2-(mix)

RESEARCH STUDY OF THE PHOTOVOLTAIC EFFECT IN CADMIUM SULPHIDE

Jet Propulsion Laboratory
Contract No. 952666

FINAL REPORT
October 28, 1970

by

K. W. Böer
Principal Investigator
Physics Department
University of Delaware
Newark, Delaware 19711

ABSTRACT

Results of the first phase (1 year) of a planned three-year effort to improve the quality of CdS photovoltaic cells are presented. The primary research effort has been concentrated in four fields: (a) General theory related to the photovoltaic effect of heterojunctions (Secs. IIA6 and 7), (b) production of materials with reproducible behavior (single crystals) (Secs. IIB1-3), (c) experimental and theoretical investigation of the behavior in the immediate neighborhood (~ 100 Å) of the CdS:Cu_xS junction (Secs. IIA2-5 and IIB3), and (d) analysis of changes in photoelectric parameters caused by radiation damage and by changes in the ambient atmosphere (Secs. IIC1-3), as such changes may be crucial for reliable operation of photovoltaic cells.

From results in part (a) information on optimized doping and on grading of a heterojunction are obtained. In part (b) successful growth and reproducible doping of CdS platelets and reproducible production of CdS:Cu_xS heterojunctions are reported. In part (c) it is suggested that the actual junction contains a $Cu_{1.96}S$ interlayer and a thin CdS layer adjacent to it under high mechanical stress. Both layers cause a marked degradation of the photovoltaic conversion efficiency. Ways to prevent or minimize the effect of these layers are suggested. In part (d) it is shown that oxygen of the ambient atmosphere influences the photovoltaic properties only in a thin (10^{-5} cm) surface-near region and that this influence can be minimized by proper defect distribution. Further inferences are obtained that the threshold for X-ray damage depends on the ambient atmosphere and the defect distribution near the surface.

Further investigations of this program will be conducted with Contract No. NGR 08-001-028 from NASA, Lewis Research Center, Cleveland, Ohio.

SUMMARY

This report describes the results obtained in the first phase (one year) of a three-year program to improve the properties of CdS photovoltaic cells, specifically to maximize the conversion efficiency and to improve the cell stability and lifetime.

The objectives during this first phase were to set-up a nine-man research team in this field, to familiarize each member with the state of the art and the general goal, and to concentrate with the three three-men groups of this team on the following subjects:

(a) 1. Theoretical analysis of the properties in the direct neighborhood of a $CdS:Cu_xS$ junction (Secs. IIA2 and 3).

2. Theoretical analysis of the properties in the neighborhood of a metal-photoconductor contact (kinetic and stationary case) (Secs. IIA4 and 5).

3. Theory of the photovoltaic effect with the final-goal to determine maximum conversion efficiency for certain junction-devices and to identify important device parameters for the purpose of optimization (Secs. IIA6 and 7).

(b) 1. Production and doping of CdS single crystals best suited for reliable and reproducible measurements of photovoltaic parameters (Secs. IIB1 and 2).

2. Creation of native defect-distribution in a desired profile for an analysis and optimization of the photoelectric behavior (Secs. IIB1 and 2).

3. Deposition and treatment of Cu_xS layers onto the CdS crystals in a reproducible manner (Sec. IIB3).

(c) Analysis of changes in photoelectric parameters critical for reliable operation of photovoltaic cells, such changes being caused by

1. Heat treatments in vacuo (Secs. IIC1 and 2).

2. Desorption and adsorption of oxygen (Sec. IIC2).

3. Radiation damage caused by X-rays (150-300 keV) (Sec. IIC3).

This approach was taken since it seems to be the most economical one for achieving technically useful results, taking into consideration the previous experience of the members of the research team (six students, two post-doctoral fellows and the principal investigator) and already known results. As more essentially basic results become available, more technical goals related to the actual device (with evaporated or sprayed-on CdS rather than single crystals) will be attacked by members of the team. (Such research will be conducted in continuation of this program under NASA Contract No. NGR 08-001-028, sponsored by the Lewis Research Center group in Cleveland, Ohio).

At the end of the first phase it can be concluded that all three groups of the team have considerably increased our knowledge in the field, -- in the theory by pointing out critical parameters of the device and practical steps for improvement and by proposing a model to understand the behavior at the actual $CdS:Cu_xS$ junction; experimentally by pointing out the reasons for the different sensitivity of CdS with different defect structure to ambient oxygen and X-ray damage, by analyzing the spectral distribution of the photovoltaic effect yielding improvements in the open circuit voltage and by development of treatment methods to improve conversion efficiency and reliability.

On the basis of these results the following recommendations are made:

1. The thickness of the device should be smaller than the random-walk length of majority carriers in each region for maximized efficiency.

2. The center range of the band gap should have minimized defect-level density for maximum spread of the quasi-Fermi levels, hence maximized open-circuit voltage.

3. The junction should be graded with a gradient thickness not exceeding the Schubweg of minority carriers in the junction field.

4. The illumination should enter through the wide band gap material.

5. The electrodes shall be not blocking for majority carriers in the n and p-region.

6. In backwall configuration an n^+-CdS layer with Ti/Al grid, desensitized to oxygen ad/desorption by a steep Cd-gradient should be used as the front electrode.

7. In a CdS:Cu_xS photovoltaic cell a short light treatment (hν > 1.8 eV) shall be used to convert an interlayer of $Cu_{1.96}S$ to bulk Cu_2S.

8. Care should be taken during production (by reducing Cu ions to Cu^+ state in the copper chloride solution) to minimize the thickness of a $Cu_{1.96}S$ interlayer.

9. The temperature of the CdS:Cu_xS solar cell should be kept sufficiently low to prevent $Cu_{1.96}S$ growth.

10. Provide a thin interlayer between CdS and Cu_xS to prevent growth of $Cu_{1.96}S$ by reducing diffusion of Cu into CdS and possibly reducing the elastic strain caused by the lattice mismatch between CdS and $Cu_{1.96}S$. Such interlayer may be provided by a thin CdS - II-VI alloy (possibly Zn/CdS/Se).

The most significant features of the first phase of the work are

1. The experimental establishment of reproducible, well-determined photovoltaic cell parameters.

2. The presentation of a model of the actual CdS:Cu$_x$S junction capable of explaining the experimentally observed photovoltaic behavior.

4. Theoretical analysis of an ideal homo- and heterojunction and recommendation of critical parameters of an optimized graded heterojunction.

5. Experimental evidence for certain environmental influences critical for device stability, yielding recommendations on a Cd-surplus gradient near the surface, to minimize this influence.

TABLE OF CONTENTS

I. INTRODUCTION

Presently the basic understanding of the photovoltaic effect at an actual heterojunction is in its infancy. Though useful devices have been developed, many questions about the processes involved remain unanswered and the overall quality of these devices can at best be classified as fair with respect to desirable parameters, most prominently the conversion efficiency.

After the technology of producing photovoltaic cells has evolved to a degree where several types can be reproducibly manufactured it is paramount that we learn to analyse the complex formation procedure to be able to optimize the characteristics of these cells.

The necessary research in this respect can be subdivided into three fields:

(a) Analysis of the physics of the photovoltaic effect with the goal

    1. to determine maximum conversion efficiencies for homo- and heterojunction cells for the solar spectrum and

    2. to identify clearly the important parameters of a photovoltaic cell for purposes of optimization.

(b) Development of experimental methods to measure the important parameters (a.2), and

(c) Selection of the most promising junction material and optimization of doping and grading of the junction.

In order to approach this goal on a wide front, simultaneous research projects in several of the above-mentioned fields were started in September, 1969, some of them by redirecting earlier work in similar fields for strategic team work.

Most central is the complex on the theory of the photovoltaic effect, currently investigated by P. Massicot, G. Dussel and the Principal Investigator. Immediate interest is focussed on the active volume (junction plus adjacent minority carrier random walk regions), the spectral distribution of the optical absorption in this volume, and the electrical parameters of the junction. Detailed studies of the actual $CdS:Cu_xS$ heterojunction are conducted on the basis of currently available experimental results. Pertinent information is also obtained from a more detailed analysis of "blocking" contacts where more experimental results are available.

The second part of the research team (L. van den Berg, J. Phillips and H. Hadley) is concerned with preparing and doping the CdS crystals, producing the heterojunction (at this time $Cu_xS:CdS$) and electrodes and investigating the electrical parameters of this system (current-voltage characteristics, high-field domains, spectral distribution of photoemf and their dependence on light intensity and temperature).

The third group (C. Wright, J. Bragagnolo and G. Storti) investigates properties of the CdS which are crucial for reliable operation under actual working condition, such as, e.g., radiation damage and influence of the ambient atmosphere.

II. TECHNICAL DISCUSSION

A. Theory

1. Introduction:

The purpose of the theoretical section of this report is threefold. One is to consider the $Cu_xS:CdS$ solar cell specifically, in order to enable us to make suggestions about how to improve it. This is discussed in Secs. IIA2 and IIA3. In Sec. IIA2 we propose a model for the cell. Sec. IIA3 describes a mechanism which could account for the previously unexplained dip in the spectral response at ~ 520 mμ for cells with thin Cu_xS layers. A second purpose is to investigate the microscopic theory of current transport in semiconductors in regions of high electric field (e.g., in a junction). It is thought that a more basic understanding of the processes occurring there than presently exists will allow us to make additional suggestions for improving cell performance over and above those which can be made on the basis of present knowledge. Our approach has been to begin by attacking the stationary and kinetic behavior of the current at a blocking contact, for which the field distribution is similar to that in a junction, and for which more experimental data is available. These developments are contained in Secs. IIA4 (stationary behavior) and IIA5 (kinetic behavior). The third purpose of the theoretical studies has been to attempt to establish general criteria for an ideal solar cell and to look for materials that could possibly meet these criteria. Sec. IIA6 discusses the ideal solar cell, a graded heterojunction, and Sec. IIA7 contains our suggestions for several possible new components for solar cells, made on the basis of the current (unfortunately limited) experimental knowledge of the properties of materials.

2. New Model for the Cu_xS:CdS Solar Cell:

We would like to propose a new model on which we hope to be able to base an explanation of many of the hitherto puzzling features of the cell behavior. The basic mechanism underlying the model was conceived very recently, and efforts to develop it are in an embryonic state. We feel it should be presented at this time in order to provide a stimulus for deeper investigation into the electrical and optical characteristics of the Cu_xS layer adjacent to the Cu_xS-CdS interface.

In this report we will endeavor to use our model to interpret some data recently published by Gill and Bube[1]. Our model contains several major assumptions, which we first list below and then discuss in detail:

1.) The band gap of Cu_2S is 1.2 eV, whereas that of $Cu_{1.96}S$ is 1.8 eV.

2.) The defect structure of Cu_xS in the Cu_xS:CdS cell is similar to that proposed by Rau[2] for high-temperature $Cu_{2-x}S$.

3.) If a small region of $Cu_{1.96}S$ is adjacent to a larger region of Cu_2S, absorption of intrinsic light in the $Cu_{1.96}S$ will cause the neutral Cu vacancies (see below) to become effectively negatively charged. They will then drift and diffuse out of the $Cu_{1.96}S$ and distribute themselves in the Cu_2S. If the original volume ratio of $Cu_{1.96}S$ to Cu_2S was small enough, the result will be the conversion of the $Cu_{1.96}S$ into Cu_2S.

Now we discuss the above assumptions: 1.) The evidence supporting a value of 1.2 eV for the band gap of Cu_2S is fairly substantial[3,4,5]. The evidence for the band gap of $Cu_{1.96}S$ being 1.8 eV is admittedly circumstantial. Several investigators who reported the value of 1.2 eV for Cu_2S also indicated a second threshold at 1.8 eV[3,4]. Two reports[6,7] listed 1.8 eV as the band gap of Cu_2S. Since it was not clear in all of these papers that the exact composition
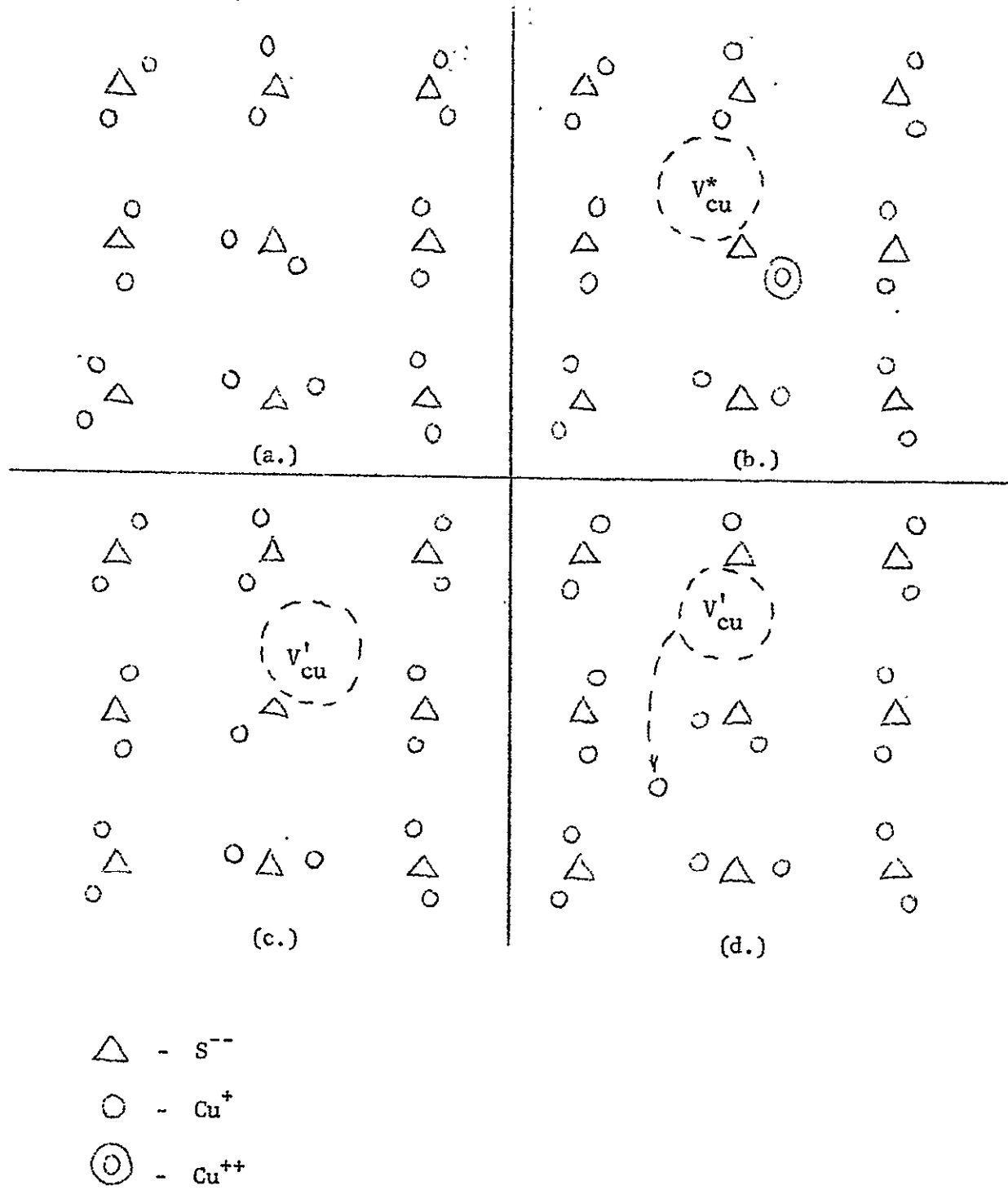
FIGURE IIA-1: Proposed defect structure for Cu_xS (After Rau[2])

of the "Cu_2S" <u>at the time of the measurement</u> had been determined, and since the composition of Cu_xS is so variable, it is reasonable to assume that these works actually measured the band gaps of two different phases of Cu_xS. We think the evidence indicates that the band gap of Cu_2S is 1.2 eV. If we then assume that Nakayama's[8] value of the band gap of $Cu_{1.96}S$ (1.5 eV) was as low as his estimate for Cu_2S (1.0 eV), we can convince ourselves that his measurements imply a value of ~ 1.8 eV for $Cu_{1.96}S$. Since the Clevite group[9] has found that Cu_2S readily converts to $Cu_{1.96}S$, it is not implausible that the values of 1.8 eV reported to have been found in studies of Cu_2S were in fact obtained from studies on $Cu_{1.96}S$.

2.) Rau studied the deviation of the composition of $Cu_{2-x}S$ from the stoichiometric Cu_2S at high temperatures (T > 500° C) and proposed a defect structure to account for his data. This is illustrated in Fig. IIA-1. Fig. IIA-1a shows the structure for Cu_2S - a highly-ordered S sublattice and a dis- ordered Cu lattice, with two Cu^+ ions associated with each S^{--} ion. (At lower temperatures the Cu sublattice may be more ordered.) A V_{Cu}^* (effectively neutral Cu vacancy) can be formed by removing two Cu^+ ions and replacing them with a Cu^{++} ion. (Fig. IIA-1b) A V_{Cu}' (effectively negative Cu vacancy) can be formed by removing a Cu^+ ion (Fig. IIA-1c). (Note that the V_{Cu}^* can be ionized by the pro- cess $V_{Cu}^* \rightleftharpoons V_{Cu}' + h^{\cdot}$, where $h^{\cdot}$ is a hole. This is probably the origin of the large hole concentration in the copper sulphides.) The formation of a Frenkel defect, as shown in Fig. IIA-1d, was shown to be inconsistent with the experimental data. The crystal can vary its composition (i.e., change x in Cu_xS) by creating V_{Cu}^*. * Moreover, Rau determined that the enthalpy of formation of the V_{Cu}^* was negative

---

* Note that Cu^{++} ions are associated with the existence of V_{Cu}^*. This will be referred to below.

at all temperatures below the melting point of Cu_2S. This indicates that it is thermodynamically favorable to form such vacancies, and it correlates with the Clevite group's finding that a crystal of Cu_2S, formed by completely converting a CdS crystal to Cu_2S by dipping it in a CuCl solution, changed completely to $Cu_{1.96}S$ after two years at room temperature[9]. It also correlates with the general tendency of x in Cu_xS to decrease when the crystals are "left on the shelf".[9] In other words, under conditions where it is possible for both Cu_2S and $Cu_{1.96}S$ to form, $Cu_{1.96}S$ will be favored thermodynamically.

3.) Consider a region of $Cu_{1.96}S$ adjacent to a region of Cu_2S. If the materials were separated initially, the energy bands would be related as shown in Fig. IIA-2a. (The Fermi level of $Cu_{1.96}S$ is assumed initially to be lower than that of Cu_2S.)

E_c ——————   —————— E_c

E_f ‑ ‑ ‑ ‑ ‑

E_v ‑ ‑ ‑ ‑ E_f

                                                      E_v
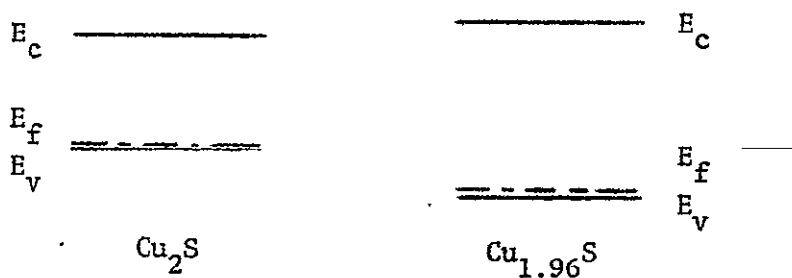
Cu_2S $Cu_{1.96}S$

(a.) Energy-band diagrams of Cu_2S and $Cu_{1.96}S$.

—————⌠————— V

(b.) Potential energy of a negative charge at a Cu_2S-$Cu_{1.96}S$ interface.

FIGURE IIA-2

When the two materials are joined, charge will flow in such a way as to equalize the Fermi levels. The resulting dipole layer will be as shown in Fig. IIA-2b. Thus there will be an electric field favoring drift of negative carriers from the $Cu_{1.96}S$ to the Cu_2S at the interface between the two. Suppose intrinsic light ($hv > 1.8$ eV) is absorbed in the $Cu_{1.96}S$. We maintain that the electrons generated by the light will be trapped at the V_{Cu}^*, thereby creating V_{Cu}'. At the boundary between Cu_2S and $Cu_{1.96}S$, there will be a concentration gradient of V_{Cu}' causing a diffusion current of V_{Cu}' to flow from the $Cu_{1.96}S$ to the Cu_2S. In addition, there is an electric field causing a drift current of V_{Cu}' to flow from the $Cu_{1.96}S$ to the Cu_2S. The Clevite researchers have shown that Cu is highly mobile in Cu_xS[10] probably diffusing in the form of V_{Cu}'. Thus the V_{Cu}' will flow out of the $Cu_{1.96}S$, (i.e., Cu^+ will flow into the $Cu_{1.96}S$), thereby converting it to Cu_2S. The Cu vacancies will distribute themselves throughout the bulk Cu_2S, converting it to $Cu_{2-\epsilon}S$, where $\epsilon > 0$. The above process will continue until the $Cu_{1.96}S$ region becomes very small and the rate of light absorption becomes so low that the process slows down*. The important point is that it is necessary to fill the V_{Cu}^* with electrons via the absorption of intrinsic light.

Before applying the above assumptions to the paper of Gill and Bube, we would like to make a brief digression. We propose that a possible thread that could be used to tie together some of the varied results reported in the literature on the Cu_xS:CdS solar cell is the idea that layers of $Cu_{1.96}S$ of different thicknesses may form initially on CdS before Cu_2S starts to grow. This is possible since Cook et al[9] reported that CdS can be converted directly to $Cu_{1.96}S$ by the

---

* Or until a drift current opposite in direction to the original one is set up, by a rearrangement of charge, to compensate the diffusion current.

dipping procedure. Different types of cells could then by expected to be created. (All of the following applies before any additional heat treatment.) For example, one could have cells with no $Cu_{1.96}S$ layer which would have a long-wavelength spectral response out to 1.2 eV and temperature-dependent dark I-V characteristics (Fig. IIA-3a; see Miya[11]), cells with a layer of $Cu_{1.96}S$ so thin that tunneling could take place and which would have a spectral response out to 1.2 eV but temperature-independent dark I-V characteristics (Fig. IIA-3b; See Gill and Bube[1]), and cells with a $Cu_{1.96}S$ layer so thick that the $Cu_{1.96}S$:CdS junction was the effective photovoltaic cell and the response would only extend to 1.8 eV (Fig. IIA-3c; See Miya[11]).
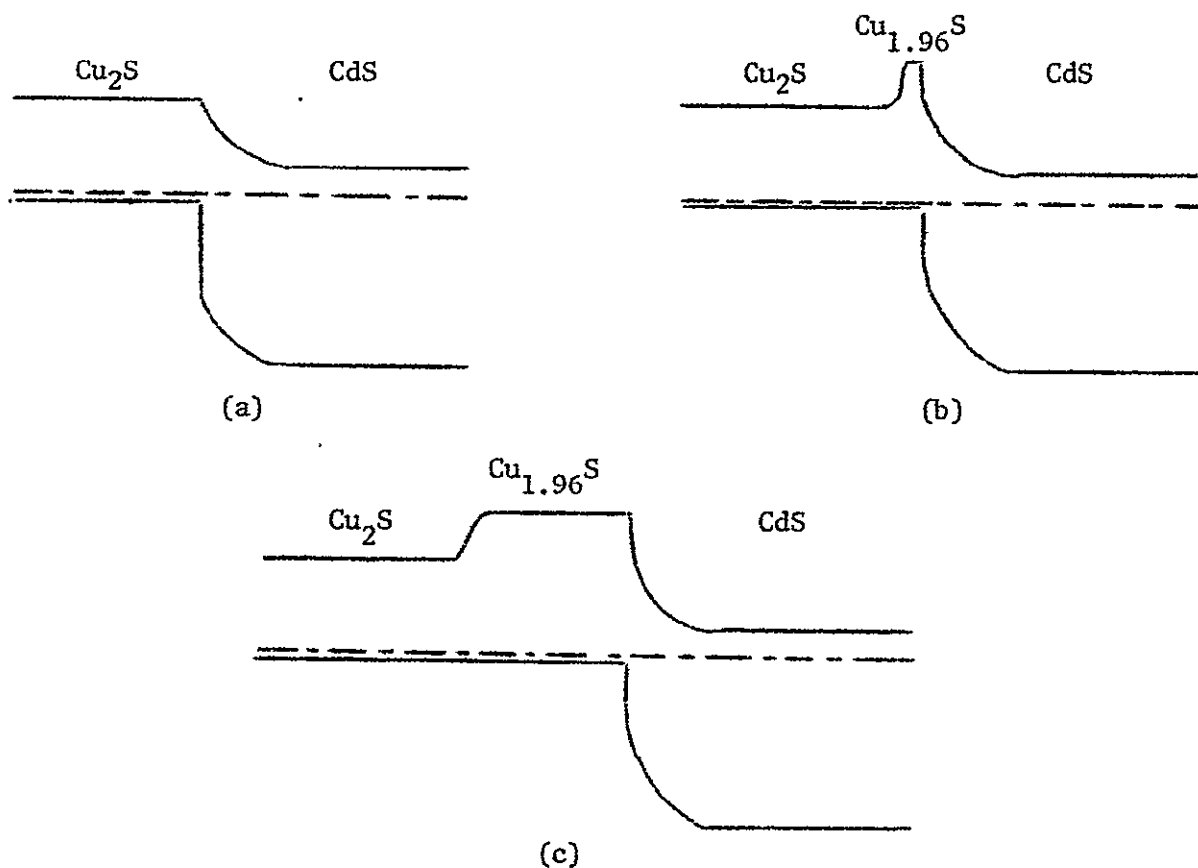

FIGURE IIA-3: Possible energy-band diagrams of different junctions resulting from dipping CdS in a copper-chloride solution.

There are several factors that could affect the formation of such a $Cu_{1.96}S$ layer: 1.) As was mentioned above, $Cu_{1.96}S$ is more stable than Cu_2S; 2.) An effort is usually made to reduce the Cu ions in the dip solution to the monovalent state, and Cu^{++} is necessary to the formation of V_{Cu}^* (and therefore $Cu_{1.96}S$); 3.) $Cu_{1.96}S$ undergoes a phase transition at 93° C, which is often close to the temperature of the dip solution; and 4.) Initially the formation of $Cu_{1.96}S$ would be favored, since it should be easier for one Cu^{++} to squeeze into the CdS lattice and replace a Cd^{++} than for two Cu^+ ions to do the same. Thus one can picture an advancing front of $Cu_{1.96}S$ eating into the CdS by means of Cu^{++} replacing Cd^{++}, with the $Cu_{1.96}S$ giving way to Cu_2S farther back from the CdS because of the preponderancy of Cu^+ ions in the solution. The above factors are currently being studied.

We now apply the model in an attempt to explain the results published by Gill and Bube[1]. We assume that the "good" cells discussed in the above article are of the type illustrated in Fig. IIA-3b; i.e., there is a very thin layer of $Cu_{1.96}S$ between the Cu_2S and the CdS. Consider the effect of a short heat treatment. Two facts should be noted: $Cu^{+,++}$ react rapidly with CdS to form Cu_xS, and the Cu_2S near the CdS would like to transform to $Cu_{1.96}S$ if it could get rid of the excess Cu. As a result of these two processes, an additional layer of CdS is transformed into $Cu_{1.96}S$ in one direction and the $Cu_{1.96}S$ layer grows at the expense of the Cu_2S in the other direction. The result is pictured in Fig. IIA-4. Due to the reduced probability that electrons can tunnel through the $Cu_{1.96}S$ barrier, the forward dark current will be greatly reduced (See Fig. 2 in ref. 1 to follow this discussion). Since light with $h\nu < 1.8$ eV can only be absorbed to the left of the barrier, the electrons it generates will still have to tunnel through the barrier to contribute to the photocurrent.* However, as $(h\nu-1.2)$ eV
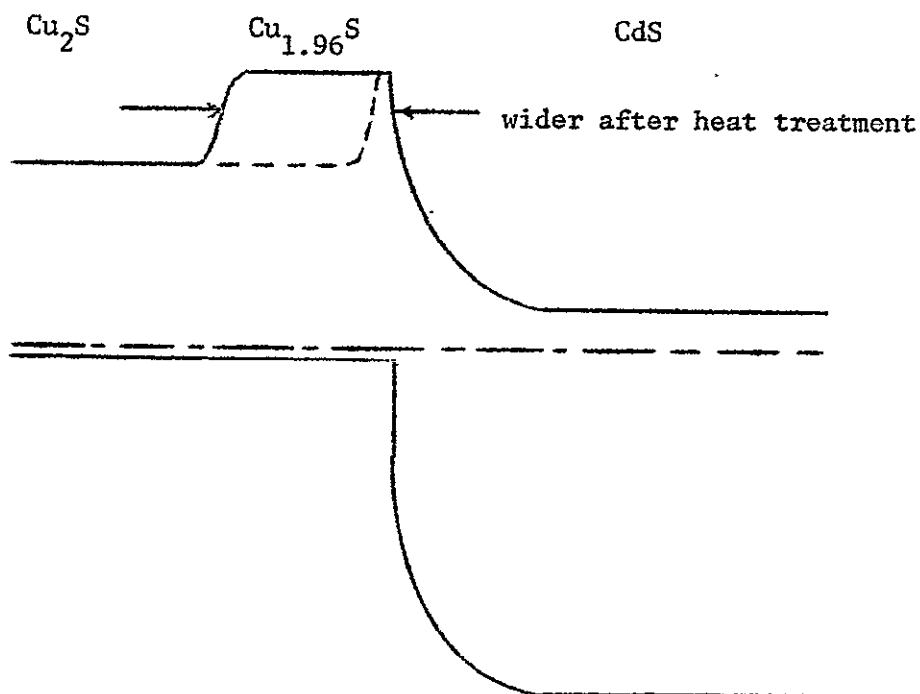
---

* Or be thermally excited over the barrier.

FIGURE IIA-4:   Effect of heat treatment on the $Cu_{1.96}S$ barrier.

increases, the electrons will be kicked higher into the conduction band of the Cu_2S; thus it may be easier for them to tunnel, and there will be a partial recovery of the photocurrent towards the pre-heat treatment value. As hν $\gtrsim$ 1.8 eV, now the light can be absorbed in the $Cu_{1.96}S$. Through the mechanism described above, the $Cu_{1.96}S$ is converted to Cu_2S and most of the barrier is destroyed. The photocurrent recovers its pre-heat treatment value. Thus the crossover of dark and light I-V curve as shown in Figure 2 of ref. (1) is

explained.*

The behavior of the spectral response described in ref. (1) is also explained on the basis of our model. Consider the response of the cell before heat treatment. It should extend from 1.2 eV to past 2.4 eV. After heat treatment, and the resultant thickening of the $Cu_{1.96}S$ barrier, there should be a threshold for response at $h\nu \approx 1.8$ eV. For $h\nu > 1.8$ eV there will be a response, since part of the light is absorbed in the barrier, where it (a) contributes to the photocurrent in the $Cu_{1.96}S$:CdS photovoltaic junction and (b) helps destroy the $Cu_{1.96}S$ barrier. (The latter condition means that electrons generated by the light of $h\nu > 1.8$ eV which is absorbed in the Cu_2S layer have less difficulty in reaching the CdS.) Bias light of $h\nu > 1.8$ eV should help erase the barrier and enhance the current for primary light with $1.2 < h\nu < 1.8$ eV. Therefore we expect a threshold for enhancement to occur at a bias-light energy of about 1.8 eV. The qualitative behavior described above is exactly that observed by Gill and Bube. However, they quoted an enhancement threshold of ~ 1.5 eV. This was obtained by considering the competition between quenching and enhancement. Their conclusion may not be unassailable, because of the difficulty in separating the two processes. Furthermore, the Clevite group[12] observed that enhancement of primary wavelengths > ~ 700 mμ (corresponding to $h\nu \lesssim 1.8$ eV) occurred when the cell was illuminated with bias white light.**

---

* Gill and Bube quote a value of ~1.9 eV as the threshold for complete recovery of the photocurrent. It is not known whether or not the discrepancy is significant. They do not discuss this threshold.

** The above behavior was observed at Clevite in cells made from donor-doped CdS. In cells formed from undoped CdS they observed enhancement of primary light with energy up to 2.4 eV with bias white light. This is explained simply as a series-resistance effect in the CdS, which must be made photoconductive by band-gap light in order to pass current easily.

For the explanation of infra-red quenching, we propose no new mechanism. We agree that Cu diffuses into the CdS during heat treatment and that it contributes to quenching in the usual way as observed in studies of photoconductivity in CdS[13]. However, at this point we do not think the Cu in the CdS plays any additional role.

The persistence of enhancement observed in ref. (1) is explained in the following way: If we take a cell which has been heat-treated and shine short-wavelength light ($h\nu > 1.8$ eV) on it, we destroy the $Cu_{1.96}S$ barrier as described above by causing Cu vacancies to diffuse out of it. If we turn off the light, the barrier will build up again (i.e. enhancement will decay) as more CdS is eaten up by the excess Cu from the Cu_2S. This decay of enhancement should be thermally activated, as is found by Gill and Bube.

Since the model is generally successful in explaining the results of Gill and Bube, we feel it is worth serious study. Furthermore, we suggest that the influence of the Cu_xS layer on the electrical and optical properties of the cell should be looked into more closely than it has been to date. We are investigating this in detail.

We would like to discuss one further point. Our model predicts the following behavior in the case of thermal cycling of the cell in vacuum. Assume that we start with a cell that has no $Cu_{1.96}S$ layer, or only a very thin one. Upon heating, the layer will grow thicker and decrease the current (because of an increase in series resistance). With further heating, small areas of the interface will gradually acquire $Cu_{1.96}S$ layers so thick that no photocurrent can get through them for $h\nu < 1.8$ eV. This will have an effect similar to that of removing part of the cell area completely, and will be manifested as a loss of short-circuit current. The areas which can still pass current have no change

in open-circuit voltage. This degradation is reversible up to an extent, since if the $Cu_{1.96}S$ layers are illuminated, they disappear, as long as Cu can diffuse into them from the Cu_2S. However, each time the layer builds up, it converts more CdS to $Cu_{1.96}S$. Thus a fixed amount of Cu is being distributed over a larger and larger volume of Cu_xS. The Cu_xS will gradually have its Cu content reduced until the point is reached where enough Cu to destroy the $Cu_{1.96}S$ barrier cannot be provided, even with the aid of light. Thus the degradation effects will gradually become irreversible, and the long-term trend would be towards first a higher series resistance, and then a loss in short-circuit current with no concomitant loss in open-circuit voltage. This qualitative behavior has been reported by researchers at Clevite[14].

3. The Dip in the Short-Wavelength Spectral Response:

Several investigators[1,3,15] have reported the existence of a dip in the spectral response of Cu_xS:CdS cells at approximately the position of the CdS band gap. The following mechanism is proposed for the dip: There is a mismatch between the lattices of Cu_2S and CdS of 4.5% and 4.8% in the plane perpendicular to the c-axis of CdS[9], which is the plane on which the heterojunction is usually formed. This misfit can be accommodated by either dislocations or elastic strain. Studies of misfit accommodation in crystals with the diamond or sphalerite structure have shown that the misfit is accommodated either completely by strain or by a combination of dislocations and elastic strain[16,17,18], for mismatches of the magnitude of the one in the Cu_xS:CdS cell. We assume that this general result holds for the Cu_xS:CdS interface also. Dislocations can provide interface states in the band gap which act as effective recombination centers[19], but this would not account for the properties of the dip. We consider the effect of strain. We assume it would be to deform the CdS adjacent to the

interface. (Deformation of the Cu_xS would have no interesting effect.) This deformation would introduce a degree of positional disorder in the ion positions. The result would be that a perturbation due to the difference in electrostatic potential between the disordered and ordered configurations of the lattice would be introduced into the one-electron Hamiltonian that determines the conduction- and valence-band electron energy levels. This would cause the conduction- and valence-band levels near the interface to be perturbed, and as a result the conduction- and valence-band edges would be deformed. (Fig. IIA-5).
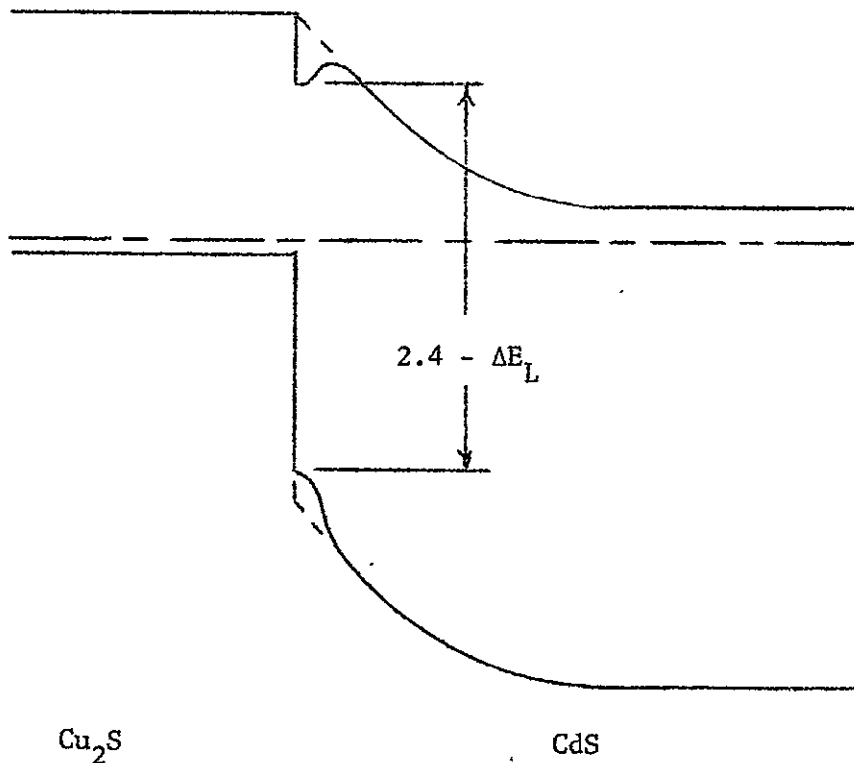

$$2.4 - \Delta E_L$$

Cu_2S . CdS

FIGURE IIA-5: Band deformation due to elastic strain in the CdS at the Cu_xS:CdS interface.

Before considering the effect these deformed bands would have on the spectral response of the cell, we examine the process of optical absorption in' general for a frontwall configuration (light incident from the Cu_xS-side). To begin with, we look at the amount of photons absorbed per unit volume as a function of the coordinate perpendicular to the junction plane, for different wavelengths. This is graphed approximately in Fig. IIA-6, using the fact that

$$\frac{\text{photons absorbed}}{\text{unit volume·sec}} = -\frac{dI}{dx} = k(\nu)I_o e^{-k(\nu)x}$$

where I_o is the incident light flux, and $k(\nu)$ is the frequency-dependent absorption coefficient. $k(\nu)$ in general increases with increasing ν for $h\nu > E_G$ and equals zero for $h\nu < E_G$, where E_G is the band gap of the absorber. In Fig. IIA-6, ν_1, ν_2, and ν_3 are such that $1.2 \lesssim h\nu_1 < h\nu_2 < 2.4 < h\nu_3$ eV. Notice that for light of frequency ν_1 and ν_2 no light is absorbed in the CdS. As the energy of the light reaches the band gap of CdS, the light is strongly absorbed there.* Therefore, if no other consideration entered, the only possible dis-continuous change in short-circuit current that could occur at the band gap of CdS is an increase, since more light is absorbed. Experimentally, however, it is observed that there is a sharp dip in current at this point, as long as the Cu_xS layer is thin enough so that an appreciable amount of light reaches the

---

* We can make an estimate of how much light of energy $h\nu_3 \gtrsim 2.4$ eV remains after the beam has gone through the Cu_xS layer. Assume $k(h\nu = 2.4) \approx 10^5 cm^{-1}$ [20] and $x_j \approx .1\mu = 10^{-5}$ cm. (x_j is the distance from the surface of the Cu_xS to the interface.) Then $\frac{I(x_j)}{I_o} = e^{-kx_j} = e^{-1}$. Thus approximately a small but significant fraction of the incident intensity remains at the interface.
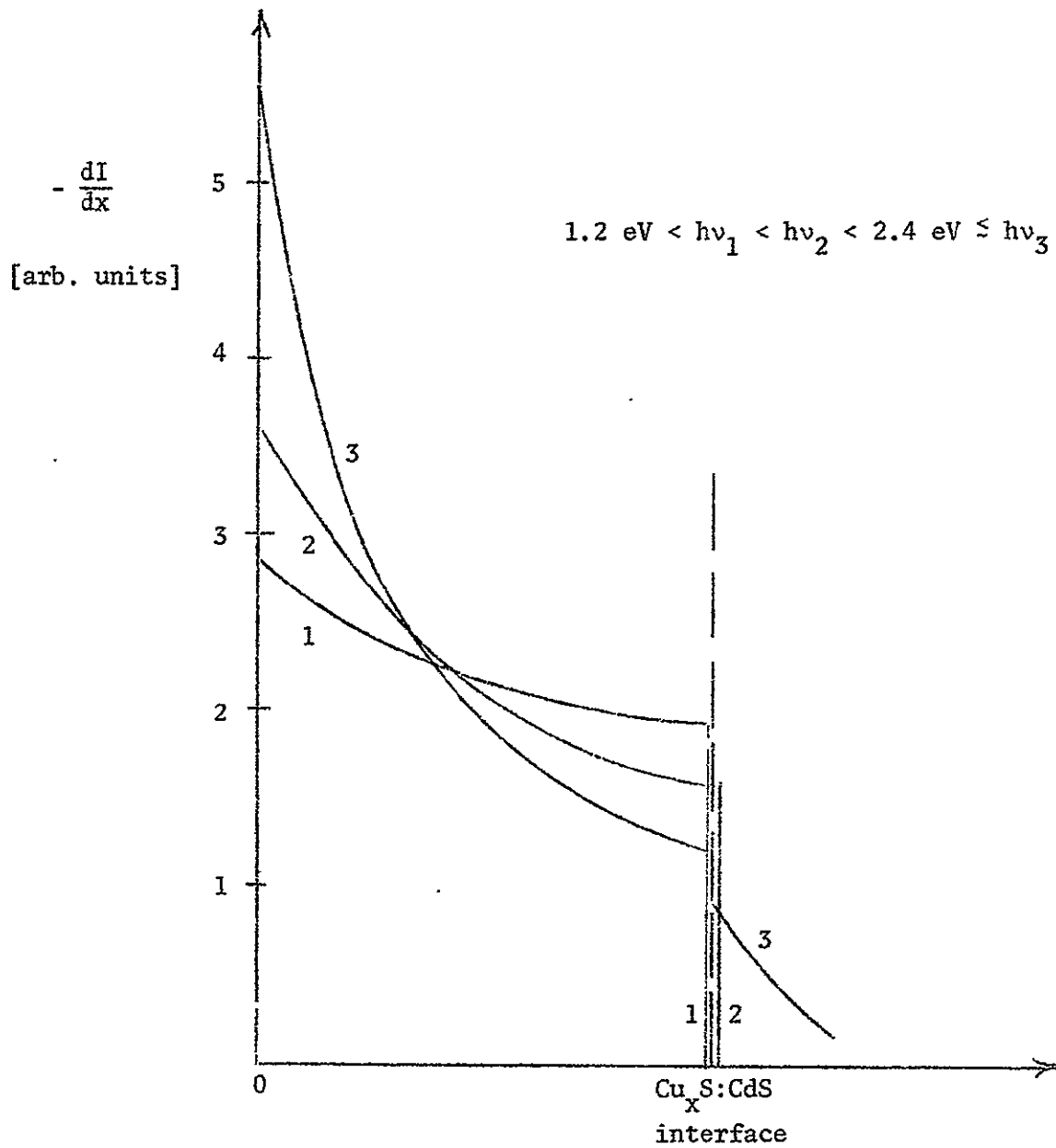
FIGURE IIA-6: Absorption of light in a cross-section of a $Cu_xS:CdS$ solar cell perpendicular to the junction plane.

junction. Therefore the extra light absorbed in the CdS must somehow subtract more from the photocurrent than it adds. The deformation of the bands in the CdS produced as a result of strain provides a mechanism for this, which we now discuss.

Let us examine the absorption of light on the CdS-side of the interface as the band edge of CdS is approached from long wavelengths. We assume that the depth of the deformation into the band gap, ΔE_L, is very small (say $\simeq kT$). This is assumed since the data show that the dip occurs very close to the band gap of CdS. For $h\nu < 2.4 - \Delta E_L$ eV, no light is absorbed in this region. For $2.4 - \Delta E_L \lesssim h\nu \lesssim 2.4$ eV, light will be absorbed as shown in Fig. IIA-7a. Electrons will be excited from the valence band into the conduction band. Due to the different curvatures of the two bands, and the resulting electric fields, the holes will be swept into the Cu_xS and the electrons will be trapped at the edge of the CdS, where they will establish a negatively-charged barrier layer. The result is shown in Fig. IIA-7b. A dipole layer will be set up with a resulting potential barrier that retards electrons trying to move from the Cu_xS into the CdS. For $h\nu > 2.4$ eV, electrons will be kicked above the deformed edge of the conduction band, and we assume that they will be swept into the CdS before they are trapped by the deformed band edge. (Fig. IIA-8).

Now let us make a "Gedanken" measurement of the frontwall spectral response of the cell. First of all, we assume that the width of the deformed region is small enough so that electrons entering the junction from the Cu_xS are swept through this region by the electric field in the junction before they can be trapped by the deformation, as long as the barrier layer has not been built up. Then for all photon energies $h\nu < 2.4 - \Delta E_L$ eV, electron-hole pairs will be generated in the Cu_xS, and the electrons will diffuse to the junction region whence they are swept
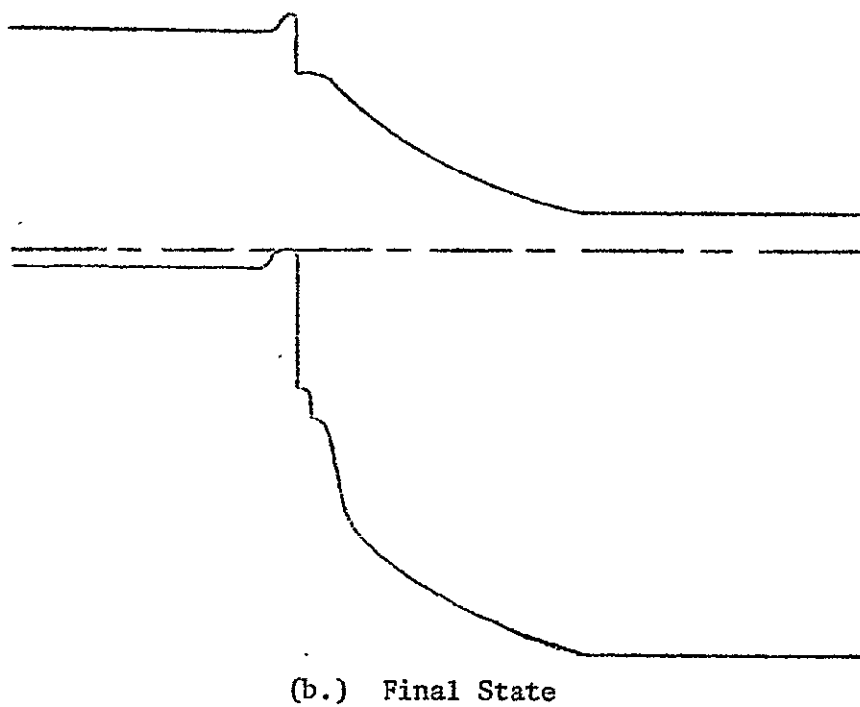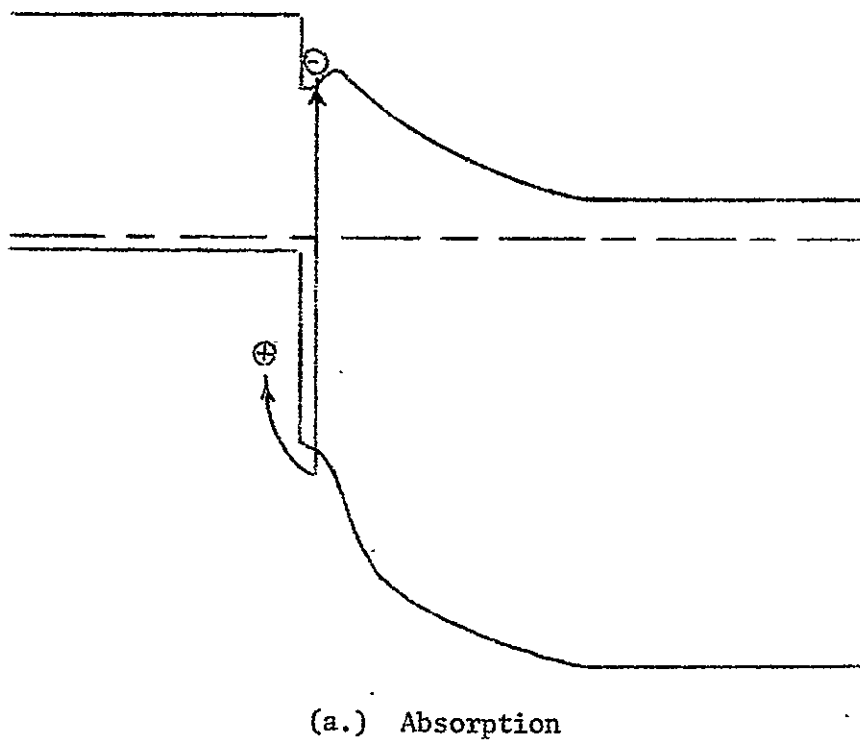
(a.) Absorption

(b.) Final State

FIGURE IIA-7: Absorption of light with 2.4 eV - ΔE_L < hν < 2.4 eV in the de-
formed-band region.
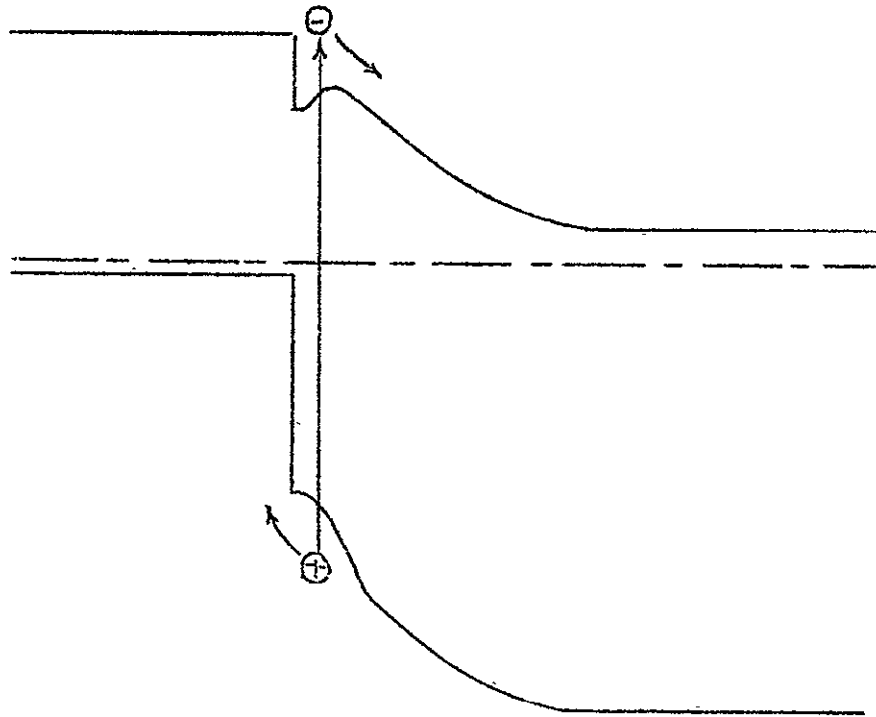
FIGURE IIA-8: Absorption of light with $h\nu > 2.4$ eV in the deformed-band region.

into the CdS and contribute to the photocurrent.

When $h\nu$ becomes large enough so that $2.4 - \Delta E_L < h\nu < 2.4$ eV, the photons reaching the CdS will be absorbed as in Fig. IIA-7a, and the deformed region will become charged. Whereas, for $h\nu < 2.4 - \Delta E_L$ eV, all of the electrons generated in the Cu_xS, within a diffusion length of the junction, diffused to and were collected by the junction, the electrons generated in the Cu_xS by light with $h\nu < 2.4 - \Delta E_L$ now will be strongly scattered by the barrier layer, and many of them will be prevented from reaching the junction before they are killed in

the Cu_xS layer. This produces a decrease in the photocurrent.

For $h\nu > 2.4$ eV, the photons reaching the CdS now generate free holes and electrons which are not trapped in the deformed region, and no barrier layer forms; hence collection of minority-carrier electrons from the Cu_xS is not obstructed. Therefore the current will rise again. Thus the dip is explained.

For backwall illumination the discussion for $h\nu < 2.4$ eV remains the same as above. For $h\nu > 2.4$ eV, however, most of the light will be absorbed farther from the junction than a diffusion length for holes because of the thickness of the CdS layer. Thus the holes cannot reach the junction and thus do not contribute to the photocurrent. Thus there will be no recovery of the response for $h\nu > 2.4$ eV. The only effect the deformed gap would have would be to cause the response to drop off more sharply as 2.4 eV is swept through from long wavelengths.

The above model is consistent with the following experimental observations:

1. The Clevite group[21] has observed that the dip is present for thin Cu_xS layers, but that it disappears for thicker Cu_xS layers. The disappearance occurs at the same thickness as that for which the response of the cell changes from increasing with increasing thickness, to decreasing with increasing thickness at all wavelengths. This is apparently related to the fact that for thick layers the light is absorbed too close to the surface of the Cu_xS for the photo-generated minority-carrier electrons to diffuse to the junction. It then follows that too small an amount of short-wavelength light will be absorbed in the CdS for the deformed gap to have an effect.

2. Chamberlin and Skarman[15] observed that the magnitude of the dip increased as the temperature was lowered. Since the electrons in the deformed conduction band can be thermally stimulated "over the hump" of the conduction band

into the CdS, thus removing the charge barrier, our model predicts this dependence on temperature. Measurements will be undertaken in our laboratory to attempt to determine ΔE_L from the temperature-dependence of the short-circuit current at the dip minimum.

3. The magnitude of the dip should depend on the amount of misfit between the Cu_xS and CdS lattices. This depends on what form of Cu_xS exists at the interface. If it is Cu_2S, then the misfit parallel to the c-axis of CdS is .4%, and those perpendicular to the c-axis are 4.5% and 4.8% [9]. If it is $Cu_{1.96}S$, then taking the values given by Clevite[9] for the lattice constants of $Cu_{1.96}S$ we calculate a mismatch parallel to the c-axis of .26% and perpendicular to the c-axis of either 5.2% and 5.7% or 7.7% and 9.1%, depending on the orientation of the $Cu_{1.96}S$ lattice to that of CdS. At any rate, the distortion parallel to the c-axis of CdS is much less than that perpendicular to the c-axis. Now consider the following experiment. We have formed Cu_xS:CdS heterojunctions with the chemical-dip method on single-crystal platelets of undoped CdS with the geometry shown in Fig. IIA-9. Backwall illumination was applied, and varying amounts of the parallel-face were shadowed as shown in Fig. IIA-10. The results are shown in Fig. IIB-17. Curve 1 is obtained with no shadow. Curve 2 is obtained with ~ 2/3 of the parallel-face shadowed. Curve 3 is taken with all but the edge of the parallel-face shadowed. As more of the parallel-face is shadowed, the response drops off much more sharply as the band edge of CdS is approached from the long-wavelength side. This behavior is explained with the aid of Figure IIA-11. Photocurrent can pass out of the Cu_xS through either the perpendicular-face $(j_\perp)$ or the parallel-face $(j_{\parallel})$. The perpendicular-face has a large lattice mismatch in both directions parallel to the junction, whereas the parallel-face has a large mismatch only in one direction. Thus the amount of distortion-induced band deformation should be larger at the perpendicular-face than at the parallel-
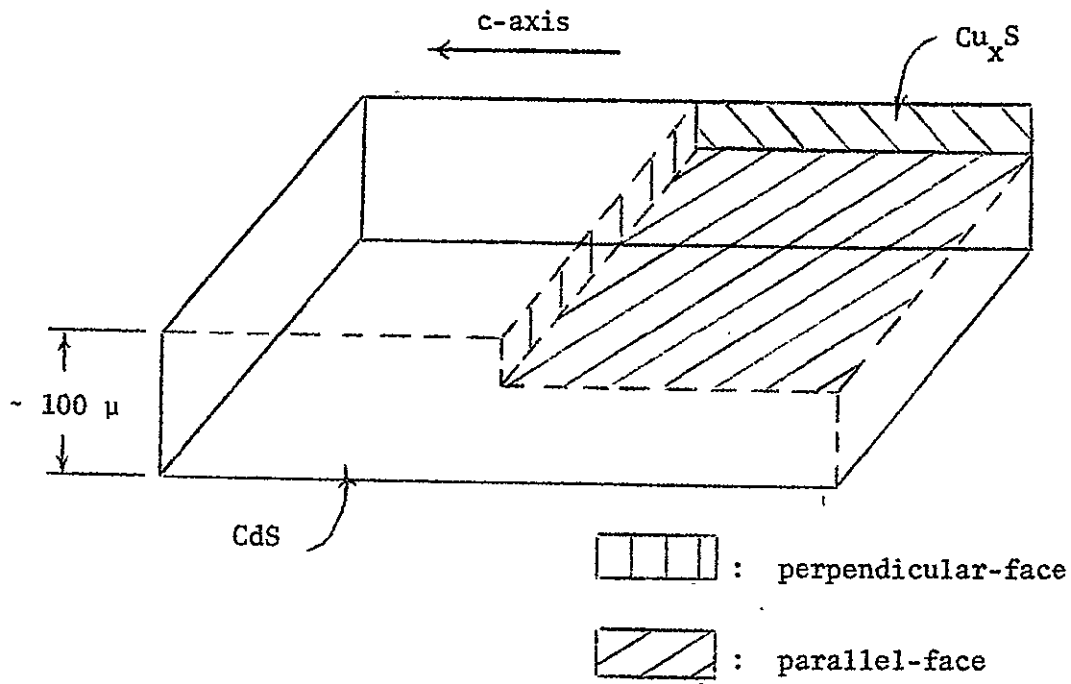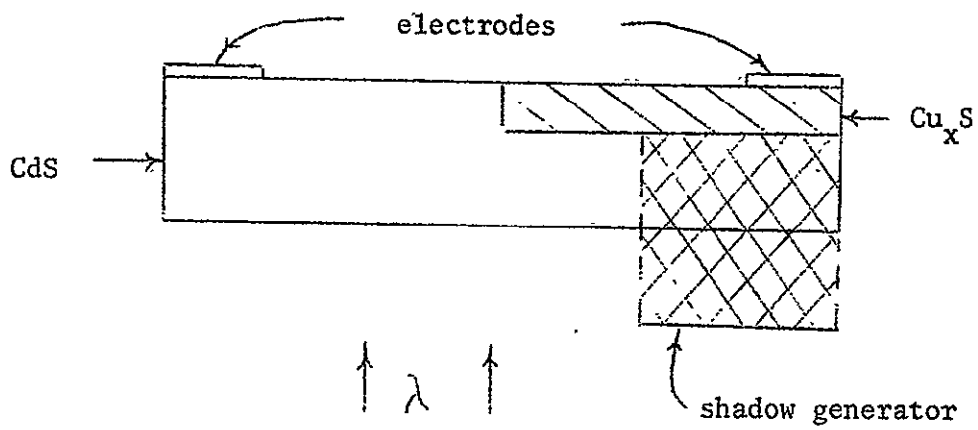
FIGURE IIA-9: Solar-cell geometry

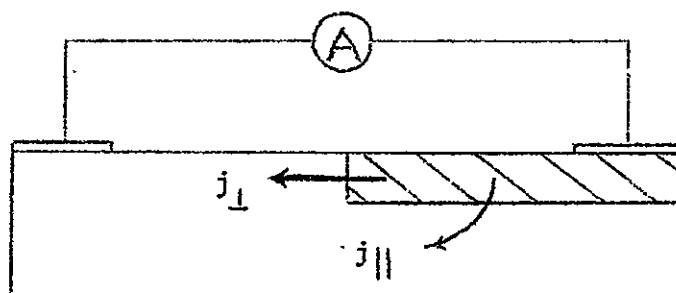FIGURE IIA-10: Method of shadowing the Cu_xS

FIGURE IIA-11: Currents through the perpendicular- and parallel-faces.

face. The relative strength of the drop-off in current at the band edge of CdS

is then simply explained by the percentages of current passing through the

parallel-face and perpendicular-face: the drop-off will be sharper as a larger

percentage of the current passes through the perpendicular face.

4. Chamberlain and Skarman[15] observed a frontwall dip which can only be

described as enormous.* We make use of our model of the Cu_xS-CdS cell as

delineated above to account for this. The spectral-response curves presented in

Fig. 4 , ref. 15, indicate that the response of their sprayed film began at

$\sim$ 700 mμ. We infer from this that the Cu_xS layer adjacent to the CdS is, in fact,

$Cu_{1.96}S$ (See the previous Sec.). Since the lattice mismatch between CdS and

---

* Their CdS layers were 1 - 1.5 μ thick, so the absorption of intrinsic light in

the CdS layer was not too great to prevent the recovery of the response after

the band gap of the CdS was reached. Consequently, they observed a dip, not just

a drop-off, in the backwall configuration.

$Cu_{1.96}S$ is even larger than that between CdS and Cu_2S, the dip should be larger. (The conduction-band edge will be deformed deeper into the band gap since the perturbation of the electrostatic field caused by the distortion of the ions is larger.)

Thus the model explains the above data satisfactorily. Additional experiments will be carried out in our laboratory to further substantiate the theory. Although the dip does not seriously affect device performance at operating temperatures, its small but finite harmful effects could be eliminated by grading the junction.

4. Stationary Current Behavior:

Two of the important problems to be clarified in connection with a heterojunction are: (a) the mechanism of generation of current in the junction, and (b) the field distribution in the junction. Both of these problems should be considered as functions of the applied voltage.

As discussed elsewhere in this report (Sec. IIB2), the high-field domain technique[22] is being used to study the heterojunction. If it were possible to establish the relation between the boundary condition (in this case at the heterojunction itself), and the value of the field within the domain, then one could gain useful information concerning the junction. From a careful analysis of the domain one could learn about the field distribution within the junction at high applied voltages.

Due to the availability of proper crystals, experimental set-up and data, it was easier to initiate this study with the test case of a blocking contact to a CdS crystal[23,24]. This case has the advantage, besides the

simplicity introduced by the fact of dealing with a homogeneous material, of having interesting technological applications, e.g., a better understanding of the gain factor and response time of a photoconductor with a blocking contact.

Part of the experimental study was conducted by Dr. R. Stirn at the Jet Propulsion Laboratory. In this discussion, the preliminary theoretical results will be presented, and an attempt to interpret in general the experimental results will be made.

Two kinds of experiments have been conducted: (1) Current-voltage (IV) characteristics, up to saturation currents, with determination of the value of the field within the domain as a function of light intensity, temperature, metal contacts, and doping (these latter by H. Hadley of our Laboratories), and (2) The measurement of the transient of the current when the voltage is applied suddenly.

The discussion will therefore be divided in two parts: (a) Stationary situations (this section), and (2) Transient situations (next section). In each case, the limiting cases of low and high applied voltages will be considered.

First we consider the stationary situation: i.e. description of the current and field distributions when the steady-state condition has been achieved. ·

(a). <u>Low applied voltage</u>: This is the usual blocking contact case. No general theory has been given, except the suggestion of basic mechanisms[25,26]. . In this case the proper contact is assumed to be totally opaque for electrons from the metal, and, therefore, only those electrons generated by light close to the cathode contribute to the current (see Fig. IIA-12). At low applied voltages, the region of generation of current $(x < x_o)$, is small compared to the length of the crystal and therefore the gain factor is much smaller than one, i.e.
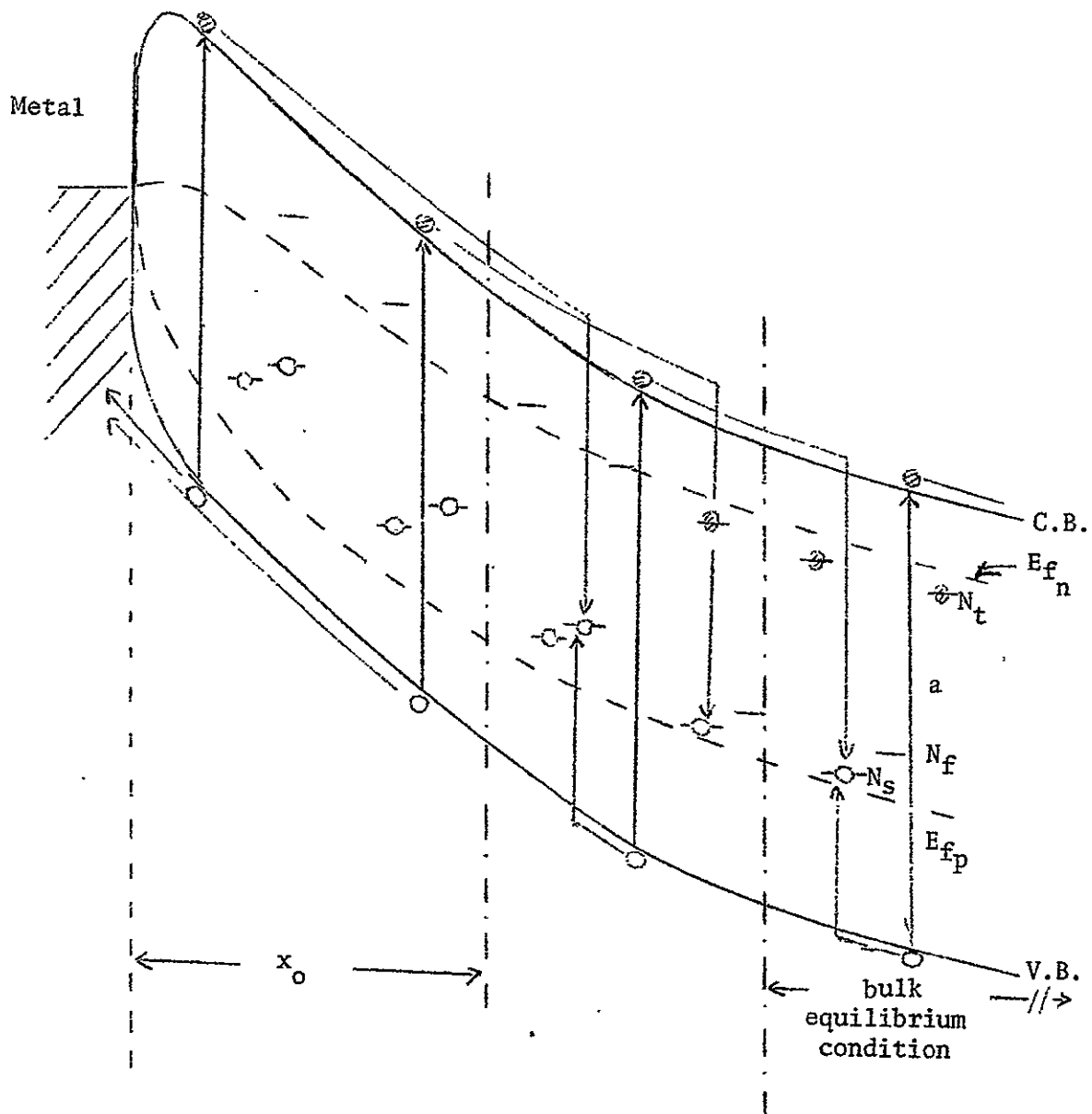
FIGURE IIA-12: Schematic model of blocking contact between metal and photo-
conductor, under light and applied voltage.

$$G = \frac{j}{eaL} = \frac{eax_o}{eaL} = \frac{x_o}{L} \qquad (1)$$

With increasing applied voltage, x_o increases, and G could approach the value of unity (when x_o becomes equal to L, i.e., the electrons contributing to the current are generated all over the crystal). Since, under these conditions, G cannot become larger than one, there should be saturation of the current as a function of the applied voltage. This condition should be achieved when the drift time ($L^2/\mu_n V$) becomes smaller than the lifetime (τ_n), i.e., for voltages

$$V > L^2/\mu_n \tau_n \qquad (2)$$

which, for typical values in CdS ($\mu_n = 10^2$ cm^2 V^{-1}s^{-1}, L = 0.1 cm, $\tau_n = 10^{-4}$s), are of the order of 1V. The saturation of the current at these low voltages is rarely observed in CdS, which suggests that some other mechanism takes over.

It is important to note at this point that the description of the blocking contact under these conditions is equivalent to that of a photocell junction, and the results should be easily extended to the latter case.

The central problem in this description is the value of x_o, i.e. the length of the region where the current is generated. We will proceed now to discuss some basic ideas connected with this problem.

In order to generate a current due purely to excitation by light in a crystal, it is necessary to separate the carriers; i.e., to force them to cross the corresponding electrodes and recombine in the metal. This is the underlying reason for the limitation in the gain factor; only those carriers close enough to the electrode to reach it before recombination (direct or indirect) with carriers of the opposite sign can contribute effectively to the current. In

fact, since equal numbers of carriers of both sign are required for recombination in the metal, that carrier that is harder to extract will determine the current.

In the absence of fields, there is no net separation of carriers. This is due to the isotropy of the distribution of recombination centers and light excitation. In this case, the probability that an electron generated at $\vec{r} = 0$ at $t = 0$ recombines at a point $\vec{r}$, is given by

$$P(r) = (\pi\Lambda_n)^{-3/2} \exp(-r^2/\Lambda_n^2) \qquad (3)$$

where $\Lambda_n = \lambda_n \left(\frac{\tau_n}{\tau_{sc}}\right)^{1/2}$ is the random walk length. (This is obtained from the fact that $P(t) = A. \exp(-t/\tau_n)$, and in a time t the electron travels a distance $r = (t/\tau_{sc})^{1/2} \lambda_n$, where λ_n is the mean free path, and τ_{sc} is the scattering time.) Therefore, if τ_n is isotropic, the distribution of the capture of the electron is also isotropic, in the absence of fields. It is of interest, therefore, to discuss what becomes of this distribution when an electric field is present. The electric field produces two main effects: (1) it deforms (tilts) the band edge; and (2) it forces the carriers to drift. The first effect, will be unimportant as long as $eF\lambda_n < kT$. This is so because in this case the carrier has no problem in traveling "up-hill". The reason for this is that while the electron travels uphill it loses energy to the field, but this loss is smaller than the average kinetic energy (kT), and therefore it is not energetically forbidden. In addition, when a collision occurs (up-hill), since the electron's kinetic energy is now somewhat smaller than kT, the electron has a tendency to absorb rather than emit a phonon (of average energy kT), and therefore, after the collision, the electron will be energetically (on the average) in an allowed state to continue traveling up-hill, if its momentum permits it. Therefore, for fields such that $eF\lambda_n < kT$, the deformation of the

band is not enough to change the isotropy of the random walk length. This simply means that the random walk length is unaffected until the electron system is "heated" by the field.

The second effect, the drift of the carriers under the influence of the field, will simply shift the "center of gravity" of the distribution, by an amount equal to the Schubweg, i.e. by $\mu_n F \tau_n$. Since the largest part of the recombination occurs within a distance of Λ_n from the center of gravity, only when the Schubweg becomes larger than the random walk length can a region close to the cathode be essentially depleted of recombination electrons. The holes generated in this region, since there are no electrons available for recombination, can now be easily extracted. The limiting field for which this occurs is given by the condition

$$F_c \gtrsim v_{th} \, (\tau_{sc}/\tau_n)^{1/2} \, \mu_n^{-1} \qquad (4)$$

Since typically $\tau_{sc} \simeq 10^{-13}$s and $\tau_n \simeq 10^{-6,-4}$s, the critical drift velocity is between three and four orders of magnitude smaller than the thermal velocity. For CdS, ($\mu_n \simeq 200 \text{ cm}^2 \text{ V}^{-1}\text{s}^{-1}$) this implies fields between 20 and 200 V/cm, which are easily obtainable in a depletion layer. Therefore, in regions close to the cathode, there is a depletion of electrons when the field is larger than this critical value. However, due to the depletion of electrons, there is a tendency to reduce the lifetime in this region. Since there are fewer available free electrons, sensitizing centers are less effective as a recombination path, and most of the recombination goes through the fast channel (i.e., the crystal is in the insensitive mode in this region). This has the effect of increasing somewhat the critical fields, as is evident from Eq. 4.

From the previous discussion it is clear that the region where the current is generated is that between the cathode and the point where the field reaches the critical value given by Eq. 4. Since in this region there are fewer electrons, there will be a positive space charge, and the field increases towards the cathode. The space charge will consist predominantly of trapped holes, and depends on the particular characteristics of the crystal under consideration. To the right of x_o, recombination becomes dominant over the sweeping out by the field; however, since there is an excess of holes at x_o, the lifetime will be shorter here than in the bulk, and this region constitutes a usual "depletion" region (i.e., the crystal has bulk properties, and the Poisson and transport equations are valid, but n at x_o is smaller than the equilibrium value in the bulk. This value of n has been used in previous publications as the boundary condition.).

Using an appropriate kinetic model, the IV characteristic can now be estimated, at least in principle. For $x < x_o$, in addition to Poisson's equation (in which the kinetic model determines the relation between the space charge and n and p), we make use of the fact that the hole current is given by $j_p = e\ a\ (x_o - x)$ (where a is the excitation rate per unit volume). The meaning of this expression for the current is that once the steady state is achieved, since the recombination in this region is negligible, all holes generated contribute to the current. At the same time, $j_p = e\mu_p\ F\ p$ is still approximately valid. The total current is given by $j_{tot} = ea x_o$. In order to calculate actually the characteristic, it may be easier to proceed in a different way: given a value of the current one obtains x_o, and using the Poisson and transport equations can obtain the voltage drop in the region x_o-L (i.e. the bulk region). Then by using Poisson's equation and the expressions for the hole current, one

can obtain the field distribution and the voltage drop in the region $0-x_0$; that is, given the current one can estimate the voltage necessary to produce it. When the voltage is increased, in order to increase the current, x_0 has to increase. Since this is the high field region in the crystal, it will have a tendency to give a sublinear characteristic (i.e. when the voltage is doubled, for the current to be doubled x_0 should increase by a factor of two; but since the field is monotonically growing towards the cathode, a region twice the initial value of x_0 has more than twice the initial voltage drop; therefore, x_0 cannot increase at the same rate as the voltage, and the same is true for the current). It is important to note that the field at the cathode is growing with increasing applied voltage, and it can reach values where additional current generation mechanisms may become active. An important consequence of the field inhomogeneity is that the limit set by Eq. 2 for the saturation of the current is no longer valid; in fact, the necessary applied voltage can be some orders of magnitude larger than the value set by Eq. 2. Therefore, it is quite possible that the saturation of the current, due to the limitation of the Gain factor, does not appear at all, since at high applied voltages some other current generation mechanism may take over.

These other mechanisms for current generation must be either field-induced thermionic emission (reduction of the cathode barrier height due to fields at that region) or tunneling through the barrier. When one of these mechanisms take over as the controlling current source, the main difference with the previous discussion is that the majority current is essentially divergenceless, and therefore the transport equation is valid within a few mean free paths from the cathode (once the anisotropy in the electron momentum distribution is erased by phonon collisions).

(b). <u>High applied voltage</u>: Experimental results[23,24] in this range of applied voltages confront us with the following situation:

i. the current is too large for the usual model of a blocking contact (i.e. the gain factor is larger than one and the current is much larger than the "thermionic" current at these temperatures determined by using known values of the work function obtained at zero current).

ii. The fields within the domains (at distances comparable to the mean free path of majority carriers from the cathode) are too small to allow tunneling directly. Therefore either tunneling does not take place or there is a high density of positive charge immediately adjacent to the cathode to build up the necessary tunneling field.

High fields extending over distances comparable to the width of the barrier would not be sufficient to provide enough reduction of the barrier so as to give thermionic currents comparable to the measured experimental currents, while they would favor tunneling currents. In order to obtain a substantial reduction of the barrier without tunneling, a dipole distribution of charge, with the positive charge close to the cathode, is required.

A more detailed analysis shows that the results cannot be explained in this way. Free holes cannot be "pinned" down close to the cathode; the image force from the metal is attractive and too strong at short distances to be overcome by any other force.

The large positive space charge could be due to a high density of trapped holes. A high density of hole traps is not observed experimentally in these crystals. If hole traps with the known densities would accumulate charge, the space-charge layer would extend too far from the cathode and tunneling would be observed. In this case, from a detailed analysis of the restrictions imposed by

the field of directions[23] it is concluded that saturation currents should

correspond to the minimum value[22], a fact which is contrary to experimental

observation. Moreover, if there were a high density of deep hole traps close to

the cathode, then tunneling of electrons from the metal would keep the occupation

of these traps low, thus reducing the space charge and the field.

From the previous discussion it is clear that the large currents ob-

served experimentally are due to either:

a. a reduction of the work function by a change in its dipole part,

    at the _proper_ boundary[27]; or

b. tunneling through the barrier.

We will discuss the possibility of tunneling in more detail, with the

crucial consideration being the storage of a high density of positive charge

next to the cathode. In this case it will also be necessary to explain why a

saturation current larger than the minimum is observed (or equivalently, why

the field within the domain is substantially lower than the known tunneling

fields).

In the neighborhood of the cathode, an ionized donor produces locally

a positive charge, that by bending the conduction band down in its neighborhood,

may contribute substantially to easing the process of tunneling[28]. In this

way tunneling fields are reduced from the usual value of 10^6 V/cm to a value of

the orders of 3 x 10^5 V/cm (This also depends on the density of centers, etc.).

Although this field is sufficient for tunneling, it is higher than the

field in the domain. Therefore there must be a transition region (with a width

on the order of the mean free path of the majority carrier), between the tunnel-

ing region and the domain, where a net positive charge is stored to reduce the

field. Usually, hole traps are acceptors, and therefore, when the hole is

captured, the center becomes electrically neutral. This leaves a neighboring ionized donor electrically uncompensated, and this has a net positive charge. Uncompensated donors close to the cathode can be produced by:

(a) Bringing in a hole to the neighboring compensating acceptor. This process could be of importance in some cases, but is insufficient to explain the transient behavior discussed in Sec. IIA5b.

(b) Extracting the electron from the neighboring compensating acceptor (e.g., by tunneling). This mechanism is not of importance here because it would not help reduce the tunneling field to the domain field. See the following discussion.

(c) Extracting the electron from a chemically uncompensated deep donor (i.e. from a donor below the initial position of the dark Fermi-level, such that it is initially not ionized), through either tunneling or field-enhanced ionization[29] (FEI). From kinetic experiments one cannot derive information about such a kind of center, nor about its density, since it would never act as an effective hole trap, except under the conditions discussed here.

The necessary density of these centers can be derived from Poisson's equation and the fact that the field decreases to the value within the domain (F_{II}) in a distance of the order of the mean free path of majority carriers (λ). Therefore

$$\frac{dF}{dx} \approx \frac{\Delta F}{\lambda} = \frac{e}{\varepsilon \varepsilon_o} \rho_1 \qquad (5)$$

For $\Delta F = 2.5 \times 10^5$ V/cm, $\lambda = 2 \times 10^{-6}$ cm, one obtains

$$\rho_1 = 1.5 \times 10^{18} \text{ cm}^{-3} = N_D - n_D = N_D^+ \qquad (6)$$

N_D is the concentration of donors and n_D the concentration of electrons in

donors. The occupancy of these levels is determined by kinetic equilibrium; i.e., the rate of capture equals the rate of emission, or

$$\frac{j_n}{e} q(F) \ (N_D - n_D) \ = \ \alpha(F) \ n_D \tag{7}$$

where $q(F)$ and $\alpha(F)$ are the field-dependent capture cross-section and emission probability, respectively.

$$\frac{n_D}{N_D} \ = \ \frac{\dfrac{j_n \ q(F)}{e \ \alpha(F)}}{1 + \dfrac{j_n \ q(F)}{e \ \alpha(F)}} \tag{8}$$

Therefore

$$\frac{dF}{dx} \ = \ - \ 10^{-7} \ N_D \ (1 - \frac{j_n \ q(F)}{e \ \alpha(F) + j_n \ q(F)} \ ) \tag{9}$$

It is clear that when the charge is generated by the process of tunneling, the only quantity affected by the field is the emission probability $\alpha(F)$, which increases strongly for fields above threshold[30]. Therefore, below threshold $e\alpha(F) \ll j_n q$ and $\frac{dF}{dx} \ll - 10^{-7} N_D$. This implies that the field cannot decrease rapidly below threshold, and F_{II} would be of the order of the tunneling fields.

If, however, the mechanism for generating space charge is FEI, which has a much smaller threshold, then at fields below those required for tunneling through the barrier there is still a substantial space charge, and the field will be decreased in a short distance, depending on the availability of ionizable donors. The threshold field (i.e., F_{II}), should be obtained from the condition

$$e \ \alpha(F_{II}) \ \approx \ j_n \ q(F_{II}) \tag{10}$$

For the mechanism of FEI, using $j_n = 10^{-5}$ a/cm^2, and the field dependence of $\alpha(F)$ and $q(F)$ derived in reference (29)[*], at T = 200° K and E_D = 0.7 eV (approximately the position of the dark Fermi-level), one obtains $F_{II} \leq 10^5$ V/cm.

From the field dependence of $\alpha(F)$ and $q(F)$, one can also obtain an implicit expression for the dependence of F_{II} on the temperature, which can be written as

$$\sqrt{\frac{e\,F_{II}}{\varepsilon\varepsilon_0}} = E_D + kT \ln [f(F_{II}/T^2)], \tag{11}$$

where $f(x)$ is a quotient of polynomials of x, and therefore a not-too-strong function of T. This would explain the experimental observation that F_{II} does

---

* It is important to note here the difference between the behavior in the contact region and that in the bulk. At tunneling distances from the contact, the distribution of electrons in momentum space is not isotropic. Due to the tunneling process, the emerging electrons are distributed in a "flat pancake" configuration, with average energy much larger than kT, and it takes several collisions to make the distribution isotropic, i.e., to make the distribution describable in terms of an electron temperature. Only when this is achieved will the bulk conditions be prevalent. As long as the anisotropy of the distribution remains, the average kinetic energy of the electrons will be larger than in the bulk under the same fields. This will have the effect of inducing a further reduction of the capture cross section $q(F)$, since this is strongly dependent on the average kinetic energy of the free carriers.

This difference in behavior between the contact region and the bulk answers the question of how it is possible to have negative space charge in the bulk (as evidenced by the existence of anode domains) for the same values of the fields ($F > F_{II}$) that in the contact region generate a positive space charge.

not change substantially with temperature in the range between 150° K - 300° K, as one would expect from a rather intuitive model. A quantitative analysis of the temperature dependence has not yet been attempted.

In summary, it is found that tunneling through the barrier is a possible mechanism for provision of the current observed in CdS, provided that there is a sufficiently high density of deep donor levels, which would be inactive in photoconductivity processes. The field in the domain would be determined by Eq. 10. The fact that F_{II} is lower than the tunneling fields in the case of CdS indicates that some other mechanism, most probably FEI, is responsible for the generation of the space charge.

5. Transient Current Behavior:

(a). Low applied voltages: When the voltage is applied, after a short time (dielectric relaxation time of the metal) a homogeneous field will appear across the crystal. This field will drive electrons towards the anode. Since there is no replenishment at the cathode, the region close to it will be depleted of electrons and a positive space charge forms there. This will have the effect of increasing the field at the cathode and decreasing the field in the bulk; i.e. the current will decrease with time. The characteristic time for this process will be that connected with the formation of the space charge; release of trapped electrons and capture of holes in hole traps, whichever is dominant. The current will approach asymptotically the value determined by the generation of current by light in the depleted region, i.e. the voltage

drop in the depleted region will grow until the field in the bulk gives a drift current equal to that generated by light in the depleted region. The current, therefore, cannot undershoot, i.e., it cannot reach values smaller than the final steady-state value.

(b). <u>High applied voltages</u>: The transient behavior of the current could be obtained by solving the Poisson, transport and kinetic equations simultaneously, with proper consideration of boundary conditions. Clearly, the system of equations is nonlinear, and a closed solution is unobtainable. In the following discussion we will attempt a very simplified model, which we expect will give the essentials of the time dependence of the current.

Previous to the application of the voltage, the crystal is assumed to be homogeneously illuminated, with one ohmic anode and a perfectly-blocking cathode (i.e., one that allows no transport of electrons from the metal electrode). It is assumed that there are no internal fields at $t \leq 0$, and therefore the quasi-Fermi level (QFL) for electrons, E_{f_n}, is flat and at the same depth from the conduction band everywhere in the crystal (the Schottky barrier at the cathode is neglected; some of the effects of the barrier are incorporated into the non-transparent contact assumed). There is a trap level distribution of density $N(E)dE$ at energy E below the conduction band. For $E > E_{f_n}$, the traps are totally occupied with electrons ($n(E)dE = N(E)dE$), while above the QFL they are increasingly empty ($n(E) = N(E) \exp [-(E-E_{f_n})/kT]$). After application of the voltage ($t \geq 0$), a field appears on the crystal

(within the relaxation time of the metal electrodes).. Free electrons are swept out by the field, and the traps begin to empty (outgassing). With increasing distance from. the cathode $(x = 0)$, the particle current increases (due to the perfectly blocking contact, at $t = 0$, j_n $(x = 0) = 0$).. Within distances large compared to the mean free path, n thermalizes and can be obtained from $n(x) = j_n(x)/e \, v_{dr}$ (neglecting diffusion currents). The outgassing of traps builds up the particle current, since the trapped charge is much greater than the free charge, i.e.

$$j_n(x) = - e \int_0^x dx' \int_{E_v}^{E_c} \frac{\partial n(E)}{\partial t} dE = - e \int_0^x dx' \int_{E_v}^{E_c} [\alpha(E)n(E)$$

$$- \beta \, n(x') \, (N(E) - n(E))] \, dE$$

or

$$j_n(x) = - e \int_0^x dx' \left(\int_{E_v}^{E_{f_n}} \beta N(E) e^{- \frac{E-E_{f_n}}{kT}} (n_0 - n(x')) \, dE \right.$$

$$\left. + \int_{E_{f_n}}^{E_c} \beta N(E) \, (n_0 - n(x')) \, dE \right) \tag{12}$$

where $\alpha(E) = \beta(E) \, N_c e^{- \frac{E}{kT}}$ and $n_0 = N_c e^{- \frac{E_{f_n}}{kT}}$ have been used. The separation between shallow $(E < E_{f_n})$ and deep $(E > E_{f_n})$ traps has been made for simplicity in calculations. At the point Δx where $n(x) = n_0$ (the quasi-thermal equilibrium density of free carriers), there is no more outgassing. Since for $x < \Delta x$, $n(x) < n_0$, in a zero-order approximation one can write, neglecting $n(x)$ compared to n_0,

$$j_n(x) = -e \int_0^x dx' \frac{\partial \rho_1(t)}{\partial t} \tag{13}$$

$$j_n(\Delta x, t) \simeq -e\Delta x \frac{\partial \rho_1(t)}{\partial t} \equiv e\Delta x \, f(t) \tag{14}$$

(The outgassing, which depends on the occupancy of the levels, is time-dependent.)

Since the traps are emptying, and initially the crystal was neutral, a space charge is built up near the cathode, i.e.

$$\rho_1(x,t) = \int_{E_v}^{E_c} dE \, [n(E,t=0) - n(E,t)] = \int_{E_v}^{E_c} dE \int_0^t \frac{\partial n(E,t')}{\partial t} dt'$$

$$= \int_0^t dt' \left(\int_{E_v}^{E_{f_n}} \beta \, N(E) \, e^{-\frac{E-E_{f_n}}{kT}} (n_0 - n(x)) \, dE \right.$$

$$\left. + \int_{E_{f_n}}^{E_c} \beta \, N(E) \, (n_0 - n(x)) \, dE \right) \tag{15}$$

This space charge forces a redistribution of the electric field. Within the same approximation as before, one obtains

$$F(x,t) = F.(o,t) - \frac{e}{\epsilon\epsilon_0} \int_0^x \rho_1(x',t) \, dx' \tag{16}$$

One can now integrate the field over the crystal length, and using the fact that the applied voltage is time independent, one obtains

$$V = \int_0^L F(x,t) \, dx = F(o,t) \, L - \frac{e}{\epsilon\epsilon_0} \int_0^L dx \int_0^x \rho_1(x',t) \, dx'$$

Using $\rho_1(x,t) = \rho_1(t)$ for $x < \Delta x$, and $\rho_1(x,t) = 0$ for $x > \Delta x$, we obtain

$$F(o,t) = \frac{V}{L} + \frac{e}{\varepsilon\varepsilon_o} \rho_1(t) \Delta x (1 - \frac{\Delta x}{2L}) \tag{17}$$

and

$$F(\Delta x,t) = \frac{V}{L} - \frac{e}{\varepsilon\varepsilon_o} \rho_1(t) \frac{\Delta^2 x}{2L} \tag{18}$$

In the region where there is no space charge (i.e., when $n(x) = n_o$, i.e. when $x > \Delta x$), the current is the current in the bulk $j(x,t) = j(\Delta x,t) = j_{bulk}(t)$, which is also essentially the measured current, since the field in the bulk is small and therefore the contribution of the displacement current is negligible there). Using $j_b(t) = e\mu n_o F(\Delta x,t)$, and Eq. (14), one obtains

$$\Delta x(t) = \frac{j_b(t)}{e\ f(t)} = \frac{\mu n_o\ F(\Delta x,t)}{f(t)} \tag{19}$$

and Eq. (24) becomes

$$F(\Delta x,t) = \frac{V}{L} - \frac{e}{\varepsilon\varepsilon_o} \frac{(\mu n_o)^2}{2L} \frac{\rho_1(t)}{f^2(t)} F^2(\Delta x,t)$$

or

$$F^2(\Delta x,t) + K(t) F(\Delta x,t) - K(t) \frac{V}{L} = 0 \tag{20}$$

where

$$K(t) = \frac{\varepsilon\varepsilon_o\ 2L}{e(\mu n_o)^2} \frac{f^2(t)}{\rho_1(t)} \tag{21}$$

At $t = 0$, $K(0) = \infty$ (since $\rho_1(0) = 0$), and $F(\Delta x,0) = F(x,0) = V/L$. As t increases, $f(t)$ decreases (there are less electrons to be outgassed) and $\rho_1(t)$ increases, and therefore $K(t)$ decreases. For times such that $K(t)<<V/L$, the solution of Eq. (20) becomes

$$F(\Delta x,t) \simeq [K(t) \frac{V}{L}]^{1/2} = \frac{f(t)}{\mu n_o} \sqrt{\frac{2\ \varepsilon\varepsilon_o}{e} \frac{V}{\rho_1(t)}} \tag{22}$$

and

$$j(t) = e \, f(t) \left[\frac{2 \, \varepsilon \varepsilon_o \, V}{e \, \rho_1(t)} \right]^{1/2} \qquad \cdot \qquad (23)$$

$$\Delta x(t) = \left[\frac{2 \, \varepsilon \varepsilon_o \, V}{e \, \rho_1(t)} \right]^{1/2} \qquad (24)$$

i.e., the space-charge region (Δx) contracts and the current decreases. At the same time, the field at the boundary increases, as obtained from Eq. (17)

$$F(o,t) \simeq \frac{V}{L} + \left[\frac{2 \, e}{\varepsilon \varepsilon_o} \, \rho_1(t) \, V \right]^{1/2} \qquad (25)$$

It may therefore reach values such that some other field-induced processes start at the cathode. One such process is FEI from deep non-ionized donors. Another is Zener extraction (tunneling out of deeply trapped electrons). The first process, depending on the energy of the donor, may require a smaller field, and therefore would occur first. From the discussion in the previous section, there should be a high density of deep levels in these crystals that could be activated by this mechanism. Due to the higher density, above a convenient "threshold" field, the outgassing from these levels can become much more important than the thermal outgassing from shallower levels. In order to deal with this situation, a simplifying assumption is that the escape rate is an on-off field-dependent rate (i.e., the mechanism is inactive below the threshold field, and is field-independent above this value). Calling F_c the threshold field and x_1 the point where $F(x_1,t) = F_c$ (the field increases monotonically from anode to cathode), and following the same procedure as before one obtains a relation between x_1 and Δx, namely

$$\frac{e}{\varepsilon \varepsilon_o} \frac{\rho_2 \, x_1^2}{2L} = \frac{e}{\varepsilon \varepsilon_o} \rho_1 \Delta x \left(1 - \frac{\Delta x}{2L} \right) - \left(F_c - \frac{V}{L} \right) \qquad (26)$$

where $\rho_2(t)$ is the charge density in the region $x < x_1$. It is obtained from

an equation similar to Eq. (15) if the field-dependence of the parameters is included.

Using this value of x_1 in the expression for the field, one obtains for the field in the bulk the expression

$$F (\Delta x,t) = F_c - \frac{e}{\varepsilon\varepsilon_o} \rho_1(t) \Delta x(t) \left[1 - \frac{\Delta x}{2L}\right] \qquad (27)$$

This indicates that if $\rho_1 \Delta x$ decreases, then the field in the bulk, and therefor the current, can increase. However, $\rho_1 \Delta x$ won't be able to decrease until the current provided at x_1 becomes comparable to $j(t)$. In this case instead of Eq. (20) one uses

$$e \Delta x f(t) = j(t) - j_n(x_1,t) \qquad (28)$$

and replacing Δx in Eq. (33) one finds

$$F(\Delta x,t) \approx \frac{F_c + \frac{e}{\varepsilon\varepsilon_o} \rho_1(t) \dfrac{j_n(x_1,t)}{e\, f(t)}}{1 + \frac{e}{\varepsilon\varepsilon_o} \mu\, n_o \dfrac{\rho_1(t)}{f(t)}} \qquad (29)$$

When the second term in the numerator takes over, the field in the bulk, and therefore the current, starts to increase. $j_n(x_1,t)$ may increase in this regime because, in spite of the decrease of x_1, the field in $x < x_1$ is increasing towards the cathode, and the larger the field the faster the excitation rate. When the deep traps in the region $x < x_1$ start to be depleted the current should decrease. However, this cannot occur unless the field in the bulk decreases. Therefore, the "high" field region (limited by x_1), moves out from the cathode. This has two effects: (a) it keeps a "large" outgassing current (since part of this region was previously inactive), and (b) it increases the voltage drop in this region, thus allowing a decrease of the field in the bulk. Therefore, at this time the current decreases slowly.

Meanwhile, the field at the proper cathode (F(o,t)) keeps growing, until it

reaches such a value that the perfectly blocking assumption is no longer valid,

and replenishment occurs by tunneling through the barrier. This leads to

the final equilibrium value of the current.

To summarize:

Stationary Situations: In the low applied-voltage limit, the usual

mechanism for generation of current by light is operative. As the applied

voltage is increased, the region where current is generated expands, and this

increases the field at the contact. With increasing voltages, the field at the

cathode may reach values that open up a new current-generation mechanism, either

thermionic emission over the field-reduced barrier or tunneling through the

barrier. At these high field values new mechanisms for the control of the space

charge may be operative. One such may be FEI, which would explain the F_{II}

values found in connection with field domains.

Transient Situations: At low applied voltages the current should de-

crease monotonically from the initial "ohmic" value to its final steady state

value.

At high applied voltages the current will first jump to its "ohmic"

value, (i.e., $= e\mu n_o \frac{V}{L}$), then decrease (thermal outgassing regime, Eq. 23).

While outgassing, the space charge close to the cathode increases. This in-

creases the field in this region, until eventually it will reach a value such

that some field-enhanced process is activated. This will provide a second out-

gassing mode in this region of the crystal. It can lead to an increase of the

current in this second regime, until the activated deep traps are depleted.

In order to maintain the current, this "high" field region grows out of the

cathode, reducing the field in the bulk, and therefore the current. Finally

the field at the cathode will reach tunneling values, replenishment of electrons will take place, and the current will grow to its final steady-state value. Thus it is concluded that the current first overshoots, then undershoots, and, if proper mechanisms are available, a second minimum can occur before the final equilibrium value is obtained.

The qualitative description of the behavior of the current as a function of time agrees with the experimental observations. Time constants for the decrease and increase of the current can be easily obtained for an assumed trap distribution in energy (that would fix the form of the functions $f(t)$ and $\rho_{1,2}(t)$). Order-of-magnitude estimates have been made that agree reasonably well with the observed values.

For a different type of crystal, in which FEI may not be effective, the maximum after the first minimum should not appear, if tunneling out of deep traps requires a higher field than tunneling through the barrier. However, the undershoot should be present, since an equation similar to (29) is valid under these conditions.

These results are preliminary, and they need further check of consistency of the results, validity of the approximations, connection between low and high applied voltage ranges, and a careful analysis of its implications as applied to CdS and other materials.

6. The Ideal Solar Cell:

(a) Graphical analysis: At the present time, an analytic solution to the equations that determine carrier behavior in a junction cannot be derived because the equations are non-linear. We have adopted a new approach to obtaining information from these equations. We construct graphs of the relevant

physical quantities as functions of the distance from an arbitrary plane normal
to the current flow; namely, electron and hole concentrations (n and p), con-
duction and valence bands (E_c and E_v), electron and hole quasi-Fermi levels
(E_{f_n} and E_{f_p}), electric field (F), space-charge density (ρ), electron and hole
diffusion currents ($j_{n_{diff}}$ and $j_{p_{diff}}$), electron and hole drift currents ($j_{n_{dr}}$
and $j_{p_{dr}}$), and ionized donor and acceptor concentrations (N_D^+ and N_A^-). For a
heterojunction, the electron affinity (χ) and the band gap (E_G) must be included.
These curves are intended to give us an indication of where we should initiate
a more exact analysis, and they suggest experiments that might be fruitfully
carried out. They are constructed in the following manner:

i. Reasonable assumptions are made as to the behavior of n(x), p(x),
$N_D^+(x)$, and $N_A^-(x)$. For example, we assume that n(x) and p(x) are constant out-
side of the junction and that they decrease rapidly as we enter the junction
from the n- and p-type regions respectively. We also assume that the ionized
impurity concentrations are constant outside of the junction and decrease
gradually in the junction. These curves are iterated self-consistently with
the other curves. From these quantities $\rho(x)$ is determined.

ii. Working backwards from $\rho(x)$ we draw the curves of F(x) and V(x),
where V(x) is the potential, using the relations

$$\frac{dF}{dx} = -\frac{e}{\epsilon\epsilon_0}\rho \tag{30}$$

$$\frac{dV}{dx} = -F \tag{31}$$

where e is the electronic charge, ε_o is the permittivity of free space, and ε is the dielectric constant. $E_c(x)$ and $E_v(x)$ can be determined directly from $V(x)$ in the case of a homojunction. For a heterojunction we have the relations,

$$E_c(x) = V(x) - \chi(x) \tag{32}$$

$$E_v(x) = V(x) - \chi(x) - E_G(x) \quad . \tag{33}$$

    iii. E_{f_n} and E_{f_p} are inferred from the equations

$$n = N_c \exp - \left[\frac{E_c - E_{f_n}}{kT} \right] \tag{34}$$

$$p = N_v \exp - \left[\frac{E_{f_p} - E_v}{kT} \right] \tag{35}$$

$$j = j_n + j_p = - ne\mu_n \frac{dE_{f_n}}{dx} - pe\mu_p \frac{dE_{f_p}}{dx} \quad {}^* \tag{36}$$

and knowledge about j (j is constant as a function of x; $j = 0$ under open-circuit conditions.). In these equations N_c and N_v are the effective densities of states in the conduction and valence bands respectively, k is Boltzmann's constant, T is the absolute temperature, and $\mu_{n,p}$ are the carrier mobilities (assumed constant).

    iv. The graphs of the various currents are obtained by using their defining relations in terms of previously-graphed quantities: For homojunctions:

$$j_{n_{dr}} = ne\mu_n F \tag{37}$$

---

* Our diagrams are not meant to be quantitatively exact and the slopes of the quasi-Fermi levels usually represent an approximate average slope.

$$j_{n_{diff}} = \frac{\mu_n \, kT}{e} \, \frac{dn}{dx} \qquad (38)$$

and similarly for the hole currents.

For heterojunctions:

$$j_{n_{dr}} = - ne\mu_n \, \frac{dE_c}{dx} \qquad (39)$$

$$j_{p_{dr}} = - pe\mu_p \, \frac{dE_v}{dx} \qquad (40)$$

The diffusion currents are the same.

Most of the useful information we have obtained from these graphs concerns the open-circuit voltage. Ordinarily the energy-band diagram gives the most information; the other curves help us construct and check the band diagram. We note that the open-circuit voltage is defined by $E_{f_n}^{(n)}(o) - E_{f_p}^{(p)}(o)$ in Figure IIA-13 which shows a symmetric homojunction under open-circuit conditions. The superscript tells us which side of the junction we are referring to and the argument gives the light intensity. For simplicity we assume uniform illumination.

Our major conclusions from the graphs are as follows:

1. The p-type material should be made as p-type as possible, and similarly for the n-type material. This can be seen by considering the case for maximum open-circuit voltage, namely when the bands are flat, as is illustrated schematically for a symmetric homojunction in Fig. IIA-14 (p. 51).
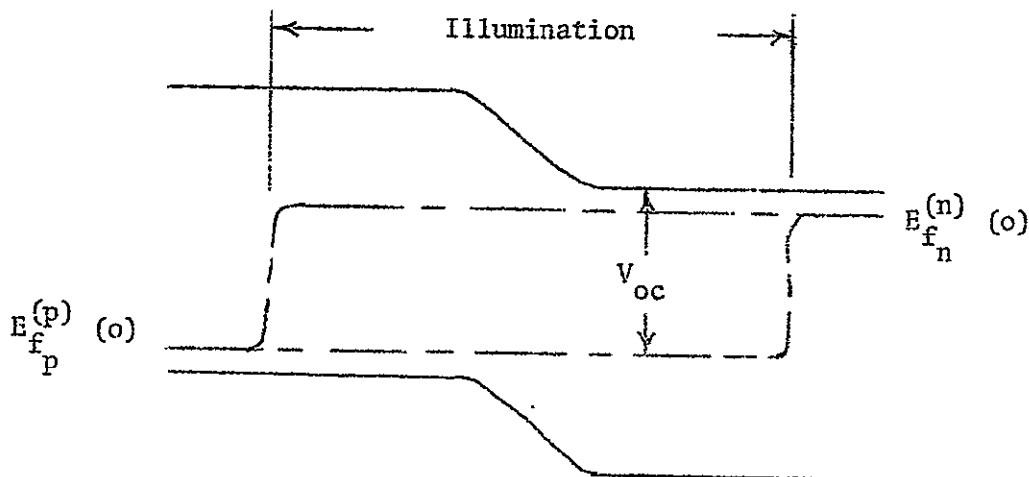
FIGURE IIA-13: Energy-band diagram for the illuminated open-circuit condition.

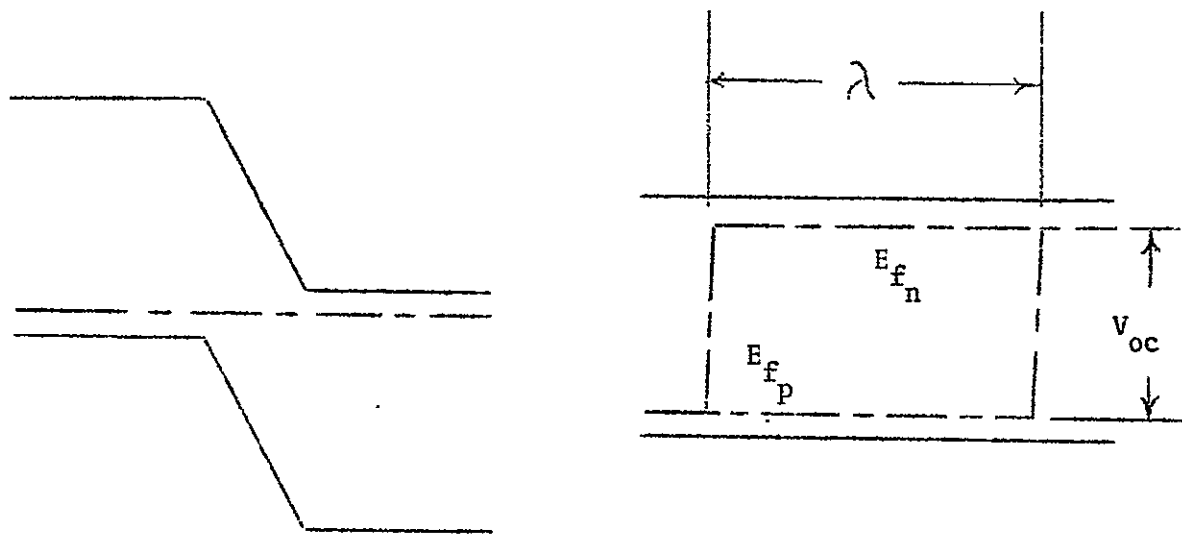2. Both minority-carrier lifetimes should be made as long as possible. This can be seen in Fig. IIA-15. We start with a symmetric junction (Fig. IIA-15a). By increasing the minority-carrier lifetime in the p-region (through doping) we raise the electron quasi-Fermi level there closer to the conduction band. (Fig. IIA-15b). (This follows from the relations

$$ n = a\tau_n = N_c \exp - \left[\frac{E_c - E_{f_n}}{kT} \right] \quad , \quad (41) $$

where a is the number of photons absorbed per unit volume per second, and τ_n is the electron lifetime). However, this results in an electron current in the junction ($dE_{f_n}/dx \neq 0$) which is not compensated by a hole current. Thus we

Dark   Illuminated

(Assume uniform illumination for
simplicity)

E_c

E_f

E_v

V_{oc}
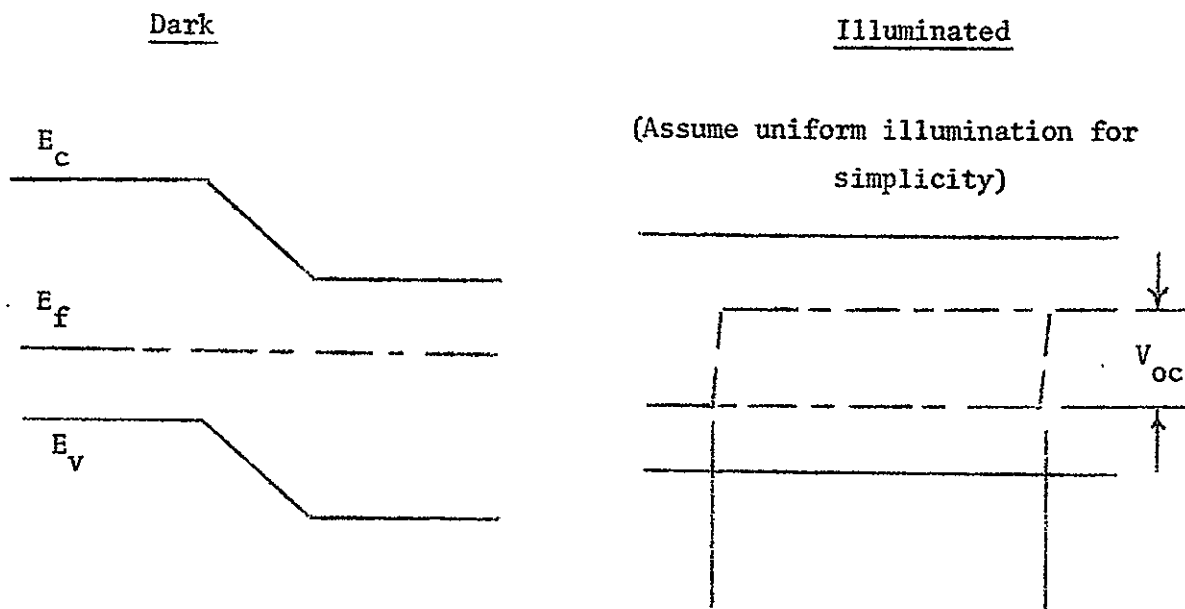
(a.) Smaller initial majority-carrier concentration

λ

E_{f_n}

E_{f_p}

V_{oc}

(b.) Larger initial majority-carrier concentration

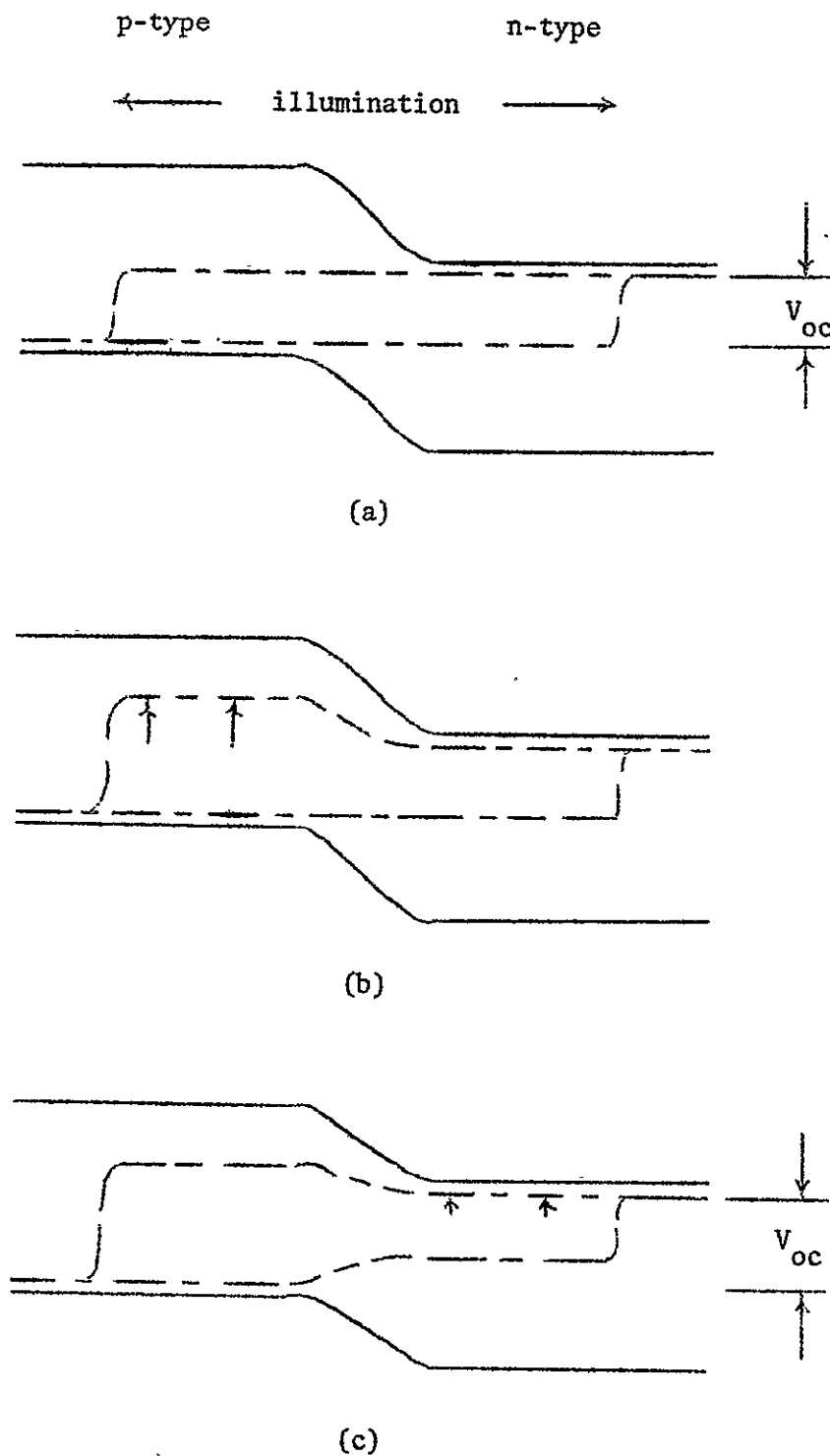FIGURE IIA-14: Effect of initial majority-carrier concentration on V_{oc}.

p-type   n-type

←——— illumination ———→

(a)

(b)

(c)

FIGURE IIA-15: A demonstration that longer minority-carrier lifetimes result in a larger open-circuit voltage (V_{oc}).

need to have $dE_{f_p}/dx \neq 0$. We cannot shift <u>only</u> the hole quasi-Fermi level in either region, since all energy differences between the conduction band, the valence band, and the quasi-Fermi levels are determined by doping. The only possibility is to shift the entire n-region of the energy-band diagram up with respect to the p-region (Fig. IIA-15c). The net result is that $E_{f_n}^{(n)}(o)$ is shifted upward with respect to $E_{f_p}^{(p)}(o)$ and V_{oc} is increased. The same result is obtained if we start by increasing the minority-carrier lifetime in the n-region. Thus the longer the minority-carrier lifetimes in the light are, the greater V_{oc} will be. This effect has been observed experimentally[32].

3. The open-circuit voltage is <u>not</u> restricted to be lower than the smaller band gap in a heterojunction (Fig. IIA-16). The disadvantage of this case, of course, is that there will be essentially no short-circuit current,
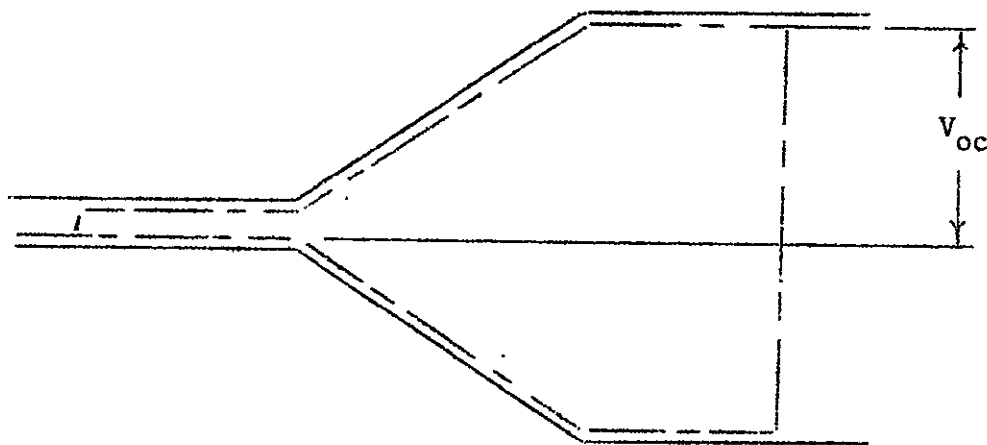

FIGURE IIA-16: Extreme case where V_{oc} > the smaller band gap of a heterojunction.

since photo-generated electrons and holes will be swept in the same direction for light absorbed in the small-band gap and junction region.* For optimum characteristics we want the open-circuit voltage to be increased as much as possible, as long as the slopes of both the conduction and valence bands have the same sign in the junction. The maximum useful V_{oc} would occur for a flat conduction band. This implies that the maximum useful V_{oc} approximately equals the smaller band gap.

4. We can suggest the reason for the unexpectedly low maximum open-circuit voltage observed in CdS cells, which is usually quoted as ~ 0.6 V as opposed to a maximum theoretical V_{oc} of ~ 1.2 V. (Chamberlin and Skarman, however, reported a value of 1.04 V for halogen-doped CdS[15]). First, we calculate the separations of the electron and hole quasi-Fermi levels from their respective bands in CdS. Bube and Gill[34] reported a value of 6×10^{-7} sec. for the hole lifetime in the CdS layer of $Cu_xS:CdS$ cells. We use the equations

$$ p = a\tau_p = N_v \exp - \left[\frac{E_{f_p} - E_v}{kT} \right] \qquad (42) $$

and an appropriate value for a, calculated below, to find the position of the hole quasi-Fermi level at the junction:CdS interface in the CdS. This will be determined by light of wavelength approximately in the range 450 mµ, since this light is strongly absorbed in this region. To calculate "a", we use the following equation:

---

* There will be some photocurrent for light generated in these regions due to electrons which are thermally assisted over the barrier. This has been observed in InSb:GaAs heterojunctions for which the proposed band diagram is essentially that pictured in Figure IIA-16 [33].

$$a = -\frac{dI}{dx} = \kappa(\lambda)I_o'e^{-\kappa(\lambda)x} \tag{43}$$

Here I_o' is the intensity of light arriving at the CdS. As noted above, this will be $\approx 10^{-1} \cdot I_o$, where I_o is the intensity of light incident on the Cu_xS. For light of this wavelength, $\kappa \approx 10^5 \text{ cm}^{-1}$ in CdS. Thus

$$a \approx 10^5 \cdot 10^{-1} \cdot 3 \cdot 10^{16} \cdot 1$$

$$\approx 10^{20} \text{ cm}^{-3} \text{ sec}^{-1}$$

where we have used the data published by Clevite[35] to obtain I_o in this range of the solar spectrum.

From the above we find

$$E_{f_p} - E_v \approx 0.3 \text{ eV} \tag{44}$$

at the junction:CdS interface. Of course $E_{f_p} - E_v$ would increase rapidly, as one moved away from the junction into the CdS, since in practice the illumination is not uniform. Now we use a value of n commonly found in the CdS used in solar cells of $n \approx 10^{15} - 10^{16} \text{ cm}^{-3}$ to find $E_c - E_{f_n} \approx 0.2 \text{ eV}$. Since Cu_xS is almost degenerate, and the hole quasi-Fermi level is very close to the valence band (within $\approx .01$ eV), we have all of the information we need to construct an energy-band diagram, under illuminated open-circuit conditions, except the position of the electron quasi-Fermi level in the Cu_xS. We obtain Fig. IIA-17.

Since under open-circuit conditions we have $j = j_n + j_p = 0$, we must have

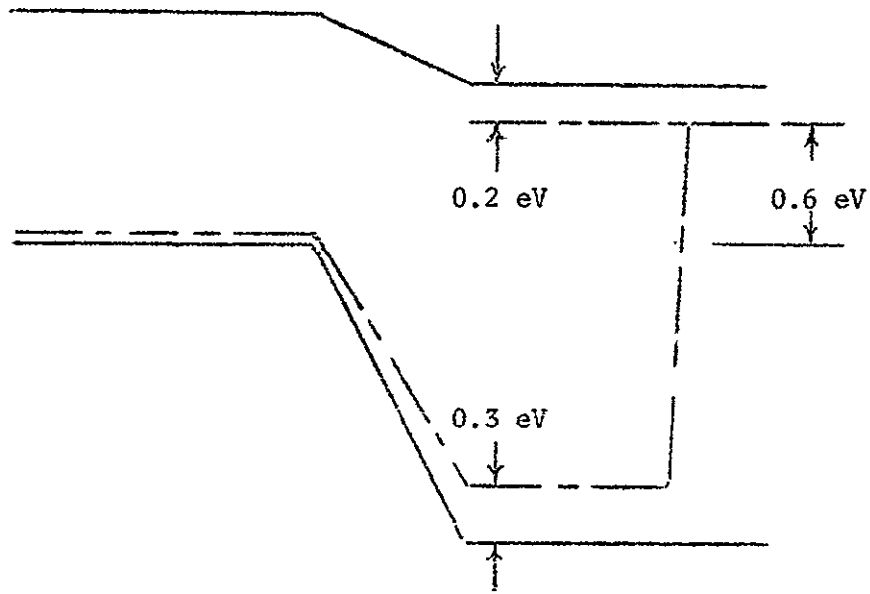$$n\mu_n \frac{d E_{f_n}}{dx} = - p\mu_p \frac{d E_{f_p}}{dx} \tag{45}$$

FIGURE IIA-17: Energy-band diagram inferred from experimental data (Illumination is assumed to be uniform at the intensity that would exist at the junction)
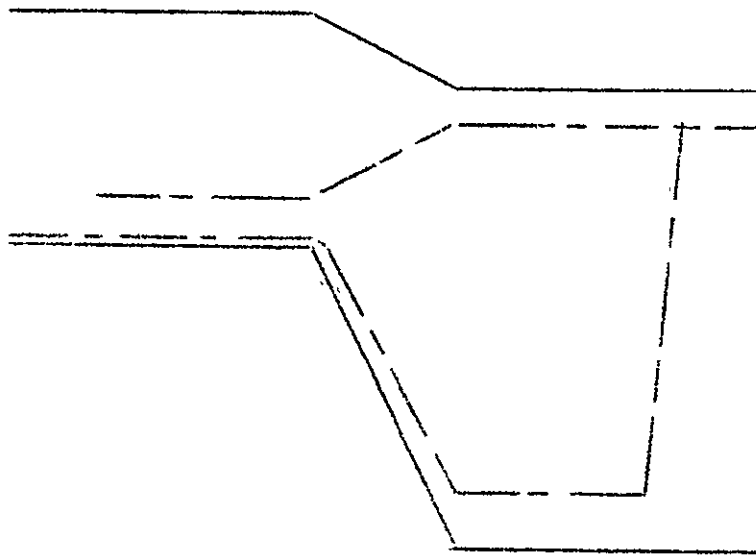

FIGURE IIA-18: Estimated position of the electron quasi-Fermi level in the Cu_xS

This would seem to necessitate having the electron quasi-Fermi level in the $\left|\dfrac{dE_{f_n}}{dx}\right|$

Cu_xS very close to the hole quasi-Fermi level, since this will give a large

in the junction to counteract the large $\left|\dfrac{dE_{f_p}}{dx}\right|$. Thus the complete band diagram

can be roughly given as in Fig. IIA-18.

Apparently, the electron quasi-Fermi level is pinned close to the valence

band by an enormous number of electron levels in the band gap that cannot be

emptied at normal illumination intensities (these would probably be V'_{Cu} -- see

Sec. IIA2). A significant reduction in the number of Cu vacancies should result

in an increase in V_{oc}.

5. The Clevite group's finding that the open-circuit voltage for cells

made from Cu-compensated i-CdS was unexpectedly low $(V_{oc} \simeq .25\ V)^{36}$, can be ex-

plained with reference to Fig. IIA-19. The i-CdS has a dark Fermi level which

is farther from the conduction band than the one in n-type donor-doped semicon-

ducting CdS. In the light the electron quasi-Fermi level drifts towards the

conduction band in the i-CdS; in the n-CdS it remains approximately stationary.

These conditions result in the energy-band diagrams of Fig. IIA-19.

(b) Critical parameters: We consider the optimum width of a junction

with respect to certain critical parameters. These are the random-walk-lengths

for recombination (analogous to the diffusion lengths), $\Lambda^{(n)}_{n,p}$ and $\Lambda^{(p)}_{n,p}$ (The

superscript indicates whether Λ refers to the n- or p-type region; the subscript

identifies the carrier referred to.), the intrinsic optical absorption length

$d(\lambda) = \kappa^{-1}(\lambda)$ $(\kappa(\lambda)$ is the optical absorption coefficient), the Debye length L_D

and the Schubwegs, $\Delta_{n,p}$ $(\Delta_{n,p}$ are the random-walk-lengths for recombination if

the carriers are drifting in an electric field.) The junction width for a homo-

junction, ℓ, is defined as the region in which there is a built-in electric

field. We restrict our attention to homojunctions for the moment.
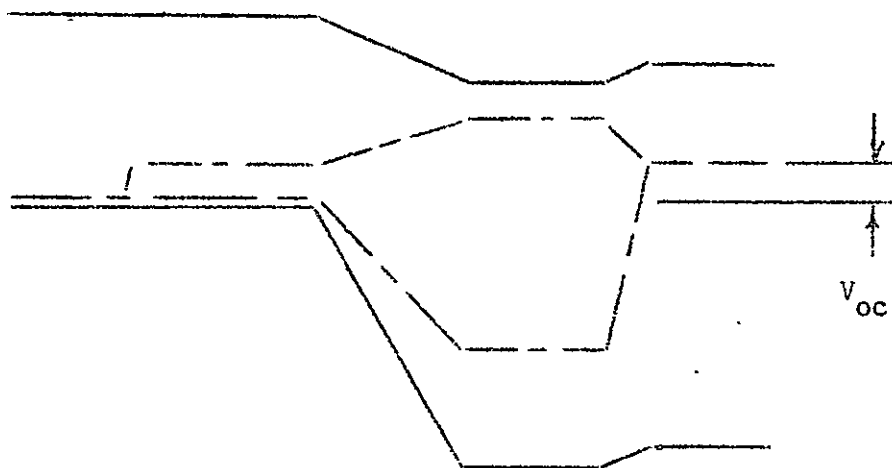
(a.) $Cu_xS:i\text{-}CdS$
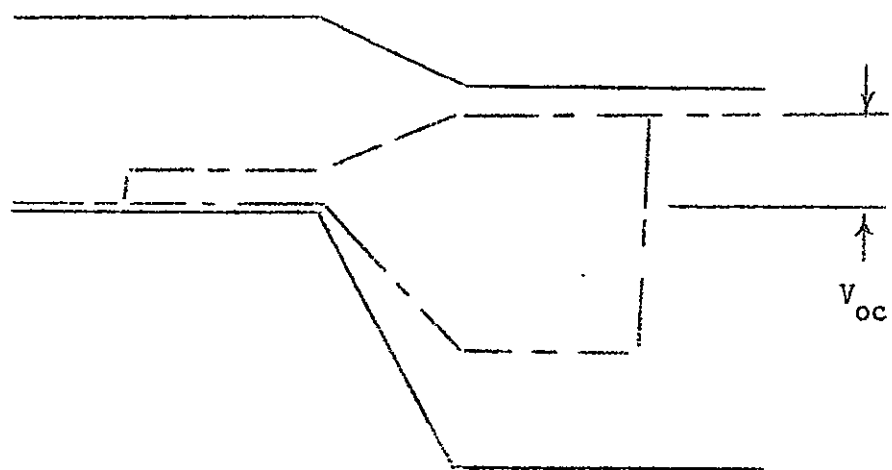
(b.) $Cu_xS:n\text{-}CdS$

FIGURE IIA-19: Comparison of V_{oc} in solar cells made from photoconductive and semiconductive CdS. (Again uniform illumination is assumed.)

To optimize photocell performance, we should realize several conditions:

1. The region which is active for optical absorption is $\Lambda_n^{(p)} + \ell + \Lambda_p^{(n)}$.
Thus we want

$$\Lambda_n^{(p)} + \ell + \Lambda_p^{(n)} \geq d(\lambda)$$

If this condition does not hold, electron-hole pairs will be excited optically outside of the region where they can contribute to power generation.

2. We would like to have the junction as narrow as possible, consistent with the above equation, so that the electric field in the junction, and hence the drift current, is maximized. At least, we should have

$$\ell < d\ (\lambda)$$

3. In the case of a homojunction, L_D is essentially a measure of ℓ, so there is no additional condition to be imposed with respect to L_D.

4. $\Lambda_n^{(p)}$ and $\Lambda_p^{(n)}$ should be maximized in order to maximize the number of minority carriers that can diffuse to the junction and contribute to power generation.

5. A minority carrier that reaches the junction should be swept through the junction before it is killed. This implies $\Delta_{n,p} > \ell$.

6. We want to collect the maximum number of carriers by the electrodes before they are killed. I.e., after the photo-generated electrons, say, have been swept into the n-region, we want the distance they have to travel to the cathode to be less than $\Lambda_n^{(n)}$. Thus we want the thicknesses of the n- and p-regions to be less than $\Lambda_n^{(n)}$ and $\Lambda_p^{(p)}$ respectively.

There are two additional considerations in the case of a heterojunction. First of all, since the graded region does not have translational symmetry, it

must be considered as a quasi-single-crystal with a position-dependent band gap[37,38], and some of the parameters will depend on position due to this fact. Secondly, there are two "widths" one can define. One is ℓ, which is the same as for a homojunction (and again closely related to the Debye length). The other is ℓ_G, which is the width of the graded region. There are two conditions on ℓ_G. One is that it be large enough so that the harmful effects of a notch and/or spike be eliminated (see Sec. IIA6 c, below). The other is that, consistent with the previous statement, $\ell_G \approx \ell$. This is so that the electric field due to space charge (existing over the distance ℓ) and the effective electric field due to band-gap grading[31] (existing over the distance ℓ_G) are concentrated in the same region. With the above-mentioned modifications in mind, we can apply the conditions previously established for homojunctions to heterojunctions.

(c) <u>Homojunction vs. Graded Heterojunction</u>: As a result of our theoretical investigations, we have come to several conclusions regarding the characteristics of an ideal solar cell. We think this should be a heterojunction, not a homojunction. The main reason for this is as follows: First of all, in a homojunction formed from a material with a band gap E_G, no incident photons with $h\nu < E_G$ are absorbed. This implies that one should minimize E_G. However, there are other considerations. All photons with $h\nu > E_G$ are absorbed within a length $\kappa^{-1}(\lambda)$. This length becomes smaller as $(h_\nu - E_G)$ increases. Consider a cell with a distance L from the surface on which light is incident to the active junction region. As $h_\nu - E_G$ increases the light is absorbed closer to the surface, and eventually the minority carriers created by the absorption will not be able to diffuse to the junction before they are killed ($\kappa^{-1}(\lambda) < L$). If we try to counteract this by making L small, eventually we will have $\kappa^{-1}(\lambda_2) \gg L$,

where $\lambda_2 > \lambda_1$, and the light with an energy close to E_G will not be strongly absorbed. Of course, for each wavelength there is an optimum L, and for a given solar spectrum there is an optimum E_G and a corresponding optimum L, but a significant amount of the incident light is not absorbed where it can generate electric power.

The situation is different in the case of a heterojunction. Suppose we construct a heterojunction from two materials with a small band gap $E_G^<$ and a large band gap $E_G^>$. We shine light on the device on the large band-gap side (backwall). All light with $h\nu < E_G^>$ passes through to the junction region where it is absorbed in the small band-gap material. We can make $E_G^<$ small in order to intercept most of the solar spectrum, and since the absorbing surface is actually at the junction, the fact that $\kappa^{-1}(\lambda)$ for small λ (such that $h\nu \gg E_G^<$) gets smaller does not matter. If we can make $E_G^>$ large and $E_G^<$ small we can have virtually all of the solar spectrum contribute to power generation.

Going one step further, we propose that a graded heterojunction, as opposed to an abrupt heterojunction, would be necessary. There are two reasons for this. The first reason is the following: If the lattices of the two components of the heterojunction do not match exactly, the mismatch will cause interface states to appear in the band gap which will impair performance. If we make the junction from two materials which have a continuous range of solubility in each other, we can grade the composition uniformly from 100% of one component to 100% of the other, with a concomitant uniform change in lattice parameters. In this way the interface states due to lattice mismatch will not be present, although there probably will be a reduction of the mobility below the values in the perfect crystals of either component[39].

The second reason involves the elimination of spikes and notches in the valence and conduction bands which are deleterious to cell performance[40]. The origin of such a spike is illustrated in Fig. IIA-20. If we connect a p-type semiconductor with an electron affinity χ_p to an n-type semiconductor with an electron affinity $\chi_n < \chi_p$, the resulting junction will have a spike in the conduction band which impedes collection of minority-carrier electrons generated by light in the p-type material. We think this spike could be eliminated in the following manner. (See Fig. IIA-21). We consider a succession of layers with conduction- and valence-band energies, electron affinity, and Fermi level all varying smoothly from one componant to the other. (Fig. IIA-21a). If these layers are joined together, the result will appear as in Fig. IIA-21b. The spikes are smaller than the spike that would have resulted if the layers farthest to
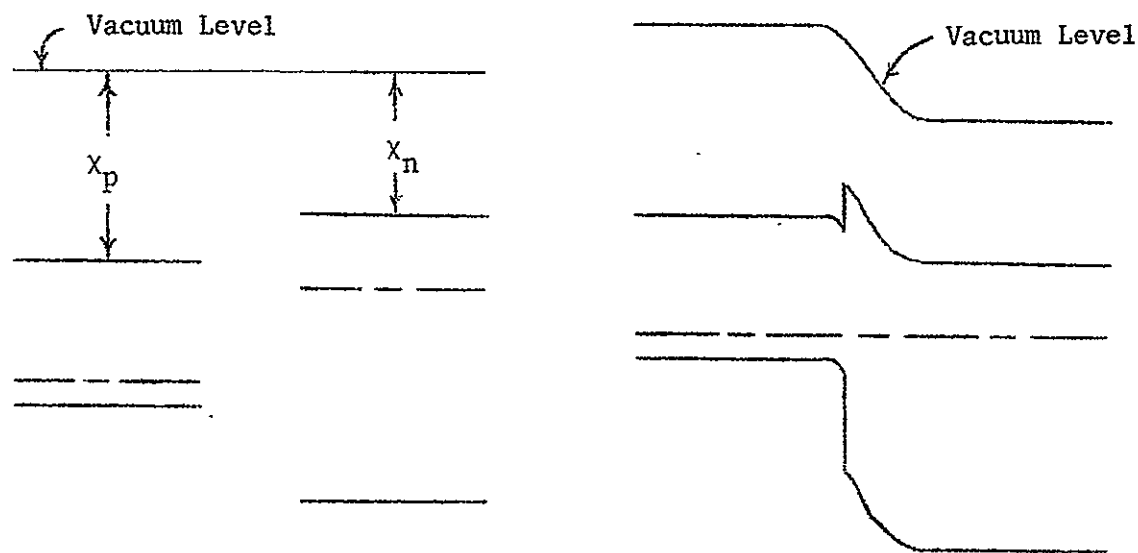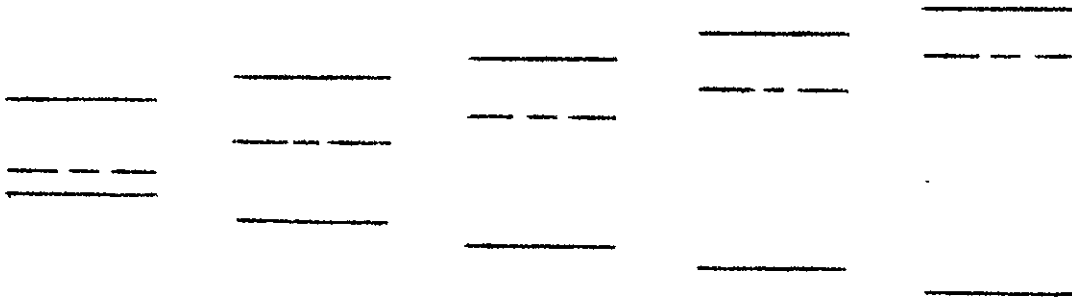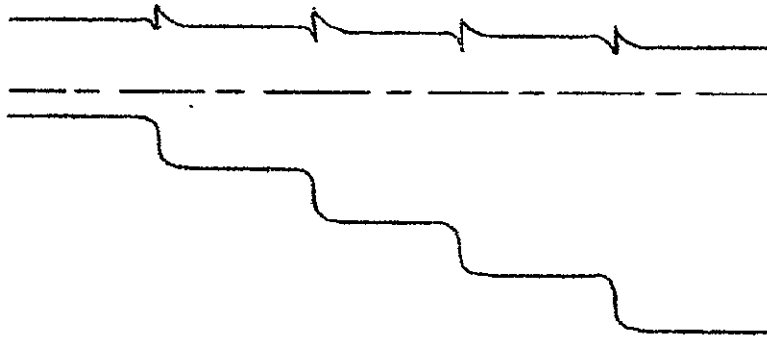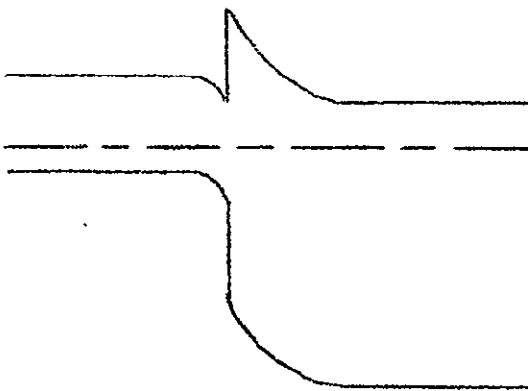

FIGURE IIA-20: The origin of a conduction-band spike.
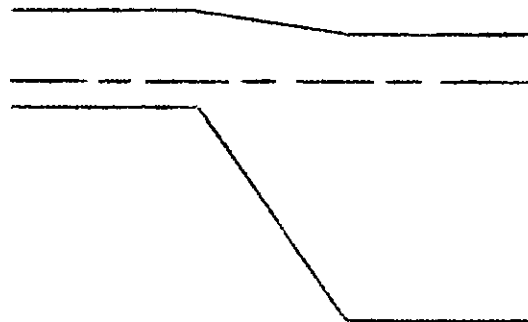
(a.) Band configuration before grading in five steps

(b.) Band configuration after grading in five steps

(c.) Abrupt junction

(d.) Completely-graded junction

FIGURE IIA-21: Grading a heterojunction

the right and left in Fig. IIA-21a had been joined (Fig. IIA-21c). As one takes thinner and thinner layers, with smaller variations in properties from one layer to another, and joins them together (i.e. forms an alloy with a continuous variation in composition), he should be able to make the bands smooth. The final band diagram of such an alloy would be independent of the electron affinities of the initial components and would only depend on their band gaps and the initial positions of their Fermi levels (Fig. IIA-21d).

There are several other criteria that the materials which would be used in an ideal heterojunction should meet. The electron and hole mobilities should be as high as possible. The conductivity type (n-type or p-type) should be of the right kind. We would like to be able to make the materials as ambipolar as possible under light (i.e. make the electron and hole quasi-Fermi levels separate as much as possible. See Sec. IIA6a.). The doping characteristics that the elements of one component exhibit upon being incorporated in the other component should be as favorable as possible. Finally, since we are interested in a practical device, we would like to be able to manufacture the materials, and especially the junction, as economically as possible. This means, for example, that we would like to be able to automate the production process. In the next section we summarize the above criteria and make specific recommendations concerning new materials we feel should be investigated.

7. Possible New Materials for Solar Cells:

We summarize our requirements for materials to be investigated as possible new components in an ideal solar cell in the following list:

1. Large $E_G^>$, small $E_G^<$.

2. Complete range of solubility in each other

3. High mobility

4. Correct conductivity type

5. Ambipolar photoconductivity

6. Good doping characteristics

7. Ease of preparation

As a first step in examining the question of which new materials are to be investigated, we have prepared a chart incorporating the first four entries in the above list for most II-VI and III-V compounds (Table I). These include a significant number of the compounds for which information on solubility is available, and the table will be expanded as more data become available. The top row of the chart gives information where available on the band gap (in eV), lattice constant (s) in Å *, electron and hole mobilities (in $cm^2 V^{-1} sec^{-1}$), and possible conduction type (n or p).** The boxes above the diagonal give the ranges of solid solubility, the numbers in the boxes corresponding to the value of x in the formula $(AB)_x:(CD)_{1-x}$, where AB is the compound in the corresponding column and CD the compound in the corresponding row. The boxes below the diagonal contain pertinent references. A word of caution is in order about interpreting solubility data. Most investigators use X-ray diffraction measurements of lattice

---

* Where one lattice constant is given, the structure is zinc blende; where two are given, the structure is wurtzite.

** An "n" or "p" in parentheses indicates that material of that type can be made, but only with a high resistivity.

Table I

$\frac{x}{1-x}$	Zns	ZnSe	ZnTe	CdS	CdSe	CdTe	β HgS	HgSe	HgTe
Latt. Const.	6.26 3.82	5.67	6.10	6.72 4.14	7.02 4.30	6.48	5.83	6.08	6.45
Band Gap	3.6 direct	2.7 direct	2.3 direct	2.4 direct	1.7 direct	1.4 direct	semi-metal	semi-metal	semi-metal
μ_n μ_p	140 5,700°K	530 30	340 110	350 15	650	1050 80	900	10000	15000
Type	n	n (p)	p (n)	n	n	n,p	n	n	n,p
ZnS		0-1	0-0.08 0.95-1	0-1			0-1		
ZnSe	45		0-1	0-1	0-1			0-1	
ZnTe	47	45		not 0-1		0-1			0-1
CdS	43	45	48		0-1	0-0.035 ?-1	0-0.43 0.6-1		
CdSe		45		45		0-1		0-1	
CdTe			45	46	45				0-1
β HgS	43			43				0-1	0-1
HgSe		51			44		51		0-1
HgTe			51			51	51	51	
AlP	53								
AlAs									
AlSb			42			53			
GaP	42	42							
GaAs	42	42	42	42					
GaSb									
InP	42	42		42	55				
InAs						54			53
InSb						53			

66

Table I (cont'd.) 67

| AlP	AlAs	AlSb	GaP	GaAs	GaSb	InP	InAs	InSb	x /1-x
5.46	5.66	6.14	5.45	5.65	6.10	5.07	6.06	6.48	(a) (c)/(a)
2.4 indir.	2.2 indir.	1.6 indir.	2.2 indir.	1.4 direct	0.67 direct	1.3 direct	0.35 direct	0.18 direct	Band Gap
		900 / 460	300 / 150	8000 / 400	5000 / 1000	4800 / 150	33000 / 450	78000 / 750	μ_n μ_p
		n,p	n,p	n,p	n,p	n,p	n,p	n,p	Type
0-0.01 ?-1			0-1	0-0.07 0.85-1		0-0.02 0.9-1			ZnS
			0-1	0-1		0-0.006 0.94-1			ZnSe
		0-0 0.82-1		0-? 0.75-1					ZnTe
				0-0 0-0		0-0 0-0			CdS
						0-1			CdSe
		0-1					0-0.38 0.65-1	0-0.05 ?-1	CdTe
									βHgS
									HgSe
							0-1		HgTe
			not 0-1						AlP
				0-1			0-1		AlAs
					0-1			0-1	AlSb
55				0-1	0-0.2 0.95-1	0-1	0-1	0-0.05 0.95-1	GaP
	55		52		0-1	0-1	0-1	0-0.15 0.85-1	GaAs
		49	52	52		0-0.15 0.85-1	0-0.3 0.8-1	0-1	GaSb
			52	52	52		0-1	0-0.05 0.8-1	InP
	50		52	52	52	52		0-1	InAs
		49	52	52	52	52	52		InSb

constant and optical determinations of the band gap to assess solubility. However, the results do not always appear to be unequivocal.

For our band gap limits we have chosen the lower bound for $E_G^>$ to be 2.4 eV (corresponding to CdS) and the upper bound for $E_G^<$ to be 1.38 eV (corresponding to GaAs). These values are arbitrary to a degree and were picked with the idea of including the maximum in the solar spectrum (Fig. IIA-22), constructed from Ref. 35). Also, GaAs was included since a considerable effort is being spent on its technology, and this might give GaAs an economic advantage over other materials. The pairs of compounds which simultaneously satisfy $E_G^> \geq 2.4$ eV and $E_G^< \leq 1.38$ eV have their solubility blocks outlined heavily. There are 27 combinations that satisfy the band-gap criteria. There exist solubility data on only 9, and only 4 have reasonable ranges of solubility: $Zn_xHg_{1-x}S$, $Zn_xHg_{1-x}Se$, $(ZnSe)_x(GaAs)_{1-x}$, and $Cd_xHg_{1-x}S$. Each one of these is discussed below:

(a.) $Zn_xHg_{1-x}S$ and $Zn_xHg_{1-x}Se$: The advantages of these two alloys are the large band gaps of the Zn-compounds and the small band gaps of the Hg-compounds. The Hg-compounds are both semi-metals, so their band gaps can be made as small as desired. On the negative side, the Zn-compounds can only be made n-type and the Hg-compounds so far can only be made n-type, although the latter have apparently not been investigated extensively. (Extrapolating from the trends in the Zn- and Cd-compounds, one would expect that possibly HgTe could be made p-type, but probably not HgS or HgSe.) Also, the minority carrier mobilities of the Zn-compounds are low. An additional disadvantage of $Zn_xHg_{1-x}S$ is that HgS (β-form) is rather difficult to make[41].

(b.) $(ZnSe)_x(GaAs)_{1-x}$: The advantages of these materials are ease of preparation of the alloy, the relatively large band gap of ZnSe, the high

FIGURE IIA-22: Solar energy and photon spectra (m = 0)
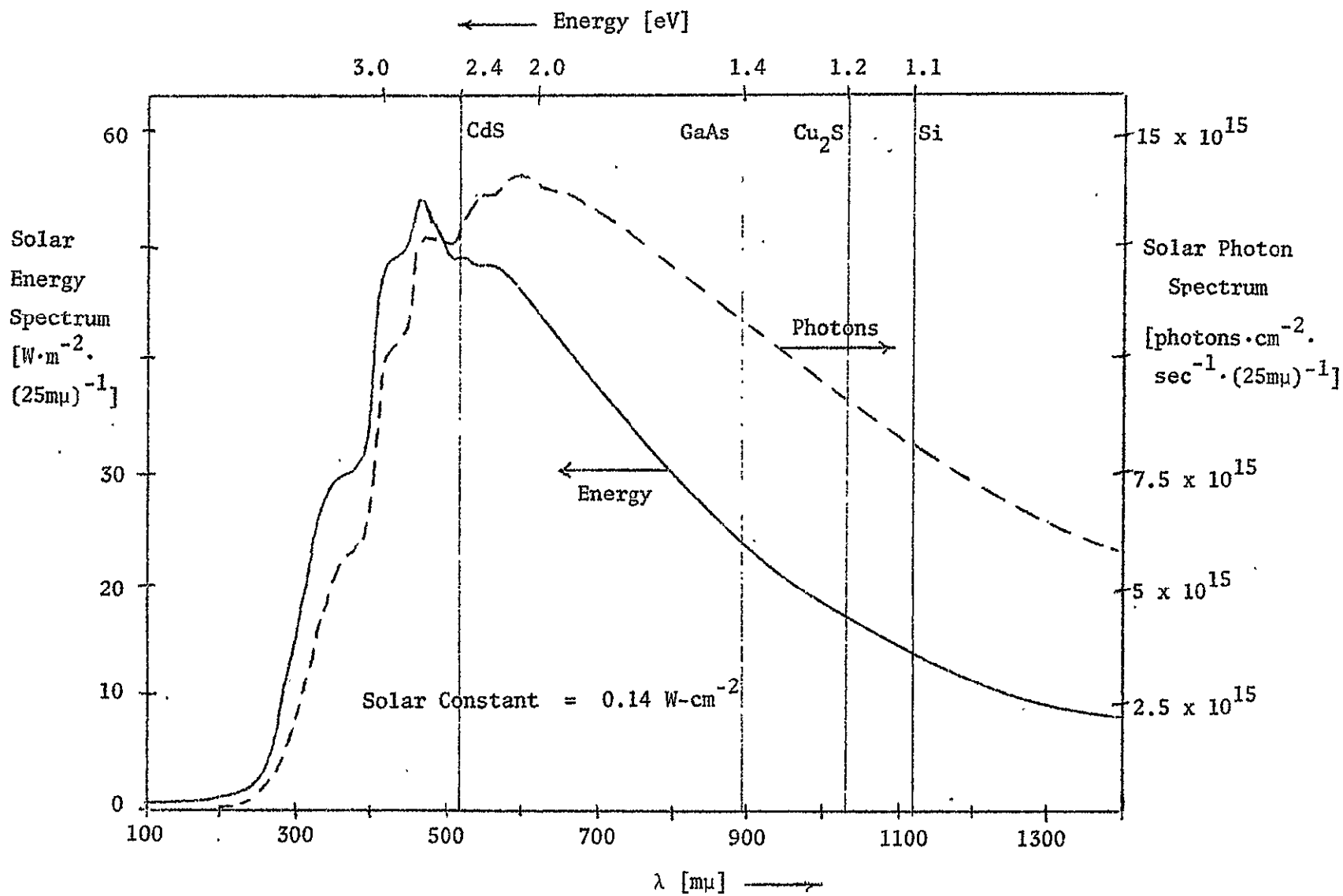
mobilities of GaAs, and the ease with which GaAs can be made n- or p-type. Disadvantages are the low minority-carrier mobility of ZnSe and the large band gap of GaAs.

(c.) $Cd_xHg_{1-x}S$: This is an intriguing system. For $.57 \lesssim x \lesssim 1$ the lattice constant and crystal structure are constant at those of CdS (wurtzite). For $0 \lesssim x \lesssim .40$ the lattice constant and crystal structure are constant at those of HgS (zincblende). For $.40 \lesssim x \lesssim .57$ the structure is that of a mixture of the two crystals. The band gap at $x = .57$ is ~ 1.3 eV. The fact that the lattice constant remains the same up to 43% HgS means the degradation of mobility due to alloying should be much less than in alloys where the lattice constant varies. That is the main advantage of this substance. Disadvantages are that HgS is difficult to make and both CdS and (so far) HgS can only be made n-type. Since each of these pairs of materials has some disadvantage, it is not clear that solar cells which are better than the Cu_xS:CdS cell could be made from them. However, although we have only suggested the above-mentioned systems as possibilities for components of a solar cell, there are probably equally promising materials that will come to light as further data are received. Also, it may be unreasonable to limit $E_G^>$ to $\gtrsim 2.4$ eV. A limit of, say, 2.2 eV would allow ZnTe, AlAs, and GaP as the wide-band-gap component. Our strongest suggestion is that due to the practical importance of developing an economical solar energy converter, a systematic investigation of graded heterojunction cells made from as many promising materials as possible should be carried out.

B. Growth and Investigation of Cu_xS-CdS Heterojunctions

1. Growth of CdS Single-crystal Platelets:

The growth of CdS single-crystal platelets during the period of this contract was directed to suit the various interests of the group.

The growth technique used is a vapor transport process at atmospheric pressure, in which a carrier gas stream transports evaporated CdS powder from a hot region in the growth furnace to a cooler region where crystallization takes place.

The growth conditions are determined by the composition of the carrier gas stream (N_2, 0 - 5 Vol. % H_2S) and the temperature gradient in the crystallization zone. A large part of the work was devoted to the growth of not-intentionally-doped CdS crystal platelets which could be used by the members of the group in their research. All crystals used by this group were obtained this way. The growth conditions required to obtain these CdS platelets are by now quite well established[56] and the growth runs made to obtain these crystals could therefore be classified as "production runs".

The remaining time was devoted to "research runs", which were geared to the following areas of interest:

a. Growth of doped crystals.

There are two interesting questions to be investigated regarding the possible effects of dopants added during the growth of the crystal:

i. Is the type of incorporation of the dopant the same as with "a posteriori" doping of an already-grown crystal?

ii. What is the effect of the dopant on the class* of the crystal?

---

* I.e., Class I or II according to the Gross-Novikov classification[57]. See Secs. IIC1 and IIC2 for a discussion of these classes.

The effect of the dopant on the crystal-growth properties was investigated by growing crystals of CdS doped with Cu. This was done by inserting a boat containing Cu in the carrier gas stream. The growth conditions of a crystal in an atmosphere consisting of N_2, H_2S, CdS and Cu have been estimated according to the same method which was used for the growth of pure crystals, i.e., by assuming that the crystals grow under near-equilibrium conditions.

About 40 pairs of growth runs were made in this program. A pair consisted of a "pure" run and a "doped" run made under identical growth conditions, so that comparison of the results was possible. Two growth conditions, H_2S concentration and temperature gradient, were changed over ranges of values which guaranteed a reasonable amount (10 or more) of usable platelets per run. These ranges were: H_2S concentration: 0 - 5 % Vol. (in N_2) and temperature gradient: 5 - 30 ° C/cm.

The results indicated that, in the case of doped crystals, the temperature at which the crystal grows becomes an important variable. Less platelets are found at the low-temperature side of the growth region in doped runs than in undoped runs. It is assumed that this effect is connected with the obstruction of the movement of dislocations by the dopant atoms. At higher temperatures this effect will become less pronounced because of the greater number and mobility of the dislocations. More explicit data shall be obtained in order that we can determine the quantitative influence of this effect on the yield per run.

b. Several crystal-growth runs were made and the crystals obtained were subsequently doped in a separate treatment to investigate the effects of the concentrations of dopants acting as acceptors (Ag) and donors (Al) in the formation of high field domains. (HFD; see the next Section for an explanation of HFD and results of the doping experiment.)

c. A series of about 20 growth runs of undoped crystals was made to investigate a possible relationship between the concentration of hydrogen sulfide in the carrier gas stream and the class of the crystals obtained, and how this relationship may be influenced by the temperature at which the hydrogen sulfide is shut off during the cooling down of the furnace. Measurements are being made to enable us to classify these crystals as Class I or II.

It is our intent to find a theoretical relationship determining the position of the line separating the class I and class II areas in a plot of the H_2S concentration vs. the H_2S-shut off temperature. This relationship should be based on the fundamental equilibria between the crystal and the surrounding atmosphere and on the model explaining the formation of Class I and Class II crystals. (See Sec. IIC2 below.)

2. Investigations of Doping and HFD in CdS Single Crystals:

For detailed investigations of the electrical characteristics of hetero-junctions experimental knowledge of the carrier concentrations and electric field in the junction would be highly useful. In suitably-doped CdS with a blocking contact, information on the concentration at the metal-semiconductor boundary and the electric field in the bulk, for zero space-charge conditions, can be obtained[22,58]. The electric field distribution near the junction in the CdS region of a $Cu_xS:CdS$ heterojunction is similar to that near a blocking contact. Therefore, in the case of a heterojunction, we expect to be able to obtain information similar to that obtained with a blocking contact. This information is derived through a study of stationary HFD, which are observed under suitable doping conditions in crystals having a range of negative differential conductivity (NDC) at high electric fields. The HFD refer to the following: If one measures the

electric field distribution in a suitably-doped CdS single crystal, he finds that under certain conditions this distribution consists of two regions of essentially constant field (the higher-field region being the HFD) with a very narrow transition region separating them[58]. The HFD can be made visible by utilizing the Franz-Keldysh effect[59,60]. The quality of the HFD is very sensitive to doping, and to improve reproducibility we carried out a study of the doping procedure. Modifications in the temperature profile of the doping furnace used led to very satisfactory results, which will be detailed below.

Before we discuss the doping, per se, we will describe a crystal property which is useful in discussions of HFD, namely, $n_1(F)$, the curve of electron concentration vs. electric field for zero space-charge density[22]. In the CdS crystals used this curve is essentially constant up to a "critical" field value. Above this value, n_1 decreases rapidly due to field quenching of the conduction electrons[61]. (See ref. 22 for the method of calculating $n_1(F)$.) The critical field at which field quenching sets in and the slope of $d(\ln n_1)/d(\ln F)$ in the field-quenching region are useful parameters to use in comparing results in different crystals. The steeper the slope is, the faster and more localized in field the field quenching is, and the better the quality of the domains is. This is made evident by experimental observation and can be discussed theoretically with the aid of the field-of-directions analysis[22].

A theoretical discussion of n_1 curves is possible using a three-level model that invokes a field-quenching mechanism[61]. Using reaction-kinetic analysis, theoretical expressions for n_1 as a function of light intensity, infrared (IR) quenching, temperature, and various model parameters controlled by doping can be obtained.

The experimental arrangement for the measurement of $n_1(F)$ curves is shown in Figure II B-1. A Leiss prism monochromator with tungsten light source
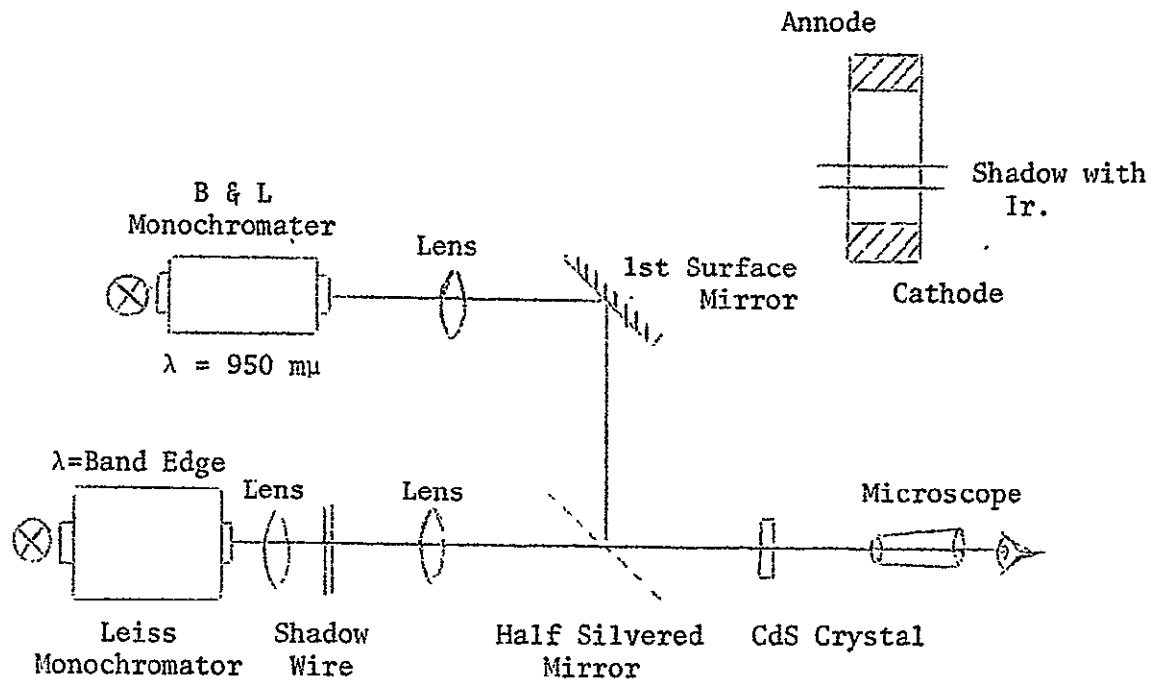
FIGURE IIB-1: Experimental Arrangement

illuminates the crystal with band-edge light. A wire creates a shadow region on the crystal to act as a pseudo-cathode. Additional IR illumination (950 mμ) is provided by a Bausch and Lomb grating monochromator and tungsten source. This IR illumination is focused into the shadow region to vary the boundary conditions of the HFD. (See insert) Crystal temperature is maintained by a cold finger and measured by a Copper-Constantin thermocouple. For certain measurements, the IR light was replaced by band-edge light.

Crystal current was monitored on a Keithly picoammeter; crystal voltage by a Simpson VOM. Both signals were recorded on an X-Y recorder for current-voltage (IV) plots. Domain lengths were measured using a graticule and microscope arrangement.

Now we will discuss the doping procedure and our results. CdS crystals were doped with differing amounts of Ag and compensated with Al to produce the NDC necessary for the production of HFD. The doping procedure consists of embedding suitable crystals in CdS powder doped with nitrates of Ag and Al followed by heating to 900° C in an H_2S-N_2 atmosphere for three hours. The nitrates dissociate below 500° C and the Ag and Al are carried into the crystal by diffusion.

The crystals for doping were selected on the basis of high optical quality. Extreme care was taken in the process to prevent the CdS crystals from sintering in contact with the CdS powder at the doping temperatures and thus reducing the optical quality.

Doped crystals had "ohmic" Ti/Al electrodes[62] evaporated on them and were tested at 210° K for HFD. The crystals showing good domains were investigated to determine the n_1 curve. Some crystals were used in a study of doping conditions by thermally-stimulated current (TSC) analysis to determine a relation between doping and electron trap distribution.

The results of doping runs were very consistent. There appears to be a correlation between doping concentrations and the quality of the stationary domain, in qualitative agreement with theory[61].

In the cases where no Al compensation was used, no domains were observed. In the case of 100 ppm Ag compensated 1:1 with Al, domains were observed in every case but one. $N_1(F)$ data indicated that the field quenching was not very efficient (i.e. the slope was too shallow; see Figure II B-2). Domains were found in each crystal doped with 50 ppm Ag and compensated 1:1 with Ag. The domains had higher field strengths, and field quenching was more rapid and set in at higher field strengths than in those crystals doped with 100 ppm Ag 1:1 Al. Further experiments are to be carried out to determine the optimum doping concentration. To determine the effects of different doping on the trap distribution, large single crystals were broken into several pieces and doped differently. The trap distribution for different pieces was then determined from TSC data. Crystals run through the doping procedure without dopants showed a greatly reduced number of traps (compared to the virgin crystals) between 0.2 and 0.7 eV from the conduction band. Crystals doped with Ag compensated 1:1 with Al showed traps at about 0.4 and 0.6 eV from the conduction band. The number of these traps increased with increasing doping concentration. In crystals doped only with Ag, the number of 0.4 eV traps was reduced. (See Fig. II B-3)

The present interpretation of these results is as follows. The doping procedure, in the absence of dopants, apparently anneals electron traps present in the virgin crystals, as evidenced by the greatly reduced TSC curves and the fact that getting a good crystal seems independent of the crystal properties (except optical quality) before doping.

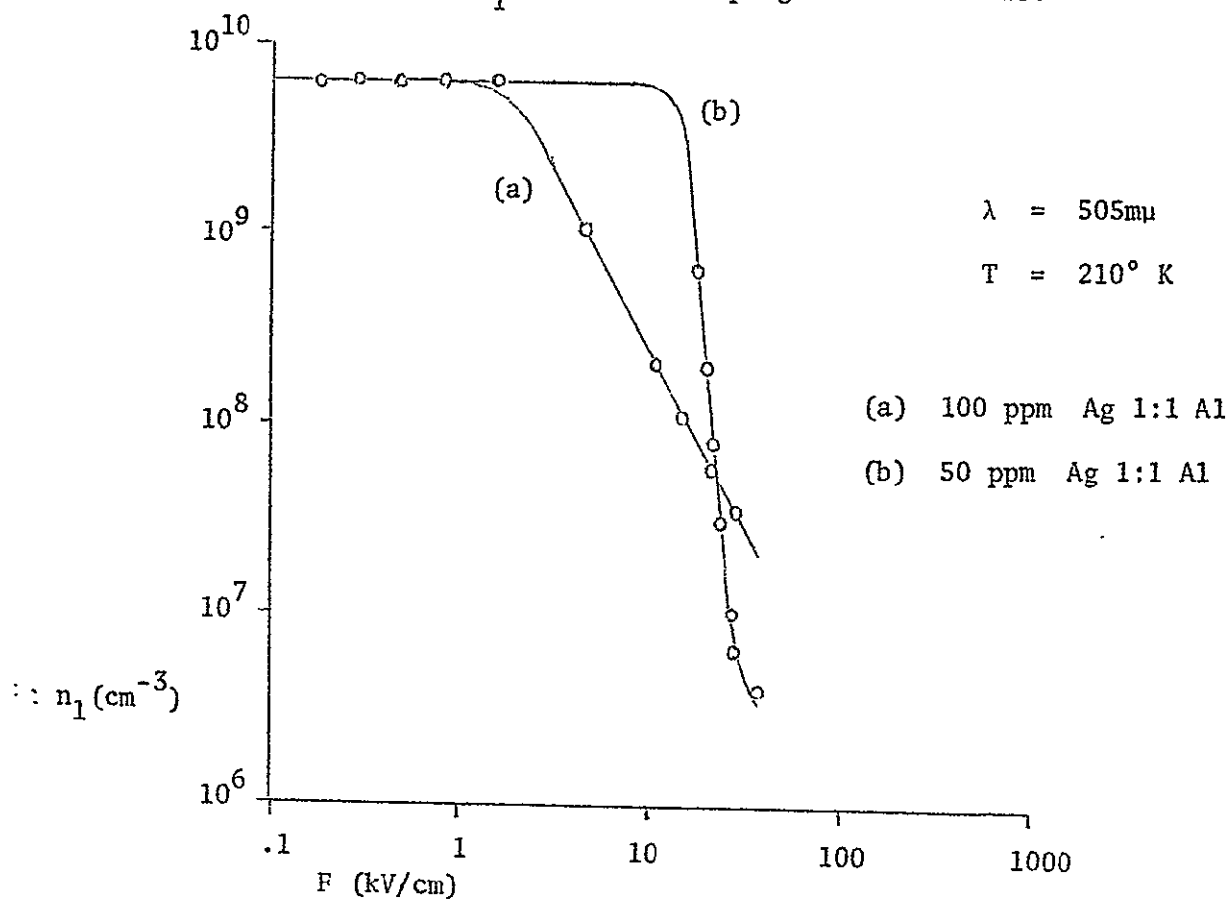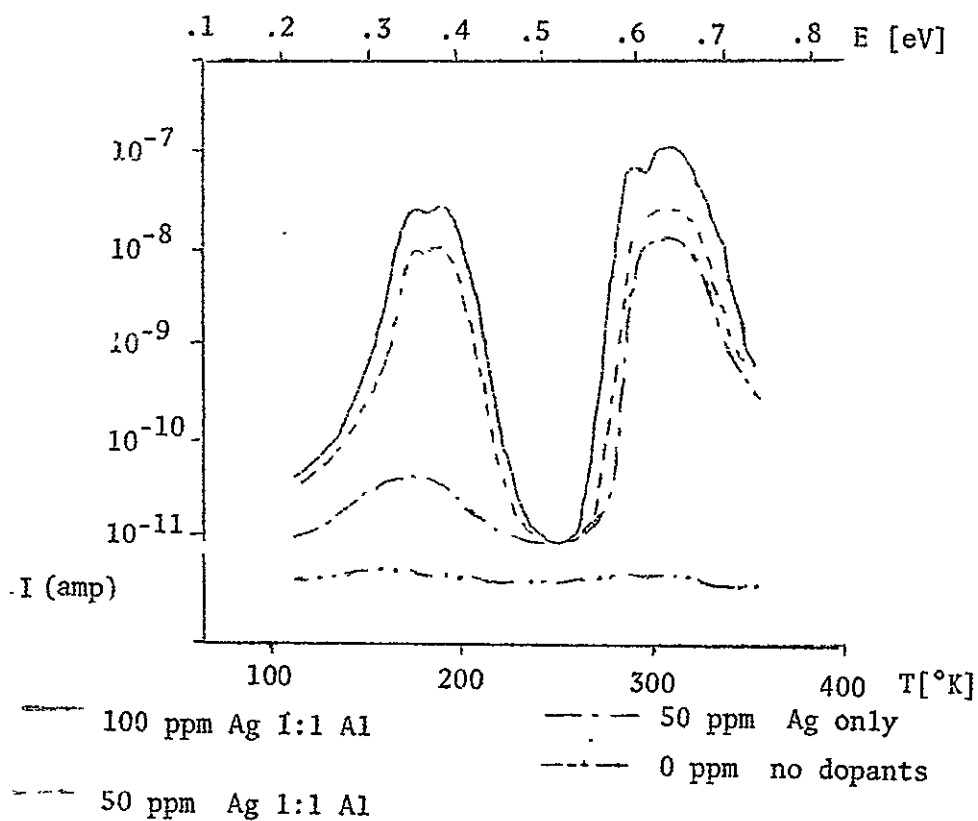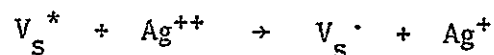Presumably, the Ag will enter as an acceptor level on Cd^{++} sites in

FIGURE IIB-2: $n_1(F)$ for two doping concentrations.

λ = 505mμ

T = 210° K

(a) 100 ppm Ag 1:1 Al

(b) 50 ppm Ag 1:1 Al

FIGURE IIB-3: TSC curves for doped crystals

——— 100 ppm Ag 1:1 Al   —·— 50 ppm Ag only

—·— 0 ppm no dopants

—·— 50 ppm Ag 1:1 Al

CdS because of the similarity of the electronic structures. Ag in this state would be doubly ionized (i.e. Ag^{++}) to satisfy lattice neutrality. In the presence of a compensating donor level, the Ag acceptor could become an ionized acceptor (Ag^+) having an effective negative charge with respect to the lattice. This would act as a Coulombic-attractive hole trap because the Ag would want to capture a hole and again be neutral with respect to the lattice.

There are several mechanisms by which the Ag acceptor levels could be ionized to produce hole traps. If Ag were the only dopant, the crystal might self-compensate itself by creating neutral S vacancies (V_s^*) that would act as donor levels. These vacancies would become singly ionized ($V_s^{\cdot}$) or doubly ionized ($V_s^{\cdot\cdot}$) by giving up their electrons to the acceptor levels:

$$V_s^* \;+\; Ag^{++} \;\rightarrow\; V_s^{\cdot} \;+\; Ag^+$$

or

$$V_s^* \;+\; 2\,Ag^{++} \;\rightarrow\; V_s^{\cdot\cdot} \;+\; 2\,Ag^+$$
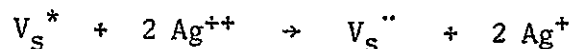
Addition of donors in the doping would result in ionizing more Ag acceptor levels, creating more hole traps and electron traps. Presumably Al will enter CdS as a donor level. If this is the case, these donors will ionize the acceptors by the reaction

$$Al^{++} \;+\; Ag^{++} \;\rightarrow\; Al^{+++} \;+\; Ag^+$$
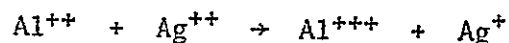
CdS appears to have intrinsic, deep-lying levels that act to keep the Fermi level above the middle of the forbidden band. These, in addition to the Ag acceptor levels and Al donor levels, would act to give the three-level model that would have Coulombic-attractive hole traps to permit field quenching[29].

This is only a qualitative idea of what happens in the doping procedure. Further experiments shall be performed to determine a more quantitative description
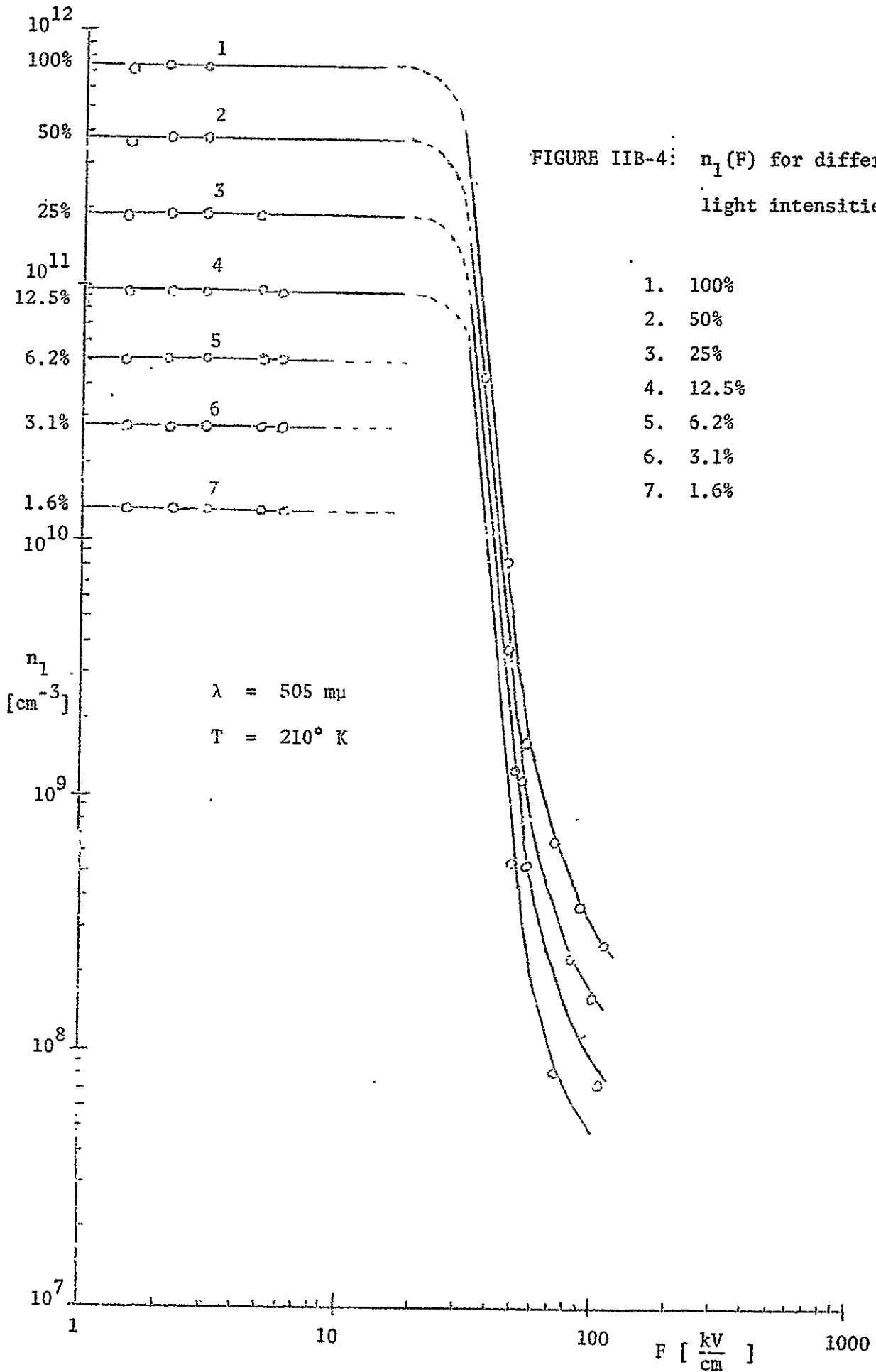
of the doping.

Observation of the HFD indicated that the doping was sufficiently homo-geneous so as to produce domains of good quality. Also, the $n_1(F)$ curves were highly reproducible at each doping concentration. Thus, the doping procedure appeared to be sufficiently reliable so as to permit investigation of various properties of the field-quenching mechanism as revealed by the $n_1(F)$ curves.

The three-level model predicts a dependence of $n_1(F)$ on light intensity. For low field values (i.e. neglecting field quenching) the theoretical dependence is linear. At higher field strengths, where field quenching is apparent, the dependence is linear in the first approximation.

The $n_1(F)$ curves for particularly good crystals were investigated to determine the dependence of $n_1(F)$ on light intensity ($h\nu \sim$ band gap).

The results are very consistent with theory at low field strengths, where a linear dependence of n_1 on light intensity is revealed. At higher field strengths the dependence is still approximately linear (within the limits of error of the n_1 measurements in this region) over a range of 2 orders of magnitude in light intensity (see Figure II B-4). Thus over the range of light intensities used, the dependence of $n_1(F)$ on light intensity can be approximated as linear to a reasonable degree of accuracy.

Measurements of the $n_1(F)$ in a homogeneously-illuminated crystal depend on the values of the electron concentration at the cathode. A pseudo-cathode formed by a shadow was used as a means of varying the electron concentration at the cathode. From IV characteristics it is possible to measure $n_1(F)$ in this shadowed region[22]. Measurements of $n_1(F)$ in this shadow vs light intensity (relative to the intensity in the fully-illuminated region) show the same linear dependence that the homogeneously illuminated crystal does. Comparison reveals

FIGURE IIB-4: $n_1(F)$ for different light intensities.

1. 100%
2. 50%
3. 25%
4. 12.5%
5. 6.2%
6. 3.1%
7. 1.6%

$\lambda = 505$ mμ

$T = 210°$ K

the "darkest" shadow intensity is about 3% of the intensity in the fully-illuminated region.

IR illumination of the crystal will produce a quenching of $n_1(F)$ from its value without IR. This method is used to "darken" the pseudo-cathode (i.e. reduce n_1 in this region) to produce domains with high field strengths. The theory predicts that the effect of IR illumination should be to cause a gradual quenching of $n_1(F)$ in the region before field quenching normally sets in. The net result would be the reduction of the "critical" field where field quenching becomes apparent[61].

Measurement of $n_1(F)$ at low fields in the shadow region (from IV curves) reveals this IR quenching. These measurements are in good agreement with previous results[29].

Measurement of $n_1(F)$ for homogeneous IR illumination was also carried out. It reveals the previously-observed low-field behavior and a high-field behavior agreeing with theory. (See Figure II B-5.) At high fields $n_1(F)$ with IR illumination approaches the case without IR illumination, as expected. We have just begun quantitative measurements of IR quenching of the knee (where the slope $d(\ln n_1)/d(\ln F) = -1$) of the n_1 curve vs. IR intensity. Preliminary results reveal an exponential dependence of the saturation current ($\propto n_1 F$) on IR intensity.

Measurements on the temperature dependence of $n_1(F)$ give a changing slope in agreement with theory (see Figure II B-6). A theoretical expression for the slope in the quenching region as a function of temperature permits evaluation of the reduction of the hole trap-barriers with field. The observed value is about 0.2 eV, in good agreement with theory[29].
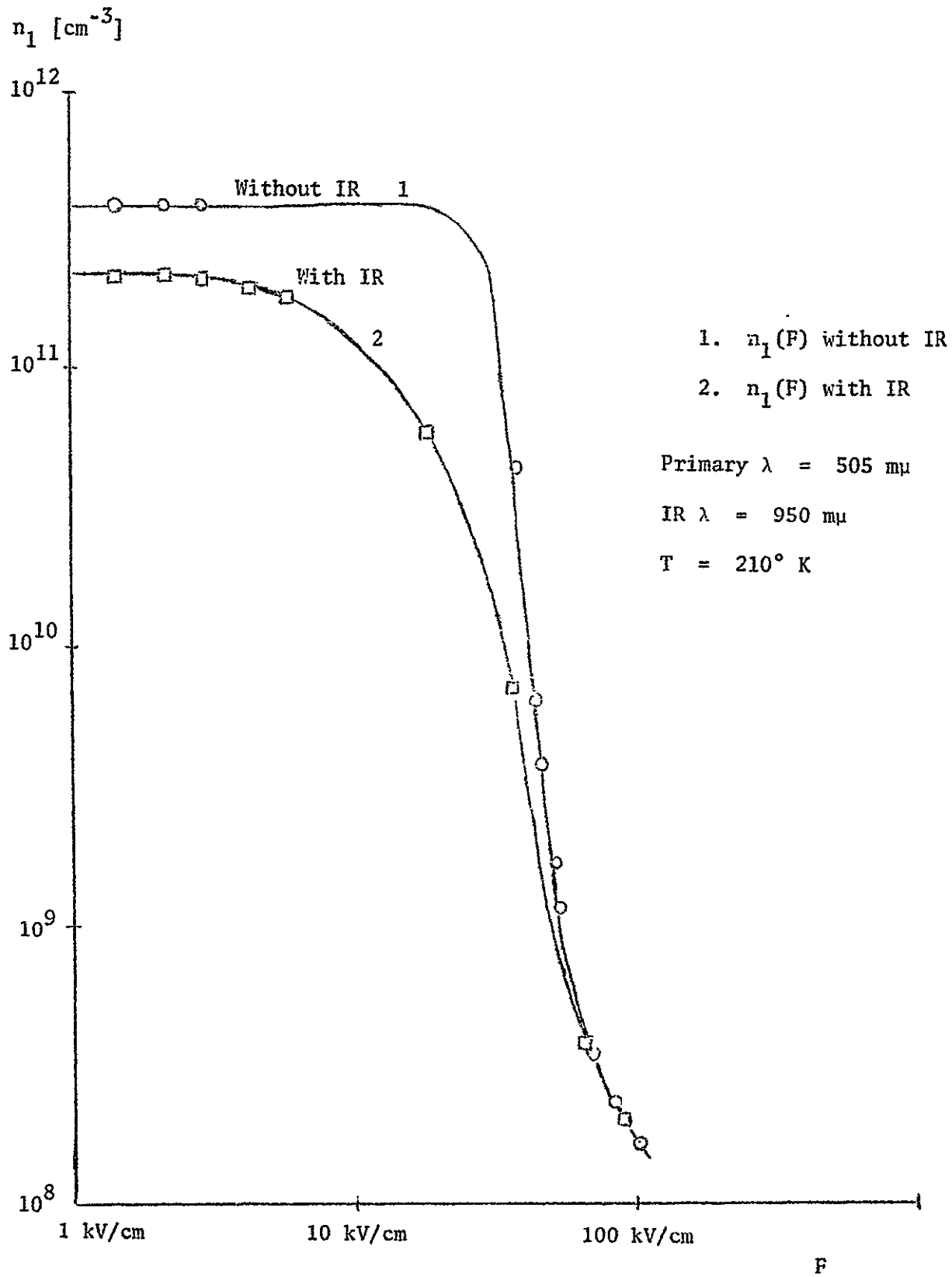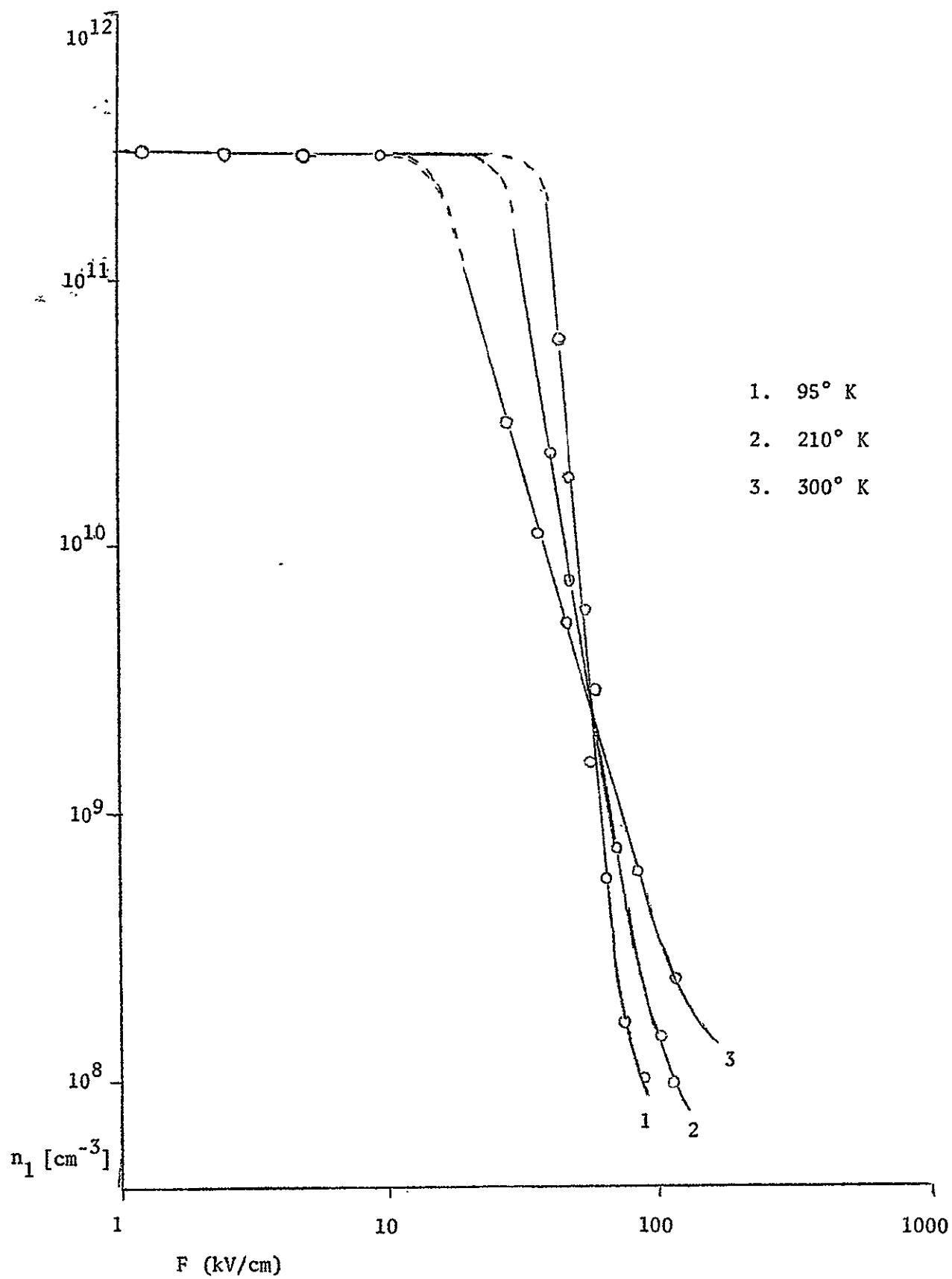
FIGURE IIB-5: $n_1(F)$ with and without IR illumination.

FIGURE IIB-6: $n_1(F)$ for three temperatures.

3. Investigation of Cu$_x$S:CdS Solar Cells Produced from CdS Single-crystals

  by the Chemical Dip Method:

Cu$_x$S:CdS heterojunctions have been made by a chemiplating process on

specially-doped (to produce stationary HFD - See Sec. IIB2) CdS single crystals

(Grown as described in Sec. IIB1). The IV characteristics of these junctions

under monochromatic illumination have been studied. In addition, stationary

HFD extending from the Cu$_x$S:CdS junction have been found and measured.

The chemiplating procedure by which the Cu$_x$S was formed on the CdS

crystals was performed as follows: An aquéous solution of CuCl was prepared by

first dissolving CuCl$_2$ in concentrated HCl with excess Cu. This was boiled until

the liquid turned clear. Then cold H$_2$O was added to precipitate out the CuCl.

The CuCl was rinsed three or four times with cold water before using. Variations

in this procedure are under study in view of the model discussed in Sec. IIA2.

Prior to the chemiplating dip, the CdS crystal (Dimensions are discussed

below.) was placed on a glass slide and encapsulated in an epoxy (Sylgard 51

Dielectric Gel made by the Dow Corning Co.) which was cured at 75° C for 3/4 to

two hours. Then the surface of the crystal on which the Cu$_x$S was to be chemi-

plated was exposed by cutting away the epoxy with a razor blade. Following this

the glass slide and the CdS crystal were dipped in a 25% solution of HCl for

about a minute to etch slightly the exposed surface of the CdS.

After this the chemiplating dip was performed. This consisted of placing

the slide with the crystal in a saturated aqueous solution of CuCl kept at 90° C

for 1/4 to 1-1/2 hours. This formed a Cu$_x$S layer 10 to 50 microns thick on the

exposed surface of the CdS crystal.

The crystal was then removed from the epoxy. Either before or after

the Cu$_x$S layer was formed, an ohmic Ti/Al contact was evaporated onto the CdS.

Electrical contact was made to the Cu_xS and Ti/Al by cementing on Cu wires with silver print.

It should be noted that after the formation of the Cu_xS layer, no heat treatments were performed; and all further measurements were made with the crystals in an N_2 atmosphere.

With regards to size, two different types of crystals have been used. The first type was the small crystals cut from a single CdS platelet at the Jet Propulsion Laboratories (Dr. R. Stirn). These were made in order to compare various Cu_xS layers on CdS crystals with the same electrical and optical properties. The dimensions of these crystals were approximately 300 x 200 x 80 microns. With these crystals the Cu_xS layer and Ti/Al contact were put on faces perpendicular to the C-axis (see Fig. IIB-7).

Only high-voltage measurements were made with these crystals because the Ti/Al contact could not be made ohmic. With the Cu_xS layer as the cathode (corresponding to reverse bias) a stationary HFD appeared adjacent to the Cu_xS junction when the IV characteristic showed current saturation. The electric field in this domain was approximately 60 Kv/cm at T = 200° K. This implied a carrier concentration $n \simeq 10^7$ cm^{-3} in the domain[29].

Because of the difficulties in making a uniform junction and an ohmic Ti/Al contact on the small crystals, CdS platelets of about 1 x 2 x .1 mm were used. The Cu_xS junction and the Ti/Al contact were put on these platelets on the large face parallel to the C-axis (see Fig. IIB-8). After the Cu_xS layer was on these crystals, the edges perpendicular to the layer and parallel to the C-axis were cleaved off to remove any possible Cu_xS on these edges that might have diffused under the epoxy. In this way illumination could be incident on the Cu_xS layer first (frontwall cell) or the CdS first (backwall cell).
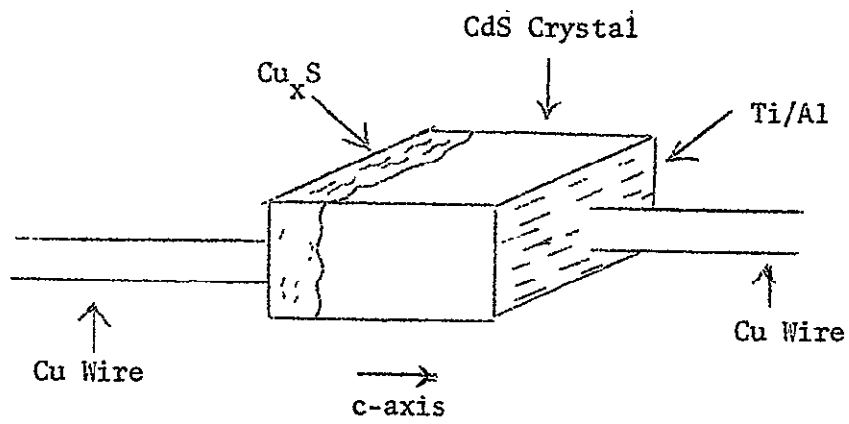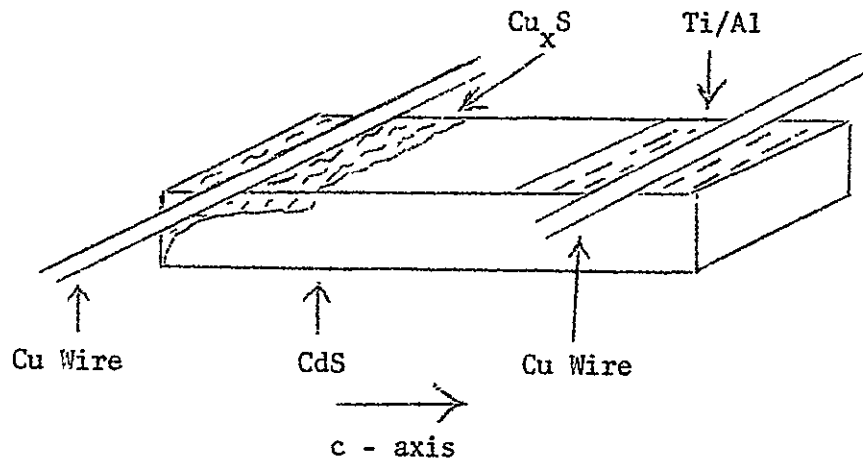
FIGURE IIB-7: Cu_xS:CdS junction on small CdS crystal.

FIGURE IIB-8: Cu_xS:CdS junction on CdS platelet.

Stationary HFD were observed with these crystals also. With these crystals, however, the current saturated before the field strength saturated in the domain. At higher voltages the electric field in the domain became a constant with a value of about 40 Kv/cm at 200° K. This implied a carrier concentration of about $n \simeq 10^9$ cm^{-3} in the domain.

IV characteristics of these devices were measured (Fig. IIB-9) under monochromatic illumination for the frontwall case (λ = .51μ at 300° K and λ = .50μ at 200° K corresponding to the band edge of CdS). The maximum open-circuit voltage observed was .54 volts at 300° K, under maximum illumination intensity (Approximately 10^{11} photons cm^{-2} sec^{-1}). In addition, the open-circuit voltage was proportional to the logarithm of the light intensity and the short-circuit current was directly proportional to the light intensity. The resistivity of our photoconductive CdS was in the range of 10^7 - 10^{10} Ω-cm. This high series resistance had the well-known effect[63] of seriously reducing the fill-factor. (We are using CdS with a high resistivity in order to enable us to use HFD as a tool for investigating the junction.)

Following this, the open-circuit voltage and short-circuit current were measured as a function of the wavelength of illumination for frontwall and back-wall cases (see Figs. IIB-10, 11, 12, 13, 14).

To reduce the effect of the variation of resistivity of the bulk of the CdS crystal with wavelength on the short-circuit current of the junction, a double monochromator system was used. The main monochromator illuminated the junction area of the crystal. Its wavelength was varied. The second mono-chromator illuminated the remaining area of the crystal and its wavelength was set at the wavelength of the photocurrent peak of the CdS crystal being measured. These measurements are shown in Figs. IIB-11, 12, 13, and 14.
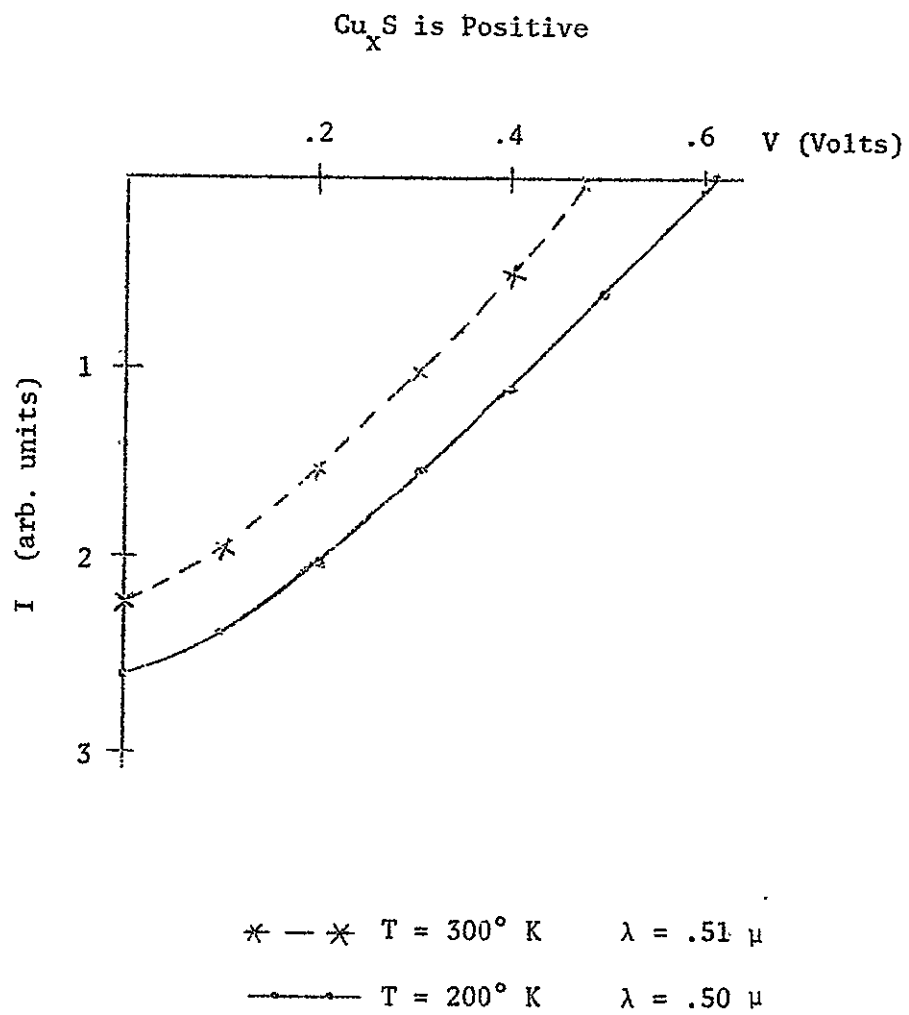
Cu_xS is Positive

FIGURE IIB-9: Current vs. voltage for frontwall illumination.
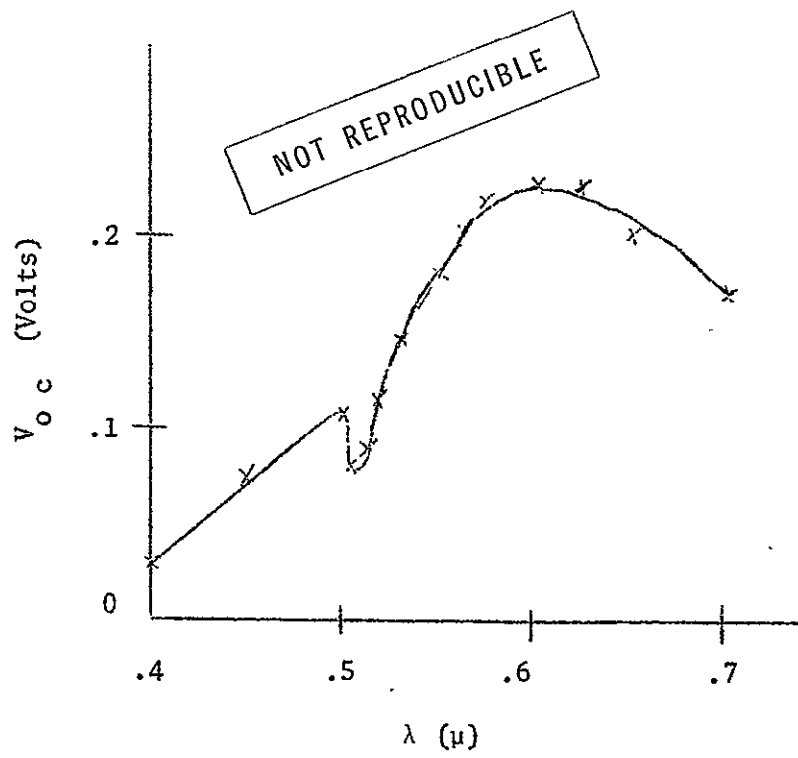
FIGURE IIB-10: Open circuit voltage vs. wavelength for frontwall illumination at T = 300° K.
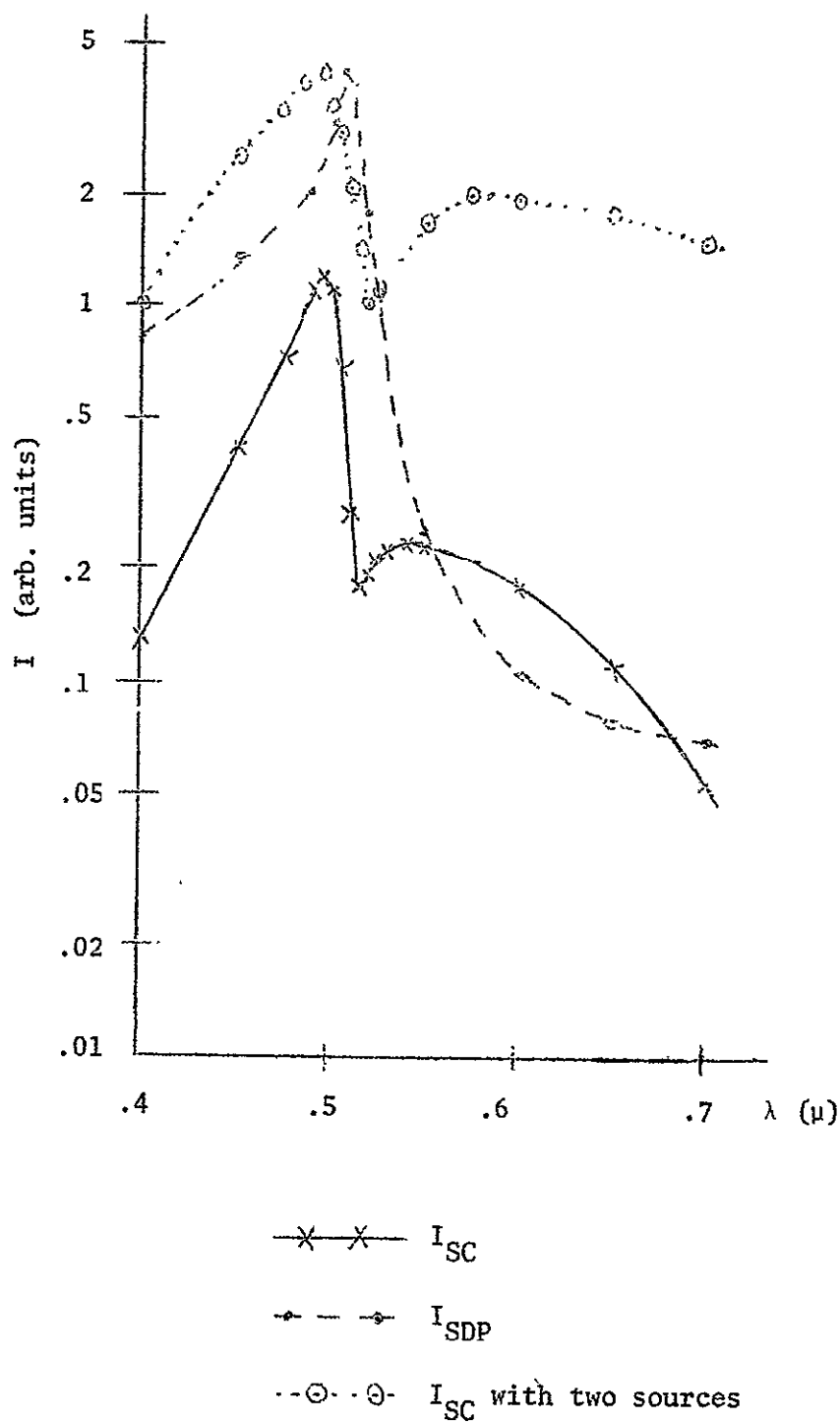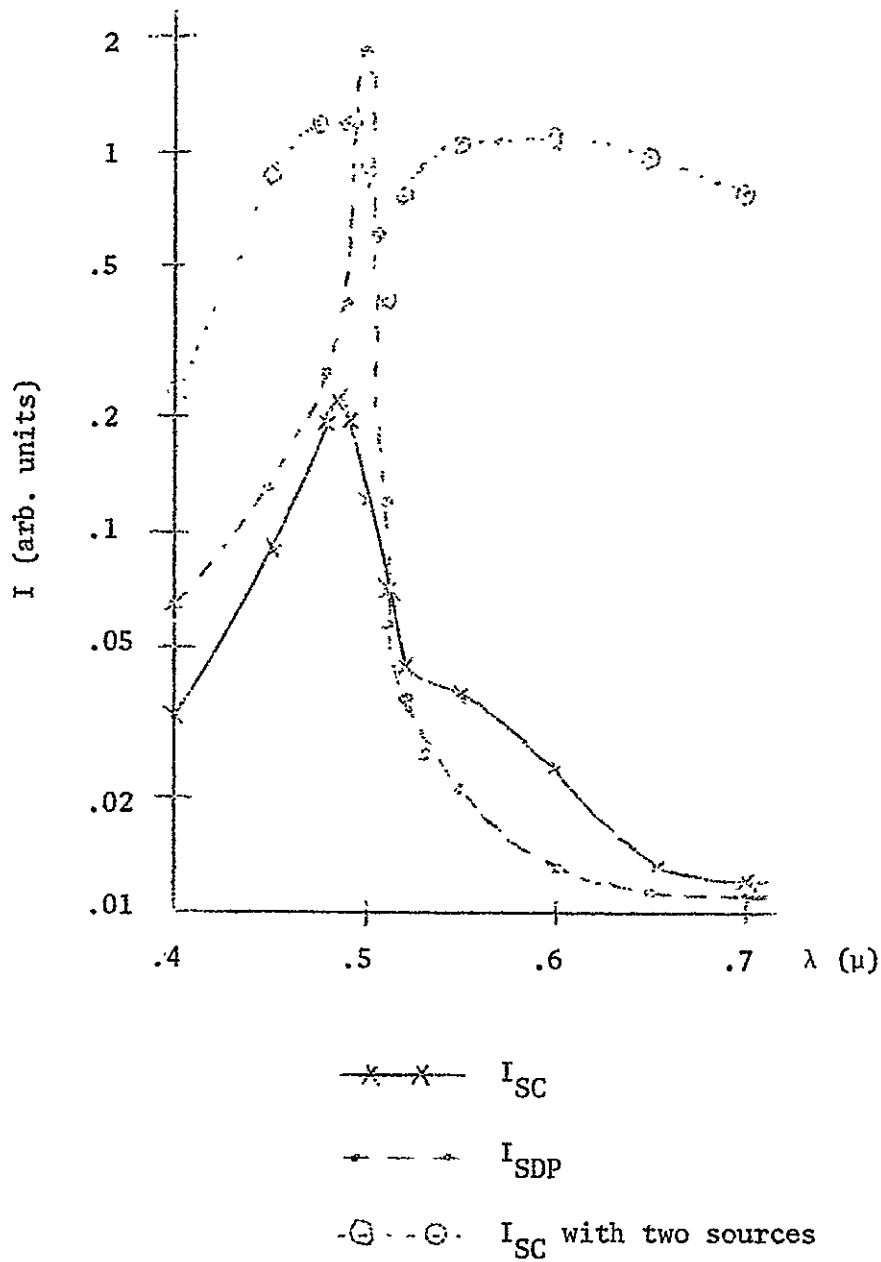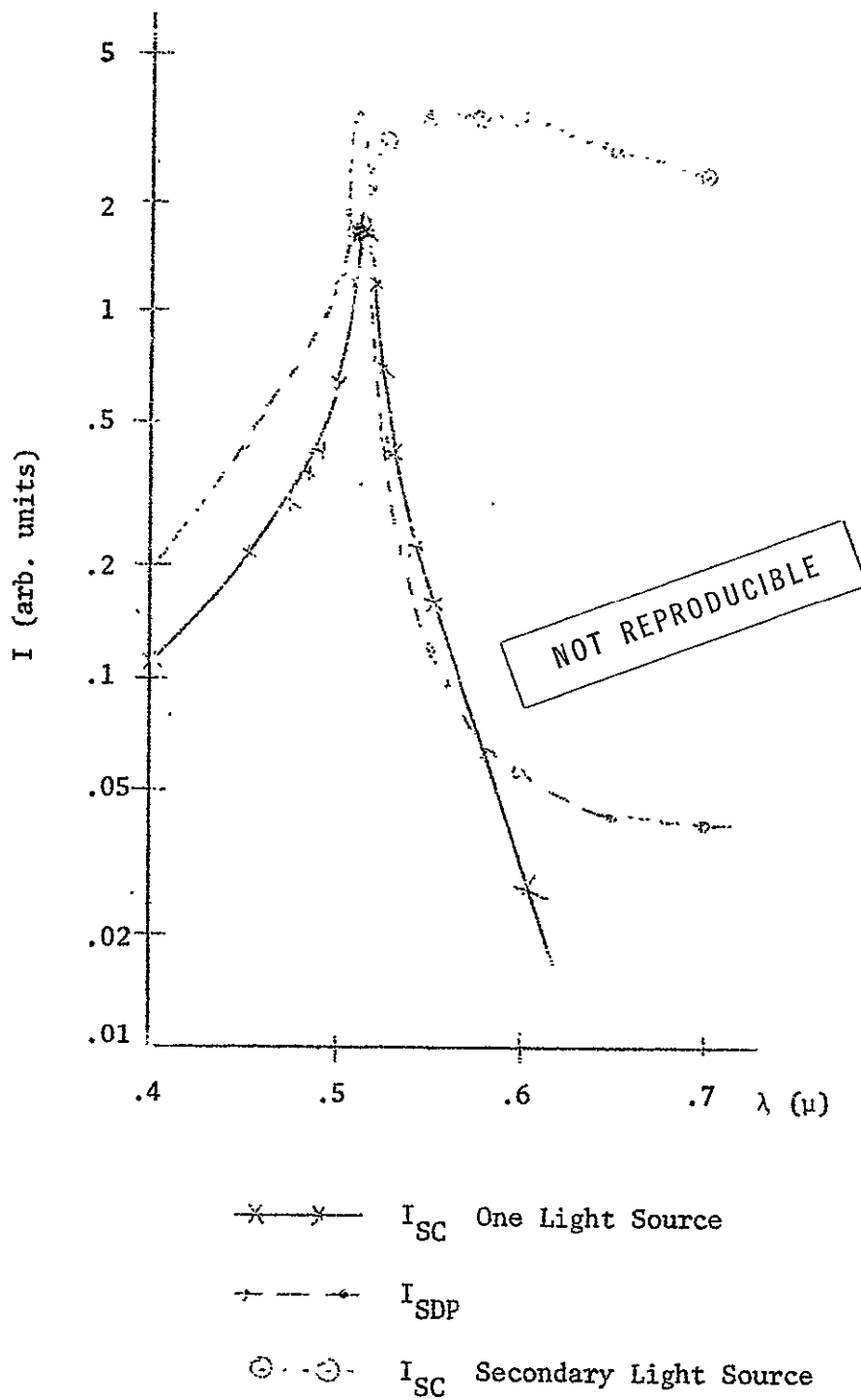
FIGURE IIB-11: Spectral distribution of photoconductivity (I_{SDP}) and short circuit current (I_{SC}) vs. wavelength for frontwall illumination at T = 300° K.

FIGURE IIB-12: Spectral distribution of photoconductivity (I_{SDP}) and short circuit current (I_{SC}) vs. wavelength for frontwall illumination at $T = 200°$ K.

FIGURE IIB-13: Spectral distribution of photoconductivity (I_{SDP}) and short circuit current (I_{SC}) vs. wavelength for backwall illumination at T = 300° K.
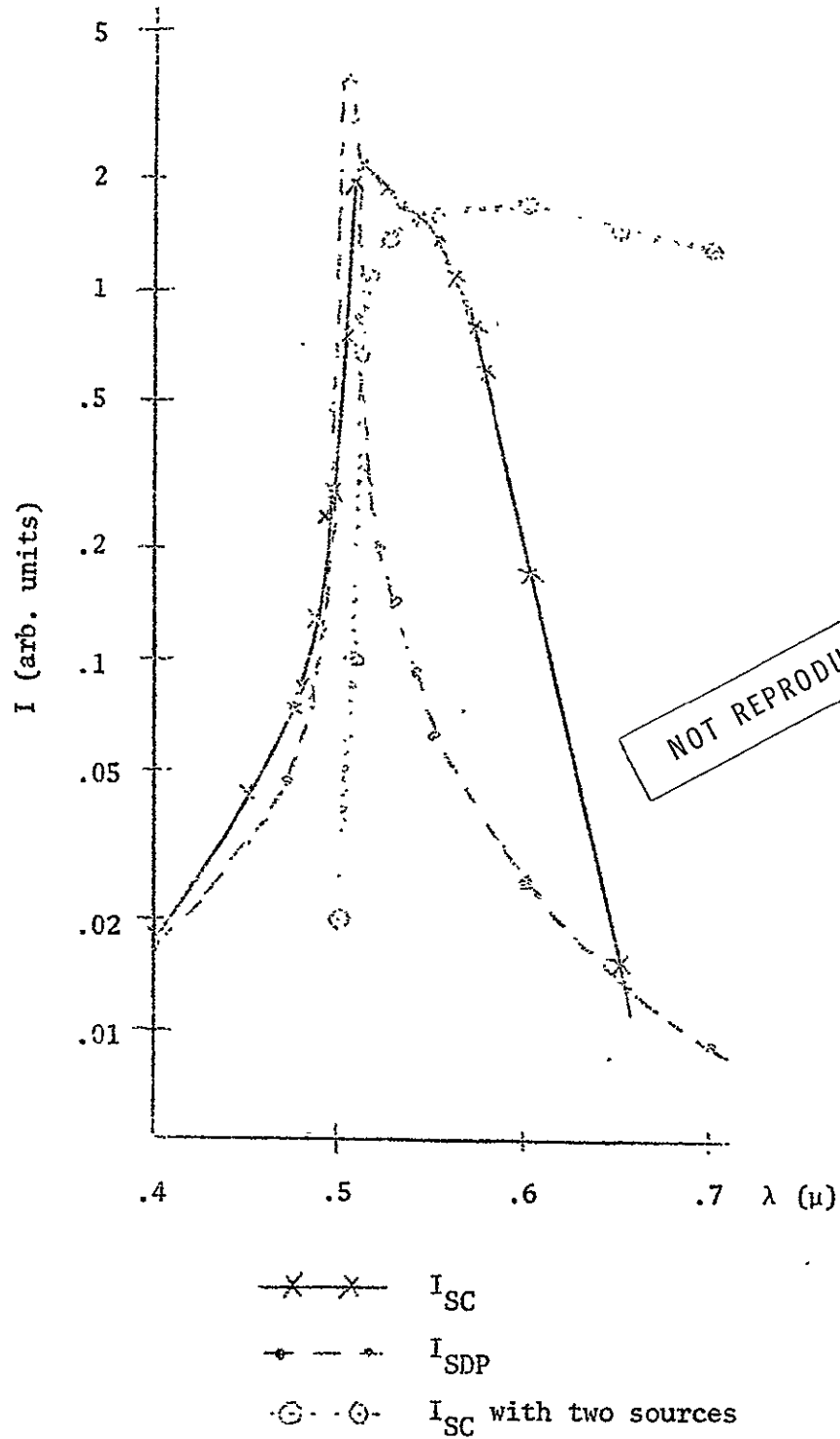
FIGURE IIB-14: Spectral distribution of photoconductivity (I_{SDP}) and short circuit current (I_{SC}) vs. wavelength for backwall illumination at T = 200° K.

In order to determine whether the spectral response of the junction was uniform, parts of it were masked off from the light, as discussed in Sec. IIA3 in relation to the dip in the spectral response of the cell at wavelengths corresponding approximately to the band-gap energy of CdS. Figures IIB-15, 16, and 17 show the different responses when different amounts of the Cu_xS-layer are shadowed.

In addition to the investigations that will be done on HFD under various types of illumination of the junction, the differing responses of different areas of the junction will be investigated to test the validity of the model proposed in Sec. IIA3 to explain the dip in the spectral response at short wavelengths. Furthermore, experiments to test the model of the junction mechanism, proposed in Sec. IIA2, will be carried out. We are in the process of initiating investigations on chemically-sprayed Cu_xS:CdS layers, in line with the planned research into improvements in the technology of practical solar cells.

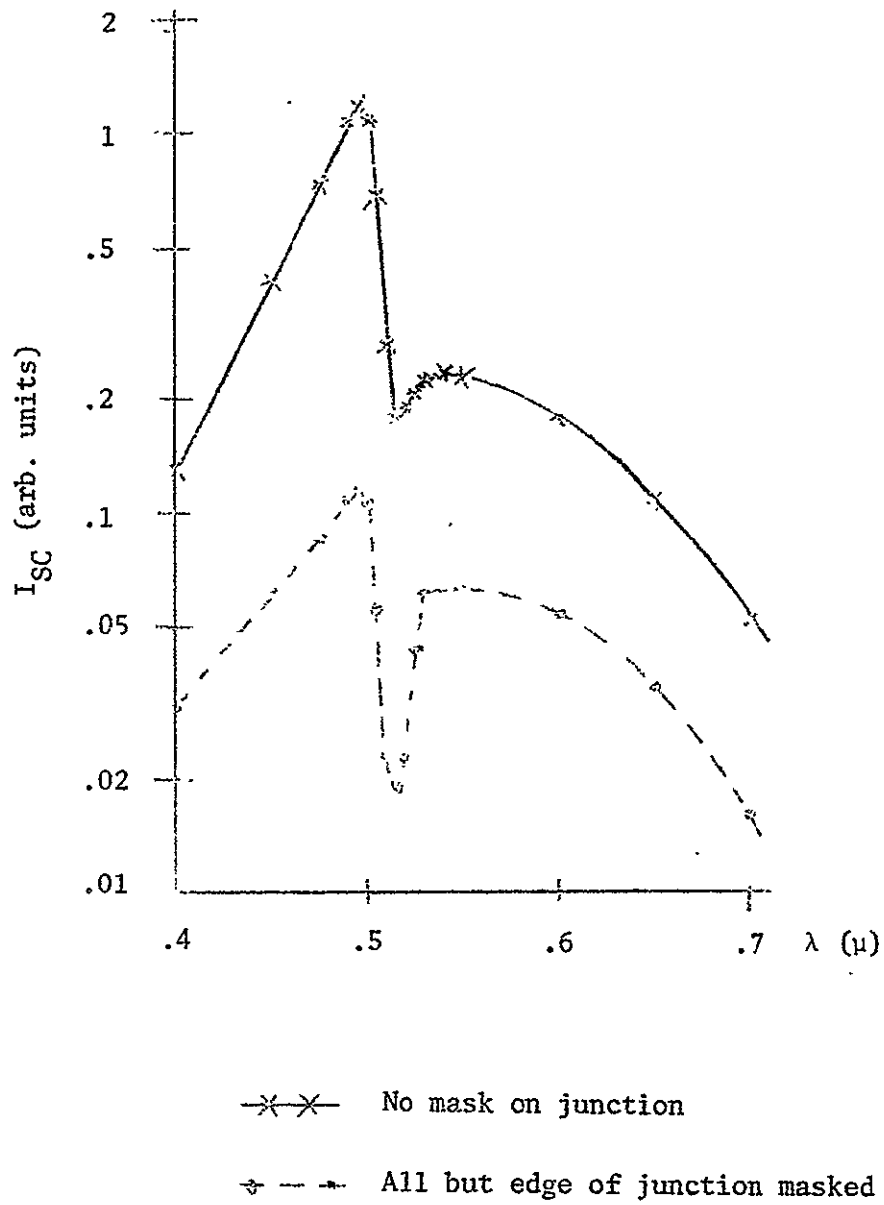FIGURE IIB-15: Short circuit current vs. wavelength for frontwall illumination at T = 300° K.
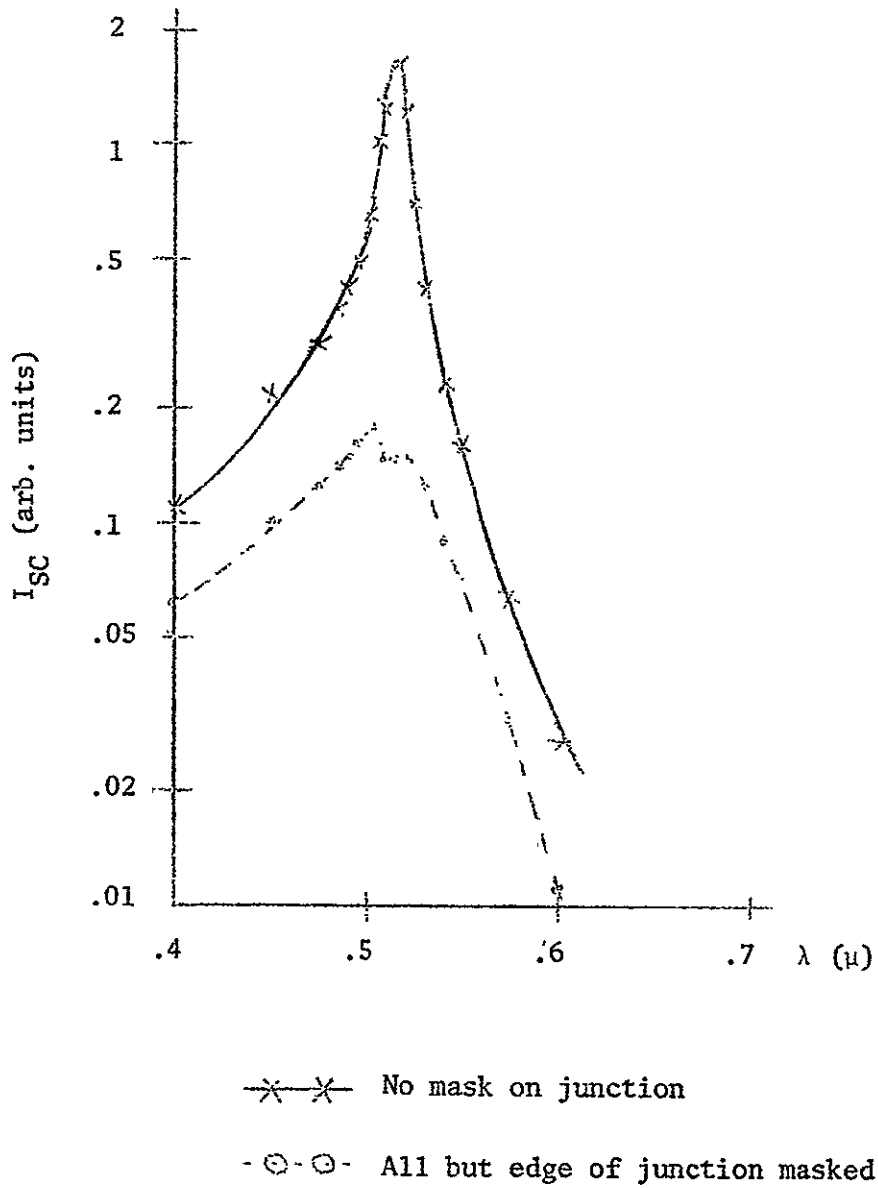
-X—X— No mask on junction

- ⊙-⊙- All but edge of junction masked

FIGURE IIB-16: Short circuit current vs. wavelength for backwall illumination at T = 300° K.
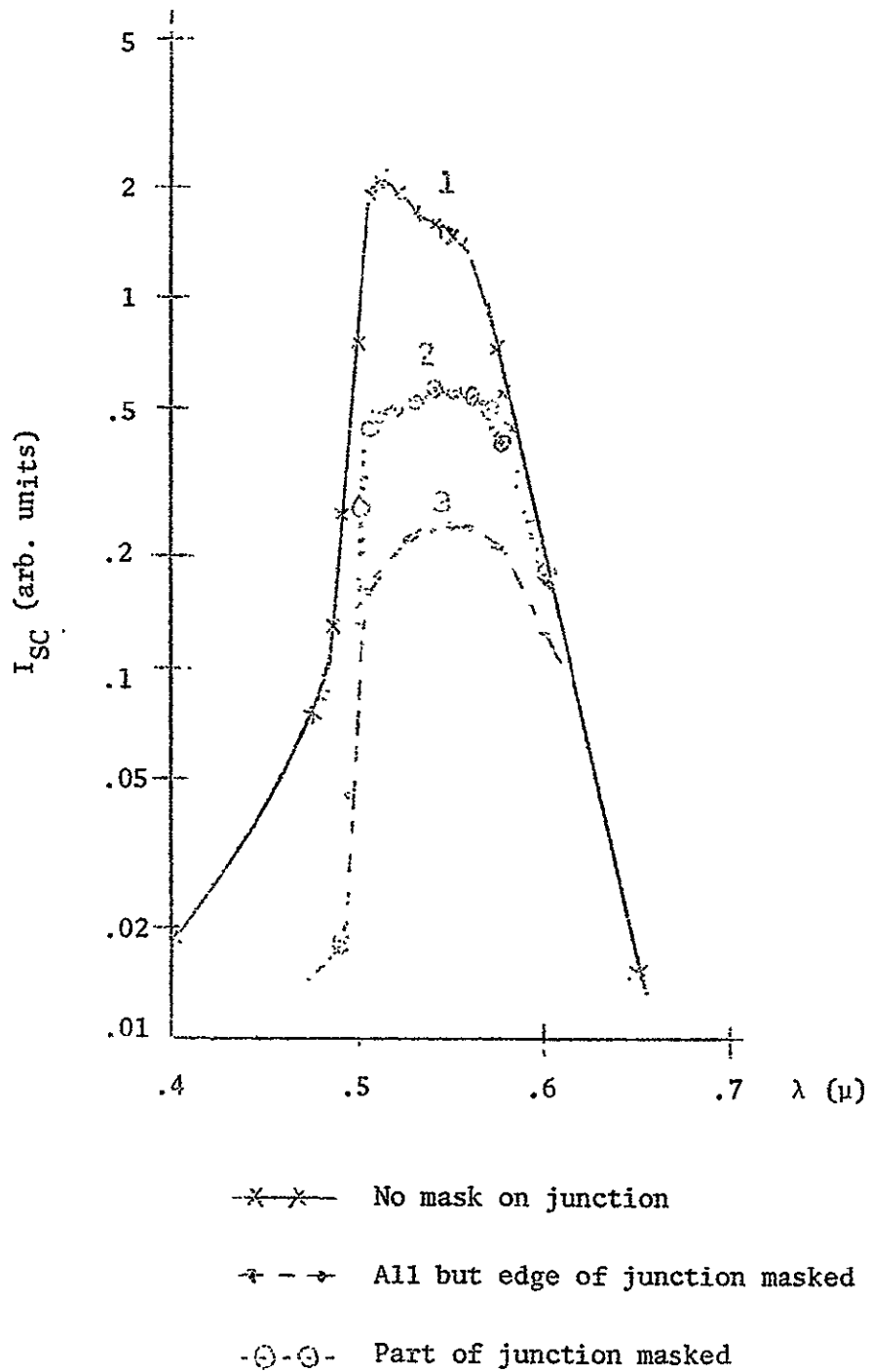
FIGURE IIB-17: Short circuit current vs. wavelength for backwall illumination
at T = 200° K.

C. Surface Properties

1. Electrical and Optical Properties with No Desorption from the Surface:

Mass spectroscopic measurements[64,65] have shown that heat treatments in vacuum cause drastic changes in the surface of CdS[64-69]. In particular, oxygen (AMU 16) and Cd desorption and Cd diffusion from the surface to the bulk can be expected[64,65].

It has also been observed that the electrical and optical properties of CdS are intimately connected with its surface structure[57,70-78,81]. A number of experimental results concerning the SDP[70-72, 74-76, 81-83] at both room temperature (RT) and liquid nitrogen temperature (LNT) and the photoexcited luminescence spectrum (LS)[81] at LNT can be accounted for if the existence of, for instance, a space-charge layer or a particular defect is assumed at the surface. The properties mentioned, together with TSC measurements, can also be used to identify defects in CdS and determine their concentrations and electronic properties. A review of the relevant information follows.

Undoped CdS platelets at RT typically exhibit SDP curves having two characteristic shapes: After reaching the absorption edge, the photocurrent either follows the absorption constant and shows a plateau or decreases very drastically, thus exhibiting a peak, as the wavelength of the incident light decreases. A theoretical analysis by H. B. de Vore[74] can be used to explain the above differences. Taking into account the recombination of carriers at the surface of CdS, one can have two possible situations. If the surface recombination rate is higher than the volume recombination rate, the carrier concentration at the surface (generated by strongly absorbed light) will be less than the carrier concentration in the volume of the material (generated by weakly absorbed

light). The SDP will show a peak in this case. If the opposite is true, then by the same reasoning the carrier concentration will increase with increasing absorption and the SDP will exhibit a plateau.

E. F. Gross and B. V. Novikov[57] were the first to observe the correlation between excitonic absorption and the SDP at LNT. According to their observations, CdS crystals could be divided into two main types: Class I crystals, for which the maxima in the free-exciton absorption spectrum appeared in the same energetic position as the maxima in the SDP, and Class II crystals, for which maxima in the absorption corresponded to minima in the SDP. This suggests that photoconductivity in CdS can be generated by two different mechanisms[79,82]:

a. Creation of free carriers through band-to-band excitation

b. Creation of free carriers from excitons through light absorption in the exciton lines.

Excitons can give origin to free carriers via three main processes:

i. Dissociation of the exciton into a free electron and a free hole through the exciton-phonon interaction[57,70,76,79].

ii. Interaction of the exciton with an impurity center. This finally results in the transfer of energy from the exciton to an electron in the impurity center which can be excited into the conduction band[57,70-72,83].

iii. Dissociation of excitons through the exciton - exciton interaction[57,80].

The way in which these processes can lead to two different CdS classes has been the subject of much speculation[57m70-72,75,76,81-83]. However, the models presented are mainly based on the assumption that the properties of the surface layer of CdS greatly differ from those of its bulk. As an example, if one assumes

that process (ii) is operative, the photocurrent increases or decreases with the absorption constant, making the crystal Class I[57]. A Class II crystal can exist if the photoactive decay of excitons is hampered by restraining their motion towards the proper centers. This can be achieved by a large concentration of defects near the surface[57].

The luminescence spectrum of undoped CdS platelets at LNT in the green and blue regions of the spectrum shows a very complex structure. Relevant to this discussion are two well-defined groups of lines: The free-exciton emission and the green-edge emission. (For a review see ref. 84 and 85). A correlation between SDP and free-exciton emission at LNT has been reported by several authors[70,83]. The green-edge emission has been thoroughly studied and its properties well established. At LNT, it is thought to arise from the radiative capture of a conduction-band electron by a hole, trapped at a center having an energy level close to the valence band. Lines arising from radiative annihilation of excitons bound to impurity centers are difficult to resolve at this temperature. The surface structure of CdS has been demonstrated to be an important factor for many of the phenomena reported in connection with these two emission groups. Again as an example, a change in the space-charge layer at the surface of CdS can cause a redistribution of carriers over energy levels in the band gap and influence the emission connected with these levels[81].

What has been said provides a powerful motivation for investigation of the relation between the surface structure of CdS and its optical and electrical properties. Once this relation becomes known one could presumably get information about surface fields and space-charge or physical properties of defects present at the surface by simply determining the optical and electrical properties. This report describes the changes in the SDP at RT and LNT, the LS at LNT and the TSC

curves as a result of heat treatments of undoped CdS platelets in ultra-high vacuum (UHV).

Our experimental arrangement was as follows. Selected undoped CdS plate-lets with evaporated ohmic Ti/Al electrodes[62], having slit geometry with 5 x 5 mm uncovered CdS and 100 μ width, were mounted in a thermally-shielded crystal holder within a stainless steel UHV chamber. The platelets used were grown in our laboratory as described in Sec. IIB1. A thin mica sheet was placed between the crystal and the Cu crystal holder to insure electrical insulation. Pt leads were pressed against the Ti/Al electrodes providing electrical contact to the crystal and preventing it from moving. It was found that Au leads tend to damage the Ti/Al electrodes because of the tendency of Al and Au to form an alloy. Al leads, on the other hand, have a tendency to scrape the electrodes when sub-ject to changes in temperature, as a consequence of the relatively high thermal-expansion coefficient of Al. The temperature of the crystal was measured with a thermocouple. The pressure was maintained with Vac-Ion and Ti-Sublimation pumps at 10^{-9} torr during the measurements, and did not exceed the 10^{-7} torr range during heat treatments.

Spectroscopic analysis was carried out with a 1 m-Jarrell-Ash spectro-meter, used as a monochromator for luminescence and photoconductivity measurements. For luminescence excitation, an HBO-200W-Mercury lamp with 365 nm and heat glass filter were used. The luminescence was recorded using an RAC type IP21 photomultiplier. The spectral slit width was about 1.6 Å for LNT measurements and 3Å for RT measurements. For infrared excitation experiments a 7-56 Corning filter and 2 W lamp were used. The TSC curves were obtained after trap-filling with intrinsic (460 nm) and extrinsic light (518 nm). Heating of the crystal was achieved by heating the Cu-crystal holder. The heating rate was about 6° C/min.

Now we discuss our results. The investigations described here were carried out in two stages. The first, extending approximately until the late part of 1969, was concerned with the effect of heat treatments on the LS at LNT. The luminescence was measured at LNT before and after heat treatments. Fig. IIC-1 gives a representative set of curves. The LS of the virgin crystal (curve 1) shows the green-edge emission with its fundamental peak at about 5150 Å. Several longitudinal-optical (LO) phonon replicas can be seen, separated by energy intervals of $E_{LO} = 38$ meV. After prolonged ultra-violet (UV) irradiation the peak at 5470 Å disappeared while the luminescence at shorter wavelengths remained unchanged (curve 2). After heat treatment at 200° C for 5 min. the edge luminescence suffered a marked decrease (curve 3). At higher treatment temperatures (Fig. IIC-1b), a growth in the peaks at 4870 and 5470 Å was observed. The green-edge emission disappeared below detection limits. It was observed that CdS crystals that were insulating in the dark and highly photosensitive always exhibited a strong green-edge emission, while insensitive crystals with a relatively high dark conductivity did not.

In the second stage of the investigation, the SDP at LNT and RT and TSC curves were determined. A reproducible SDP at LNT was obtained by scanning from shorter to longer wavelengths after pre-illumination at 4850 Å. Fig. IIC-2 shows the SDP at both RT and LNT of a crystal with a strong green-edge emission. The position of the peaks in the SDP at LNT coincided with the position of the inflection points of the reflectivity spectrum (i.e. the maxima of optical absorption) due to light absorption by the A(n=1) and B(n=1) excitons. The slight difference between the positions obtained here, and those of the A_1 and B_1 peaks at 77° K, is probably due to heating of the CdS above that temperature in the vacuum system used. From the temperature shift of the absorption spectrum
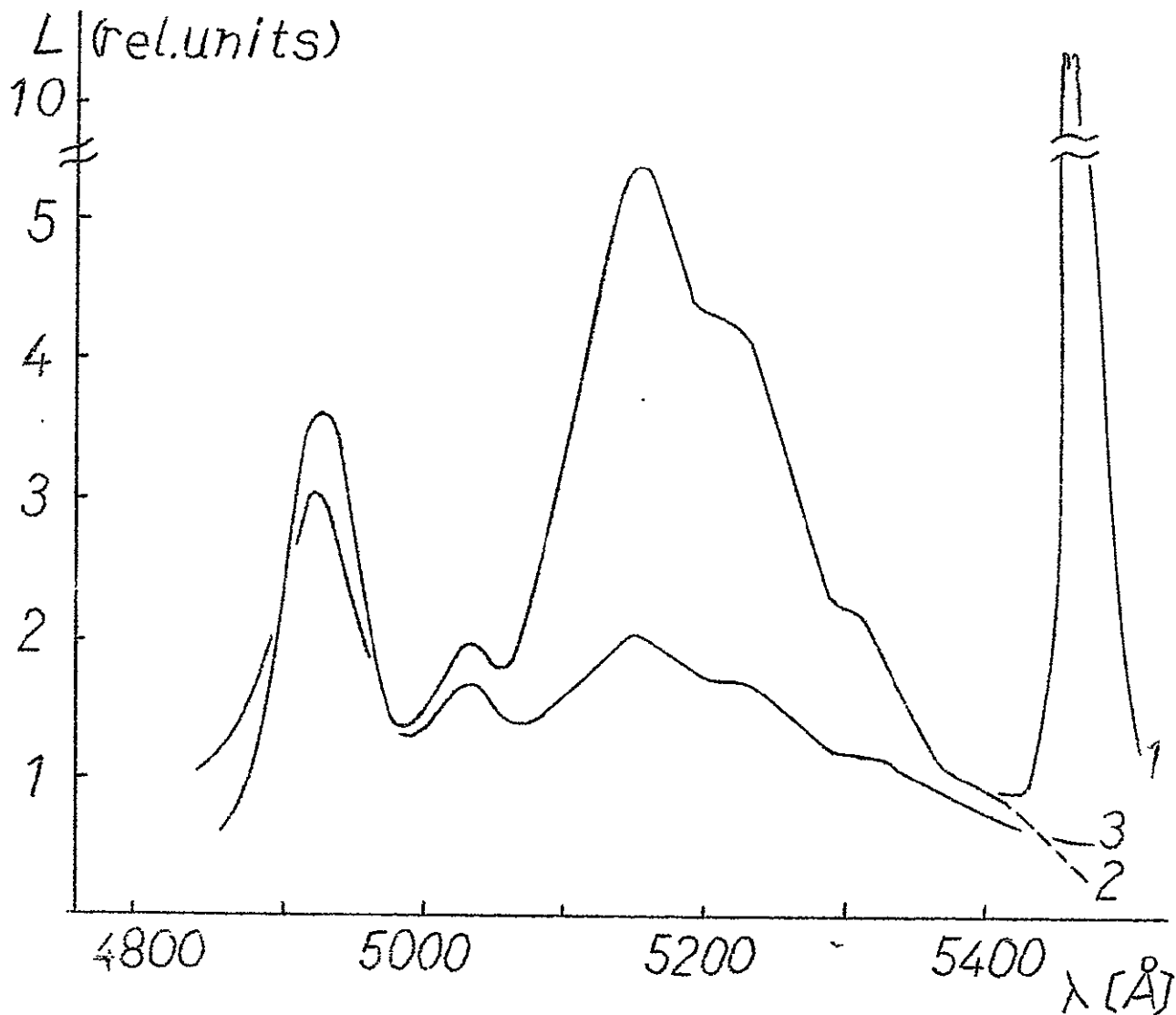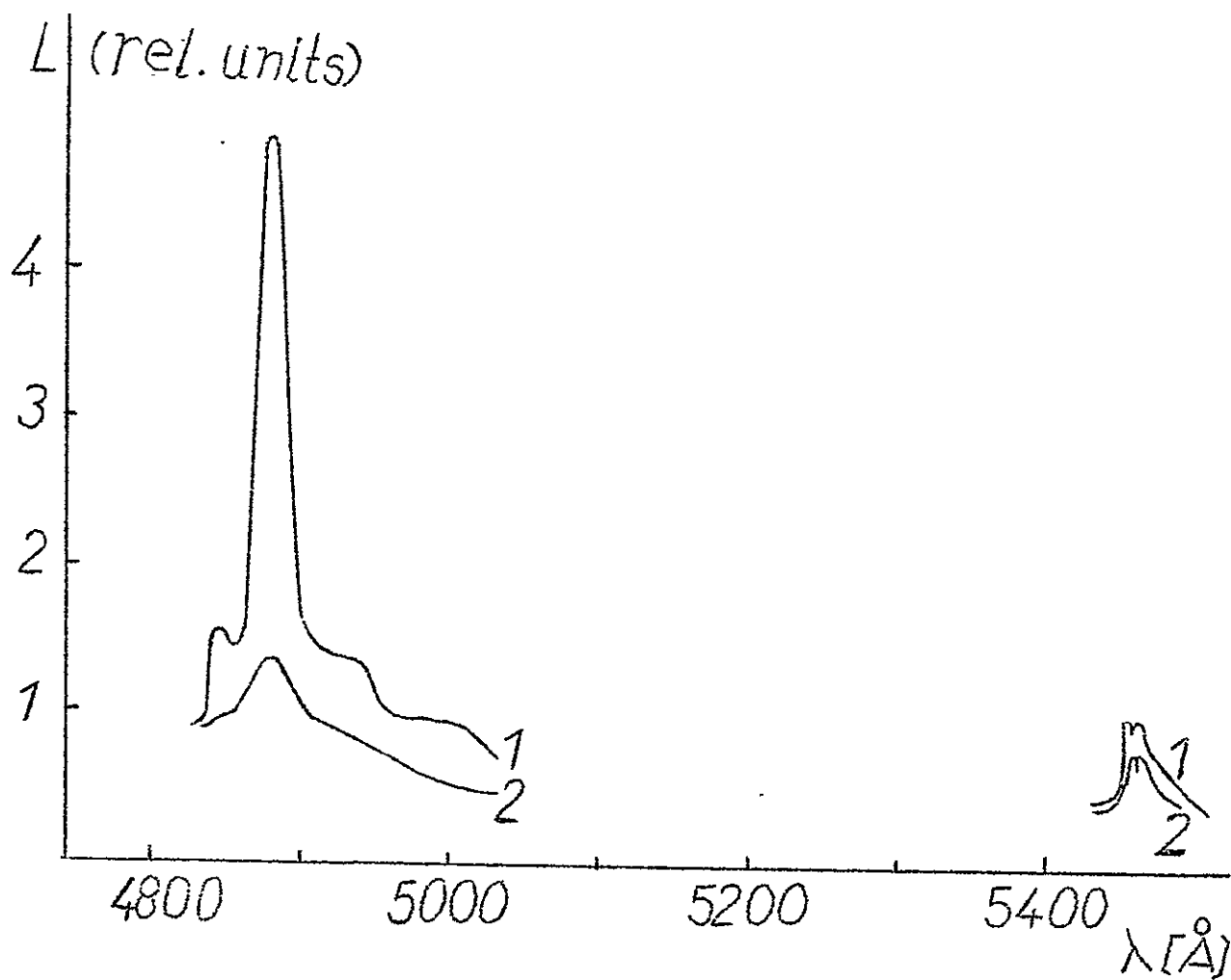
Curve 1: Untreated crystal

Curve 2: After prolonged UV irradiation
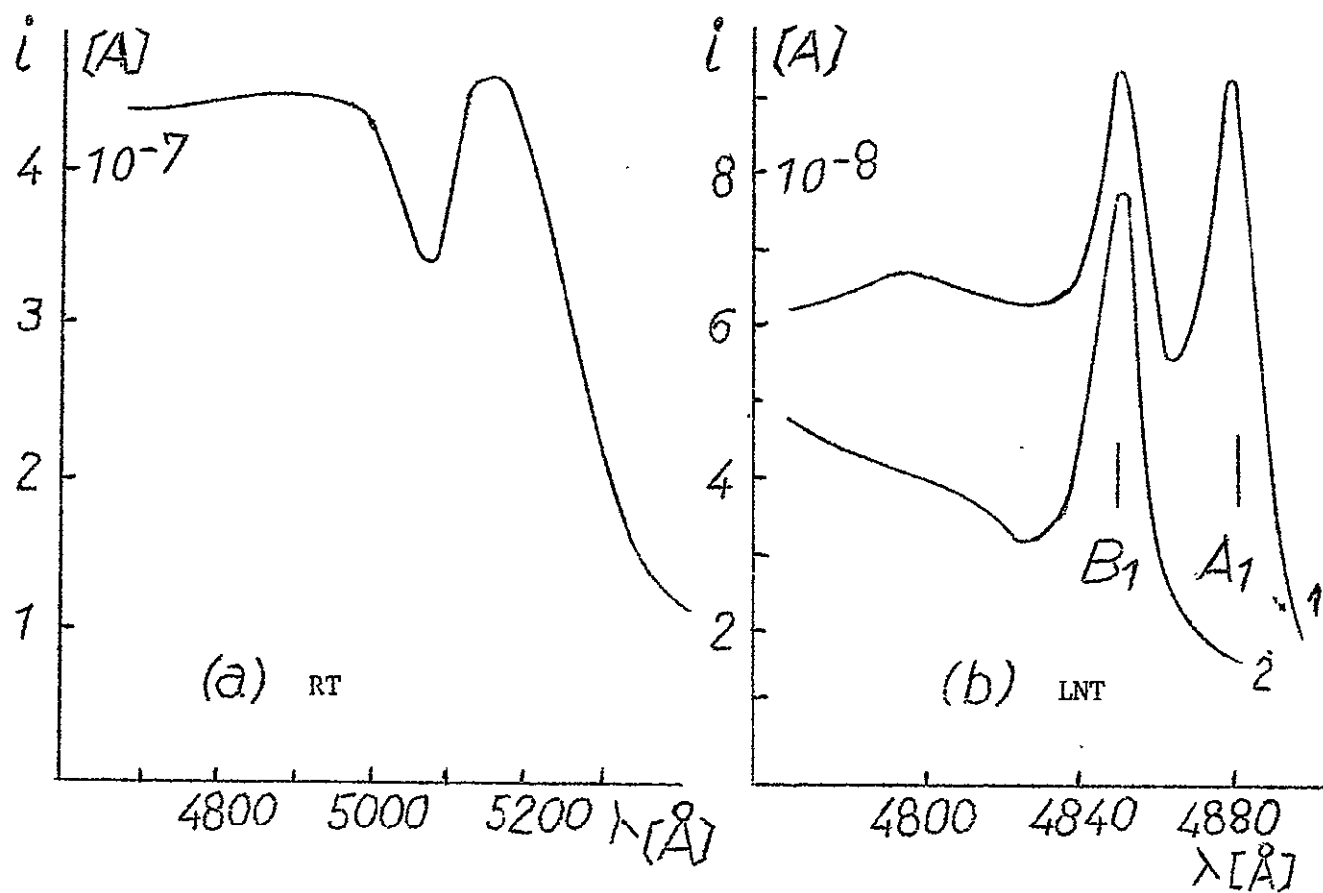
Curve 3: After heat treatment at 200°C

FIGURE IIC-1a: Luminescence spectra of CdS at LNT – Influence of

heat treatments.

Curve 1: After heat treatment at 300°C

Curve 2: After prolonged heat treatment at 300°C

FIGURE IIC-1b: Luminescence spectra of CdS at LNT - Influence of
slightly longer heat treatments.

FIGURE IIC-2: SDP of untreated CdS crystal at RT and LNT.

observed by Voigt and Spiegelberg[86], a temperature of 95° K is estimated for the crystal. After a treatment at 200° C, the SDP increased and the shape of the curves changed completely. At LNT, minima appeared where maxima previously occurred. At RT, a drastic decrease of the intrinsic-to-extrinsic photoconductivity ratio was observed (Fig. IIC-3). The TSC curves also showed changes after a heat treatment at 200° C.

Measurements carried out on other crystals show this to be a characteristic behavior: To a strong green-edge emission at LNT there corresponds a well-defined SDP. At RT the SDP generally follows the absorption spectrum presenting a plateau with a high intrinsic-to-extrinsic photocurrent ratio. At LNT, the SDP also follows the absorption spectrum. There is coincidence between SDP peaks and exciton peaks in absorption. A heat treatment at approximately 200° C yields in all cases a crystal that shows no green-edge emission; anticoincidence between SDP and absorption at LNT, and a peak with a very low intrinsic-to-extrinsic current ratio in the SDP at RT. Oxygen backfilling does not affect a crystal in this state. On the other hand, a short heat treatment (5 min) at about 150° C causes no major changes in the SDP and LS at LNT. The changes in the SDP at RT are in coincidence with those reported in relation to the thermal desorption experiments in the following section. Upon heat treatment at 180° C, important changes are seen in the SDP at LNT.

Figure IIC-4 shows the effect of heat treatments on the SDP at LNT of a strongly green-edge luminescent crystal. The virgin crystal exhibited coincidence between SDP and absorption (curve 1). Treatment at 150° C did not alter the SDP. After a treatment at 180° C the exciton peaks became "submerged" in the background and a broad band appeared towards longer wavelengths, seemingly composed of two peaks (curve 2). After backfilling with O_2, the broad band was resolved
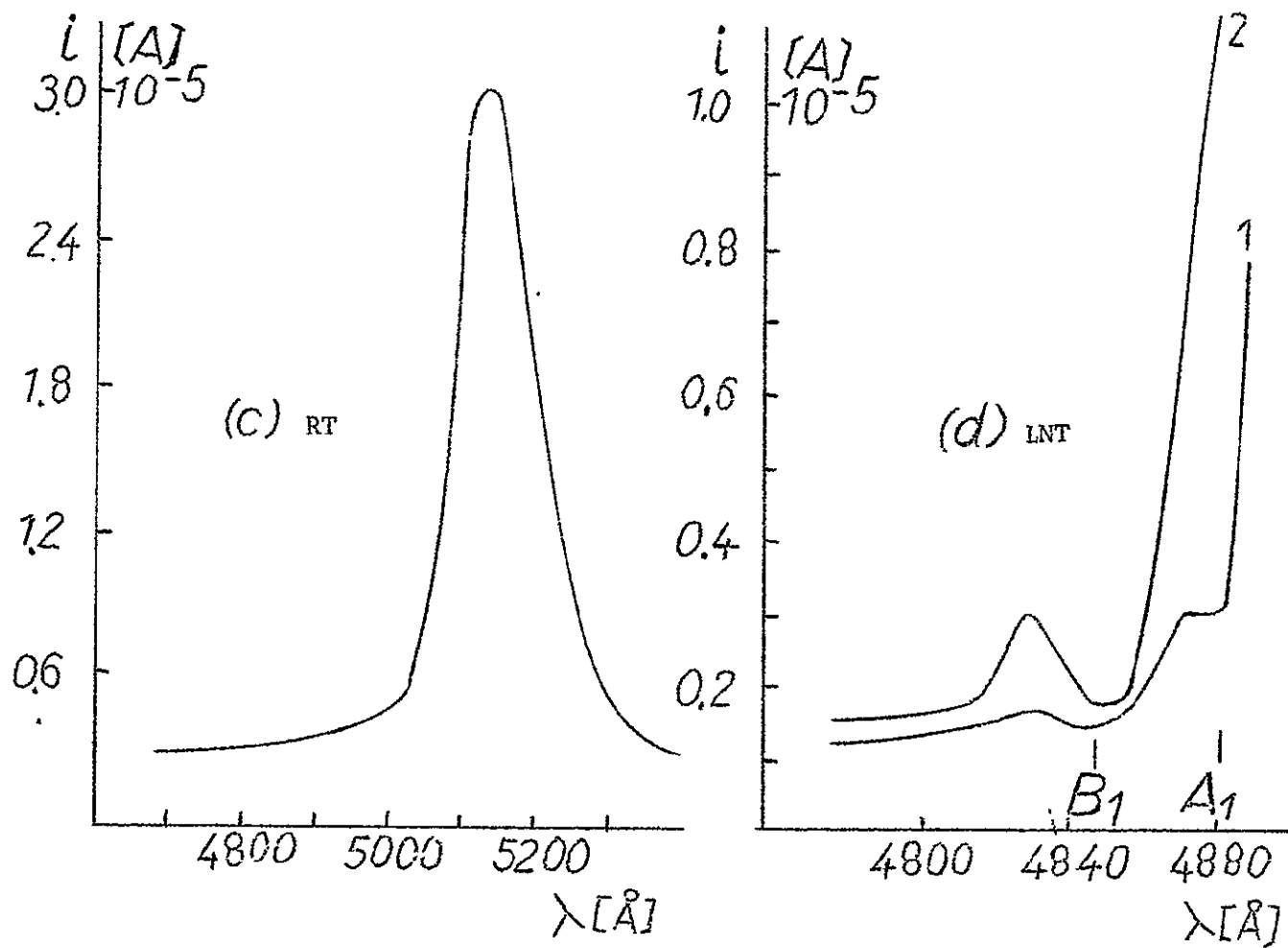
FIGURE IIC-3: SDP of CdS crystal after 200°C heat treatment at RT and LNT.
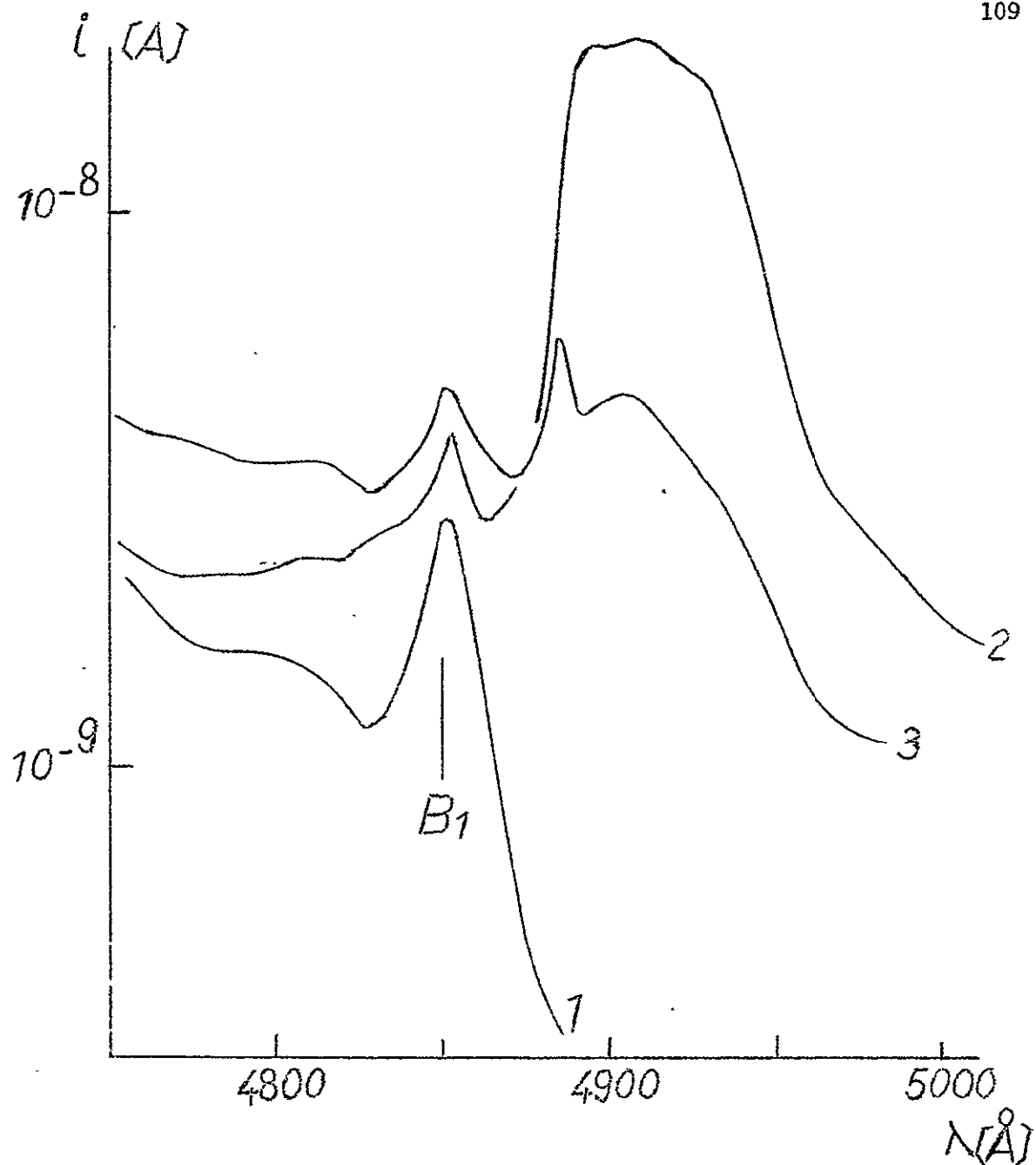
Curve 1: Untreated crystal

Curve 2: After 180°C heat treatment

Curve 3: After backfilling with oxygen
         and subsequent pumping

FIGURE IIC-4: SDP of CdS crystal at LNT, E‖C.

(curve 3) into a narrow and a broad peak, the latter having decreased more than the former. After a new heat treatment to 120° C the SDP recovered its shape previous to the O_2 backfilling (Fig. IIC-5).

The effect of IR excitation can be seen in Fig. IIC-5. Photocurrent decrease was more marked in the broad band than in the exciton peaks. With the highest IR intensity, only the broad peak within the broad band seemed to remain. TSC curves are shown in Fig. IIC-6. For intrinsic excitation (460 nm), virgin state (curve 1) and after 180° C treatment (curve 2). For extrinsic excitation (518 nm), virgin crystal (curve 3) and after 180° C treatment (curve 4).

Now we discuss our results. According to the Gross-Novikov classification[57,70], the crystals investigated here are of Class I when in their virgin state. This classification was originally made in connection with the SDP of CdS at LNT. On the basis of the reported results, however, it is possible to extend this definition to include the following properties:

a. Coincidence between free exciton peaks in the SDP and the absorption spectrum at LNT.

b. A shoulder in the SDP at RT (at about 480 nm), also implying coincidence with the absorption spectrum at that temperature.

c. A large intrinsic-to-extrinsic photoconductivity ratio at RT.

d. A strong green-edge emission.

A heat treatment at about 200° C changed the investigated crystals to Class II. The definition of Class II crystals can be properly extended as follows:

a. Coincidence between minima in the SDP and free exciton peaks in the absorption spectrum at LNT.

b. A peak in the SDP at RT (at about 518 nm)

c. A small intrinsic-to-extrinsic photoconductivity ratio.

d. No green-edge emission.
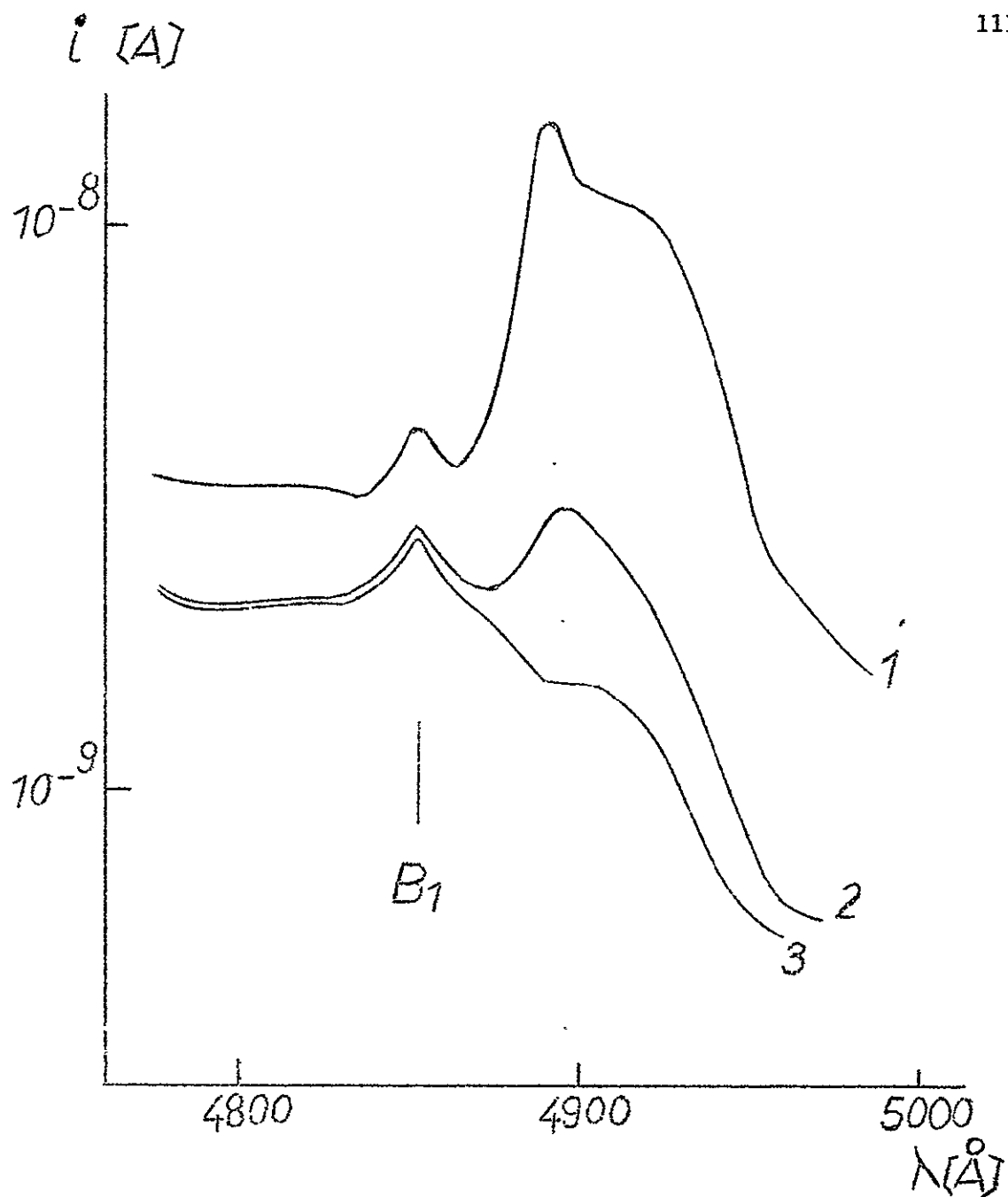
Curve 1: No IR light
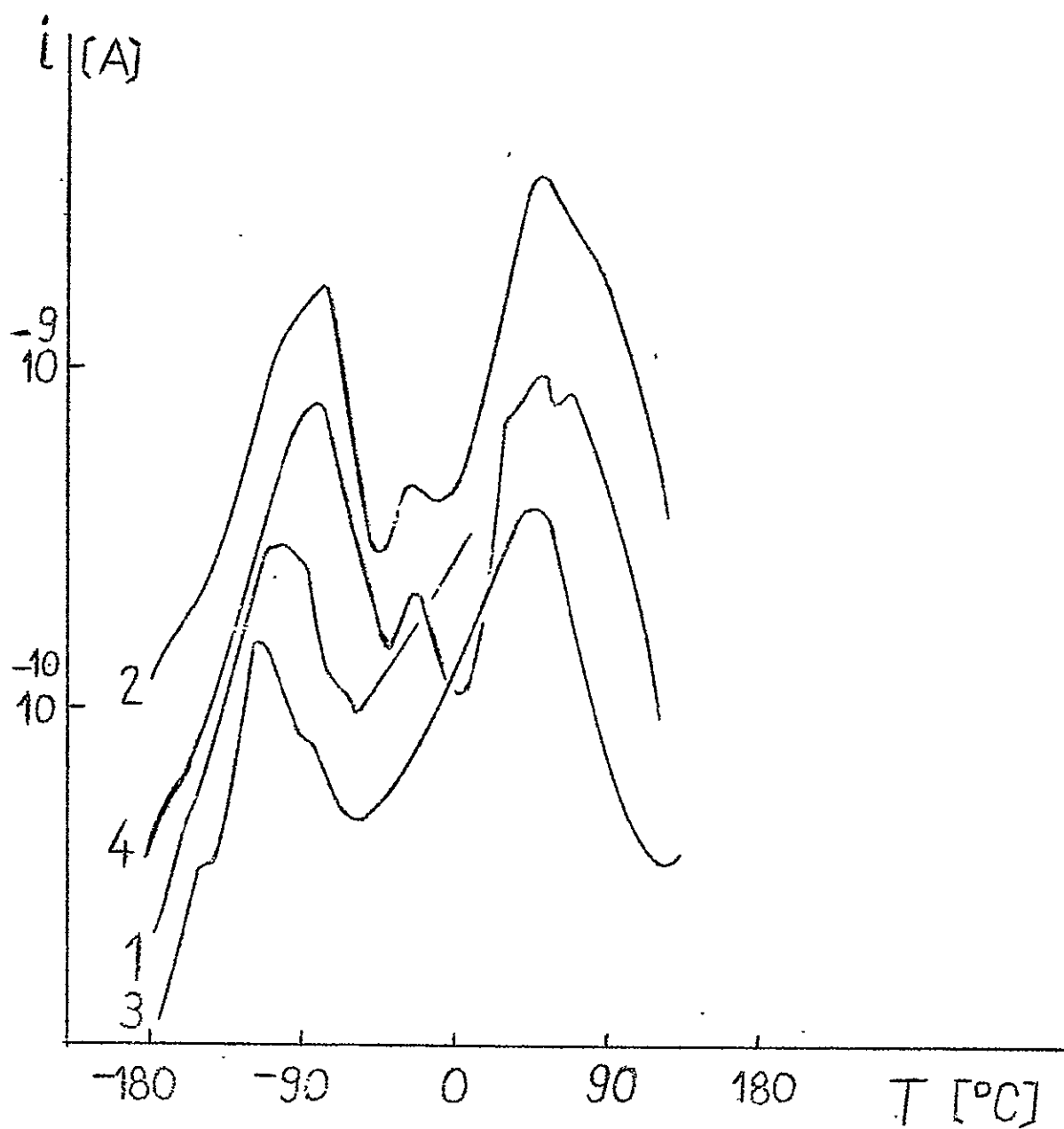
Curve 2: With IR

Curve 3: With double the previous IR intensity

FIGURE IIC-5:   Effect of IR excitation on the SDP of CdS at LNT.

Curve 1: Untreated crystal, intrinsic excitation

Curve 2: After 180°C heat treatment, intrinsic excitation

Curve 3: Untreated crystal, extrinsic excitation

Curve 4: After 180°C heat treatment, extrinsic excitation

FIGURE IIC-6: TSC curves of CdS.

14

A very similar extension is also suggested by the results of experiments carried out in this group in connection with thermally stimulated desorption (TSD)[64,65] and reported in Sec. IIC2. It is interesting to note that the behavior of the SDP at RT reported here is essentially consistent with the behavior observed in the previously-mentioned experiments[64,65]. Also the same model[64,65] can be used to explain both sets of measurements.

The coincidence between the SDP and free-exciton absorption at LNT can be explained in terms of the existence of a surface-near region in CdS[64] with certain properties. This region is produced during cooling of the crystals after the growth and has a width of about 10^{-5} cm[64,65]. It is Cd-rich and is characterized by a high concentration of donors. Oxygen adsorbed at the surface partially compensates this high donor concentration, and an accumulation layer is finally created. Thus the difference $E_C - E_F$ is a strong function of the distance from the surface and, within the surface-near layer, we can expect the lifetime τ_n of optically-excited electrons to decrease when that distance increases (accumulation layer). Following the assumptions by Voigt and Ost[76] that (a) the exciton diffusion length does not exceed those for electron and hole diffusion and that (b) excitons dissociate into free electrons and holes by collision with phonons, one sees that absorption of light in an exciton band will produce a photoconductivity peak.

Heat treatments at less than 180° C cause oxygen desorption[64,65], with the effect of a release of electrons, from levels associated with the oxygen, that fill the donors in the surface-near region. The SDP shows no change of shape. A heat treatment at 180° C causes a broad band to appear to the low-energy side of the free-exciton peaks, consisting of a narrow and a broad peak. This broad peak has been attributed to the free carriers created by dissociation of an

exciton bound to a neutral donor[79,85]. It is proposed that its appearance might be due to the neutralization, by electrons released from the oxygen at the surface, of a previously-ionized donor in the surface-near region. Backfilling with O_2 partially reverses this process (curve 3, Fig. IIC-4). IR light re-creates ionized donors (possibly by release of holes from neutral acceptors), and thus prevents the excitons from being trapped at the centers. This also causes a decrease in photoconductivity (Fig. IIC-5).

Heat treatments at higher treatment temperatures cause Cd evaporation from the crystal and diffusion to the bulk[64,65]. The effect of these two process-es is a bulk sensitization and homogenization of the photoconductivity. This makes possible the formation of a depletion layer at the surface, and the electron lifetime can become an increasing function of the distance from the surface. With the previous assumptions on the exciton diffusion length and the dissociation mechanism, absorption of light in an exciton band produces minima in the photocurrent.

The temperatures for which the transition from Class I to Class II occurs, as determined in this work, are consistently lower than those observed in thermal-desorption experiments. This difference can be attributed to the fact that in this case, with a lower heating rate, the crystal spends more time at the higher temperatures. Current research in this laboratory is concerned with different experiments on both halves of a cleaved CdS crystal of Class I.

We summarize this section with the following discussion. It has been shown that CdS crystals can be separated into two classes. Class I CdS crystals present a surface layer of adsorbed oxygen and an accumulation layer connected with the presence of excess Cd in the surface-near region. They are very sensitive to the thermal desorption of oxygen[64,65]. Heat treatments at about

200° C cause an irreversible transition from Class I to Class II crystals because of evaporation and diffusion to the bulk of excess Cd. Class II crystals are bulk-sensitized and present a depletion layer in the surface-near region. They are not sensitive to thermal desorption. The presence of an accumulation or a depletion layer can be determined by measuring the SDP at LNT. An accumulation layer implies coincidence between exciton peaks in photoconductivity and absorption at LNT. A depletion layer implies coincidence between exciton minima in photoconductivity and exciton maxima in absorption at LNT. The SDP at LNT can also give useful information about the identity of the donors connected with excess Cd in the surface-near region.

2. Effects of Adsorption and Desorption on Electrical and Optical Properties:

As was mentioned in the last section, a number of investigations[87] have shown the significant influence of adsorbed gases, principally oxygen and water vapor, on the electrical properties of CdS single crystals. These effects have been attributed to surface-charge accumulation, changing surface recombination velocity, photochemical reactions, and photodesorption, in the above references.

It is the purpose of this section to determine the changes in the electrical properties of CdS single crystals caused by the TSD of adsorbed gases, principally oxygen and water vapor, in UHV.

A stainless steel and OFHC-Cu vacuum system capable of ultimate pressures of 10^{-11} torr after baking was used. Total system pressure was measured by a cold cathode discharge gauge (Fig. IIC-7).

A General Electric 90° magnetic sector partial pressure analyser capable of measuring a 10^{-13} torr partial pressure was employed in the TSD measurements.
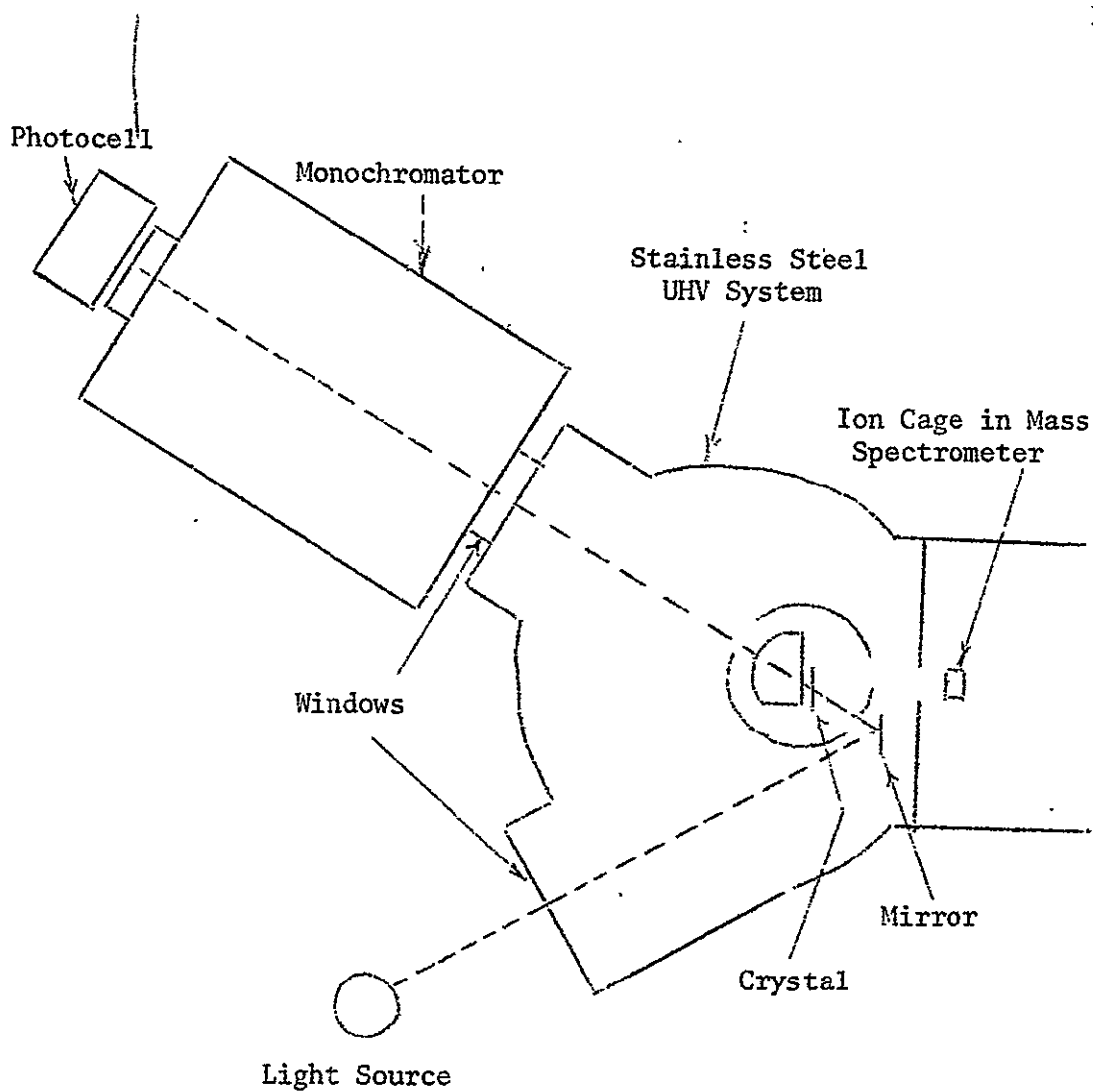
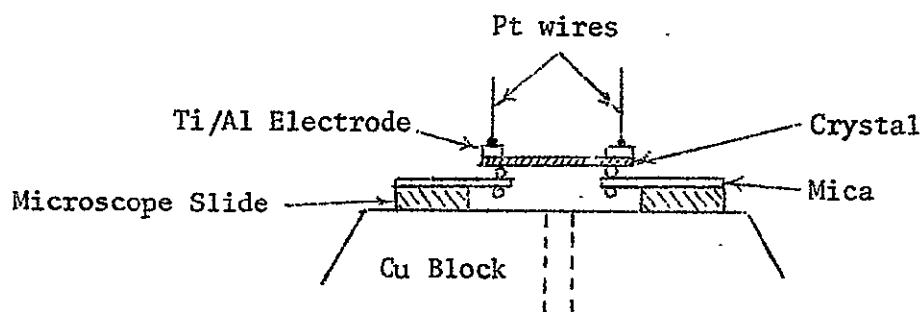FIGURE IIC-7: Experimental set-up.

FIGURE IIC-8: Method of mounting crystal for TSD measurements.

The CdS crystal was insulated from the Cu-block cold finger, both thermally and electrically by microscope slides, mica and Cu wire (Fig. IIC-8). The crystal was heated by utilizing its own Joule's heating and an enhanced photocurrent, resulting from a 6000-foot-candle power W-lamp. The temperature of the crystal was measured by a Bausch and Lomb monochromator blazed at 1350 lines/mm which monitored the thermal shift of the band edge. A feedback heating circuit was employed which sensed the shift of the band edge, thus enabling a time-linear heating rate. Typical heating rates are 8-10° K/sec.

Oxygen of 99.999% purity was used in all oxygen backfill measurements and the water vapor backfills consisted of $[H_2O]:[O_2] = 5\%$.

The crystal was supplied with narrow Ti/Al electrodes evaporated at $p \lesssim 10^{-6}$ torr on one side of the platelet. Platinum lead-in wires were used and all SDP measurements were taken with 10 VDC applied to the crystal.

As a preliminary to the discussion of the experimental results, we list some properties of Class I and Class II crystals. As was noted above, a Class I crystal's SDP at RT has a shoulder at approximately 480 nm, whereas a Class II crystal's SDP has the "typical" CdS peak at 518 nm. Also, Class I crystals are over-stoichiometric in cadmium in the surface-near region[64] and are extremely sensitive to heat treatment and ambient atmosphere, whereas Class II crystals are quite insensitive in these two respects.

Now we discuss changes in the electrical properties of CdS crystals as a result of TSD. The SDP of a Class I crystal is extremely dependent upon heat treatment. Placing such a crystal in UHV results in approximately a one-order-of-magnitude increase in the SDP. Subsequent incremental heating of the crystal (up to 275° C) followed by SDP's at RT can result in an increase of six orders of magnitude in the extrinsic photoconductivity and four orders in the intrinsic.

Also, the relative blue-to-red photosensitivity decreases from an initial virgin value of 10^3 to approximately 2 (Fig. IIC-9). If the crystal is heated above 300° C, the SDP is no longer reversible upon oxygen backfill and also the SDP begins to decrease. The relative blue-to-red sensitivity also starts to increase again until a TSD temperature of 400° C has been reached. At this point the Class I crystal changes to a Class II crystal, i.e., the SDP exhibits a peak at 518 nm.

The SDP of a Class II crystal, on the other hand, is virtually insensitive to TSD heat treatment. Incremental heating of a Class II crystal in UHV up to 300° C results in an increase of a factor of 3 in the extrinsic photoconductivity and an order-of-magnitude increase in the intrinsic photoconductivity. TSD heat treatments in excess of 300° C result in a decrease of the SDP to within a factor of 3 of the virgin crystal's SDP in UHV (Fig. IIC-10).

The results of oxygen backfill on a Class I crystal's SDP following TSD heat treatments is shown in Fig. IIC-11.

It has been observed that when a Class I crystal has been converted to a Class II crystal by TSD, the Class I state can be restored by a 3.5 keV electron bombardment for two hours with a beam current density of $\sim 10^{-7}$ amps-cm^{-2} [65] (Fig. IIC-12). This restoration is realized in UHV, 10^{-9} torr, and is thus far not maintained upon backfilling to 1 atm oxygen, i.e., the restored Class I state in UHV reverts to the Class II state upon backfilling.

Mass spectroscopic measurements in UHV of thermally desorbed gases from a Class I crystal show that oxygen (AMU 16) is desorbed from the crystal starting at a temperature of 135° C and reaching a maximum at 325° C. The activation energy for the TSD is 0.75 eV and the associated surface concentration is $\sim 10^{15}$ atoms-cm^{-2} (Fig. IIC-13). The oxygen desorption spectrum, however, is not
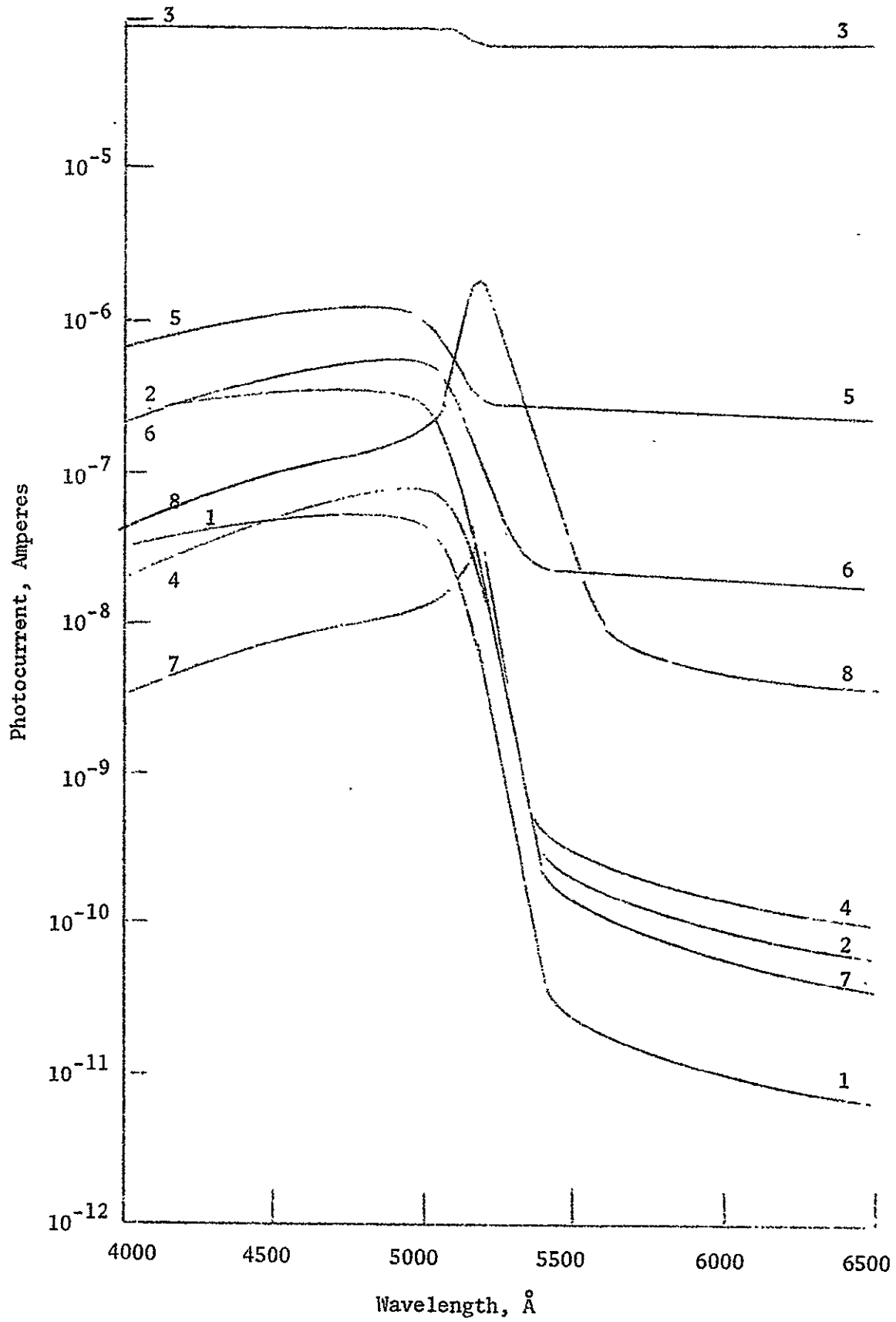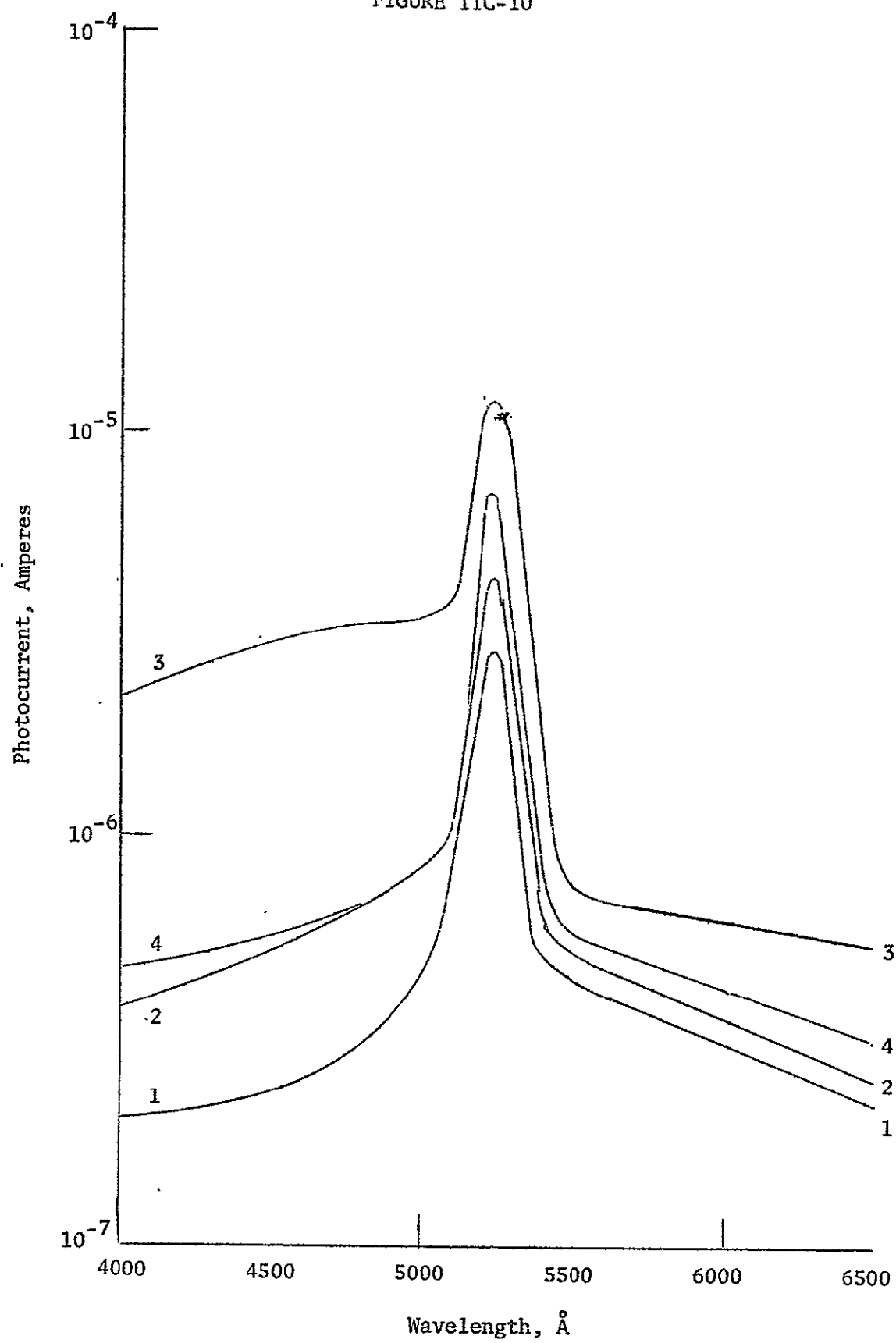
FIGURE IIC-9

FIGURE IIC-10

Figure Captions

FIGURE IIC-9:   Spectral dependence of photoconductivity measurements showing

the transition of a Class I crystal to a Class II crystal, --

all measurements taken at room temperature.

    1   Pressure of 1 atm air - Virgin Class I crystal

    2   $P = 10^{-9}$ torr

    3   $P = 10^{-9}$ torr - after heating to 275° C

    4   $P = 1$ atm O_2

    5   $P = 10^{-9}$ torr - after heating to 365° C

    6   $P = 10^{-9}$ torr - after heating to 380° C

    7   $P = 10^{-9}$ torr - after heating to 400° C

    8   $P = 10^{-9}$ torr - after heating to 525° C

FIGURE IIC-10:   Spectral dependence of photoconductivity measurements showing

the behavior of a Class II crystal as a result of TSD.

    1   Pressure of 1 atm air - Virgin Class II crystal

    2   $P = 10^{-8}$ torr

    3   $P = 10^{-8}$ torr - after heating to 300° C

    4   $P = 10^{-8}$ torr - after heating to 400° C
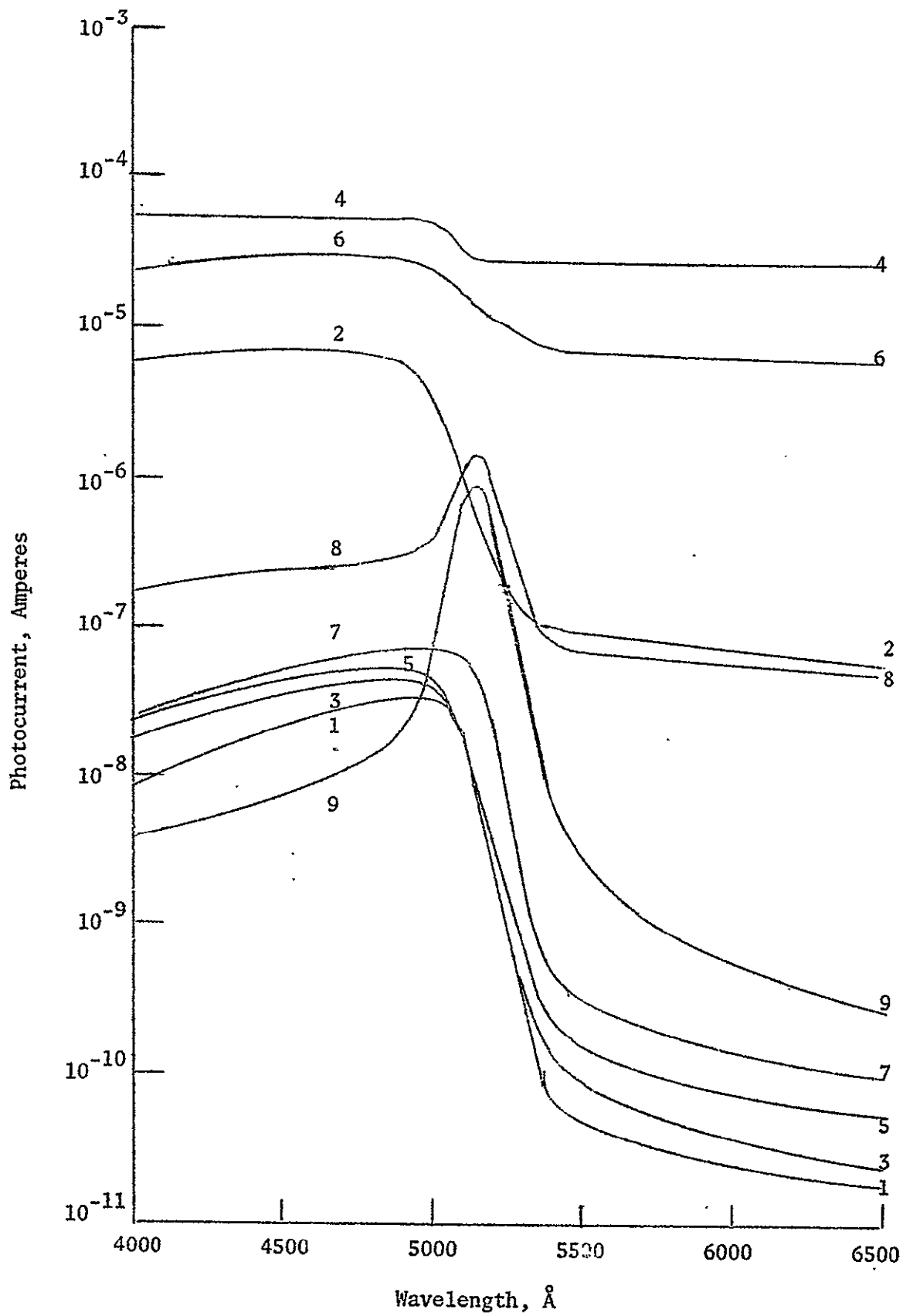
FIGURE IIC-11

FIGURE IIC-12

Photocurrent, Amperes

Wavelength, Å
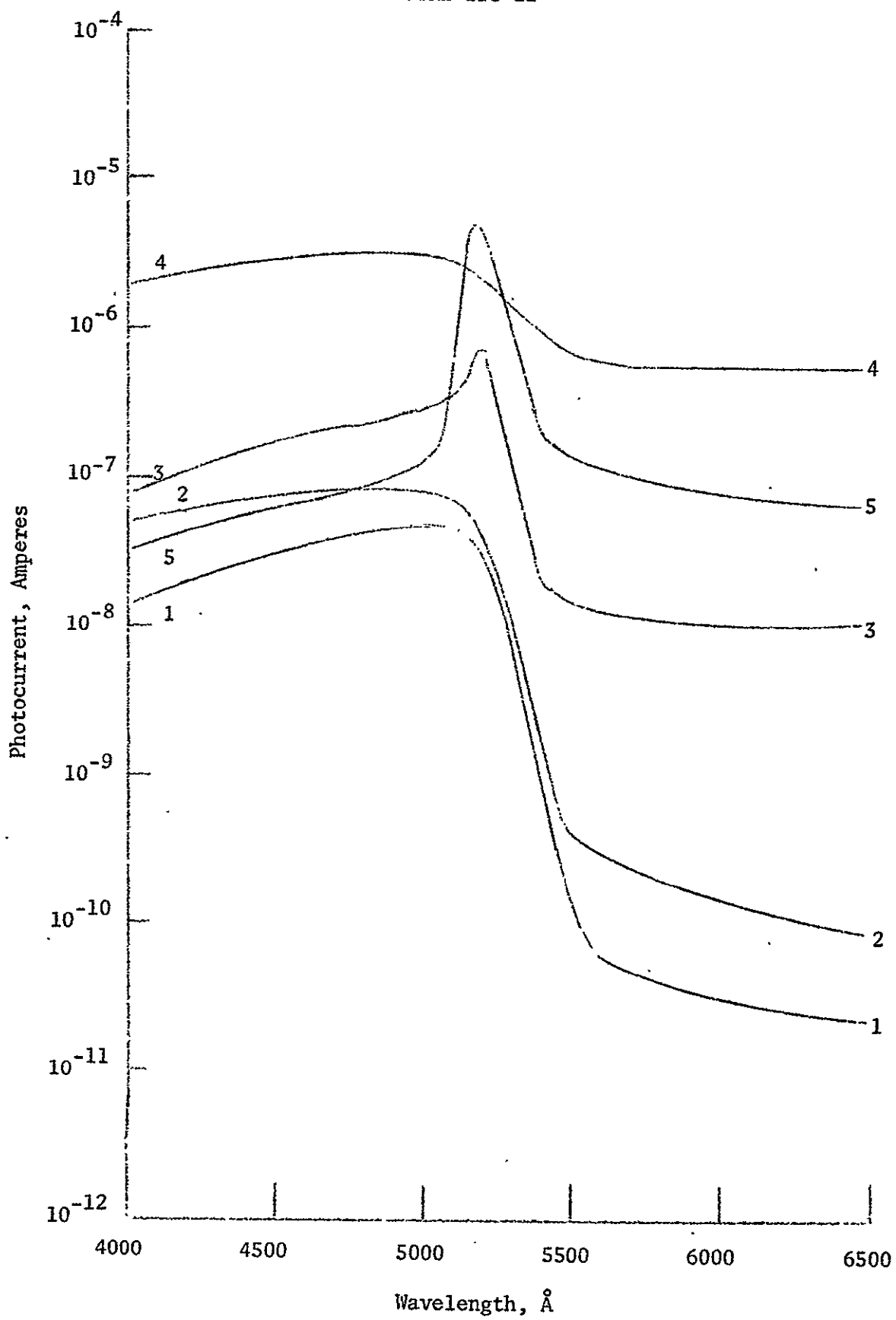
Figure Captions

FIGURE IIC-11:   Effects of oxygen backfill on the SDP of a Class I crystal after various TSD treatments.

1   Pressure of 1 atm air - Virgin Class I crystal
2   $P = 10^{-8}$ torr - after heating to 200° C
3   $P = 1$ atm O_2
4   $P = 10^{-8}$ torr - after heating to 250° C
5   $P = 1$ atm O_2

6   $P = 10^{-8}$ torr - after heating to 375° C
7   $P = 1$ atm O_2
8   $P = 10^{-8}$ torr - after heating to 475° C
9   $P = 1$ atm O_2

FIGURE IIC-12:   Spectral dependence of photoconductivity measurements showing the transition of a Class I crystal to a Class II crystal and the subsequent restoration of the crystal to the Class I state by electron bombardment.

1   Pressure of 1 atm air - Virgin Class I crystal
2   $P = 10^{-8}$ torr
3   $P = 10^{-8}$ torr - after heating to 550° C
4   $P = 10^{-8}$ torr - after 3.5 keV electron bombardment for two hours
5   $P = 10^{-8}$ torr - after heating to 550° C

FIGURE IIC-13: Thermal desorption spectrum of oxygen from a Class I crystal.
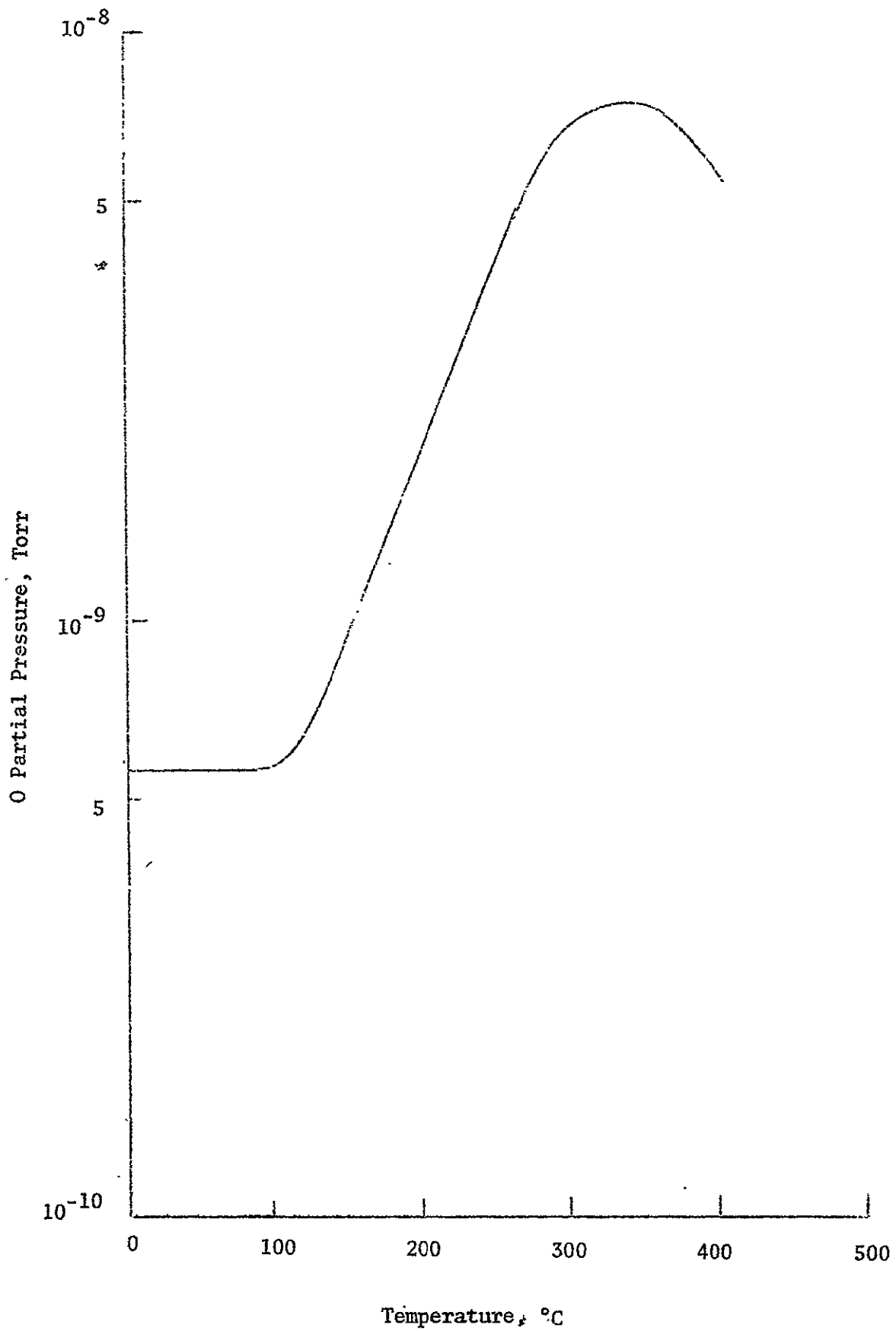
reversible upon backfilling to 1 atm oxygen and subsequent TSD in UHV. Similar measurements of thermally desorbed cadmium show that cadmium desorption starts at 275° C, goes through a plateau at 450° C, and starts a very abrupt increase at 500° C. The initial activation energy for desorption is 1.32 eV and the associated surface concentration is $1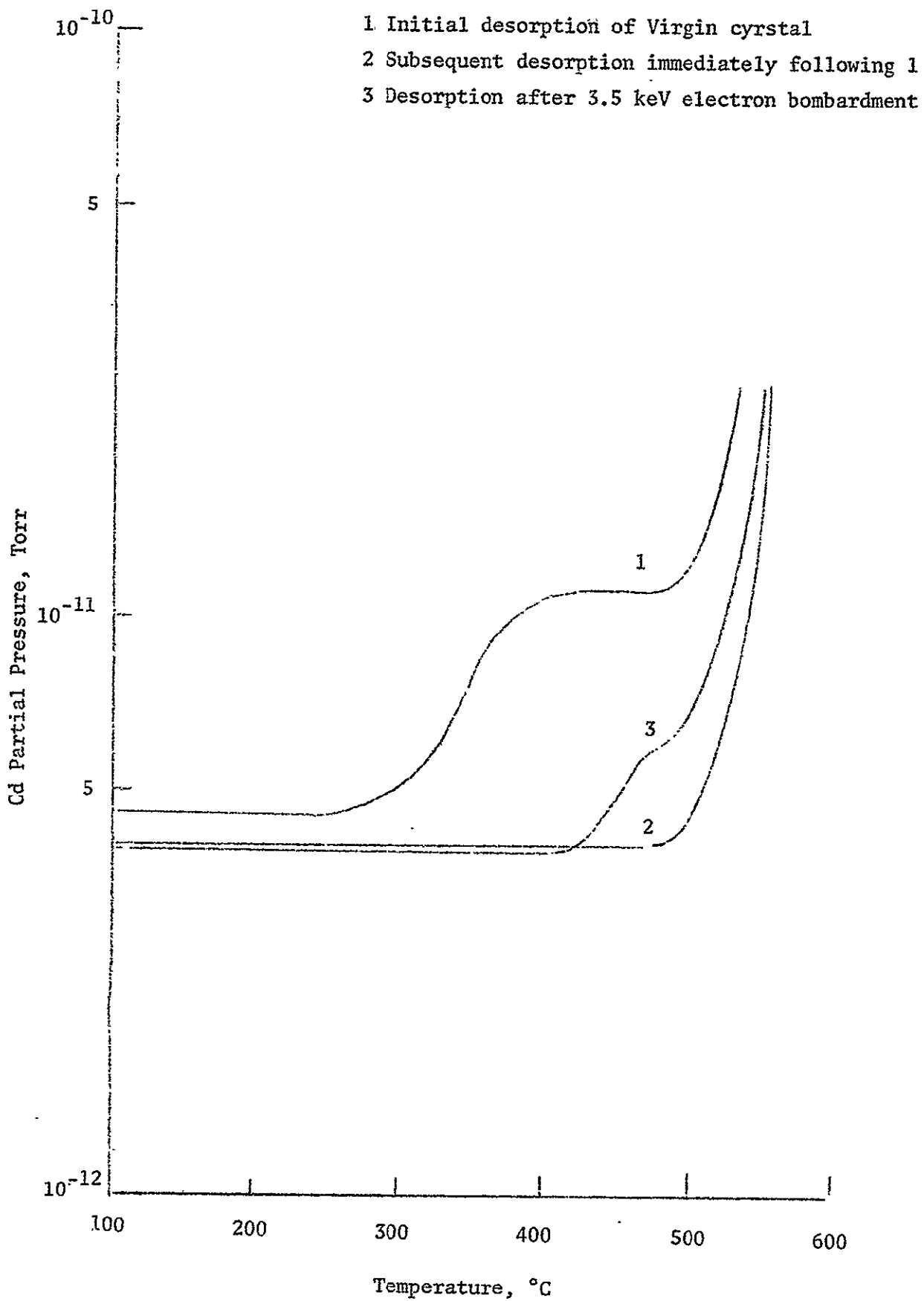0^{13}$ atoms-cm^{-2} (Fig. IIC-14, curve 1). Curve 2 of Fig. IIC-14 is a cadmium desorption spectrum taken immediately following curve 1; as can be seen, the plateau portion of the spectrum was completely removed in the initial heating.

Following an electron bombardment at 3.5 keV for two hours with an associated beam current density of ~ 10^{-7} amps-cm^{-2}, the cadmium desorption spectrum was again measured. As can be seen in curve 3 of Fig. IIC-14, the plateau portion of the spectrum is again present, although somewhat diminished in concentration.

Now we discuss the results. It has been suggested[64] that the Class I CdS crystal has a thin surface layer 10^{-5} cm thick with a high density of donors-- presumably a cadmium surplus--which is responsible for the greatly enhanced photo- sensitivity near the crystal's surface, and that the adsorbed oxygen partly com- pensates this accumulation layer. With the desorption of this compensating oxygen, the accumulation layer becomes fully active. Hence trapped electrons are freed from the oxygen and recaptured in the surface-near region, causing an electronic sensitization. Consequently the photoconductance increases. Fig. IIC-15 illustrates the change in the potential distribution close to the surface with progressive oxygen desorption. The adsorbed oxygen compensates electronically the high donor concentration in the surface-near region (curve 1). With the desorption of oxygen more and more electrons from the surface are re- leased and fill the donors in the surface-near region, thereby lowering the

FIGURE IIC-14:   Thermal desorption spectrum of cadmium from a Class I crystal.

1 Initial desorption of Virgin cyrstal

2 Subsequent desorption immediately following 1
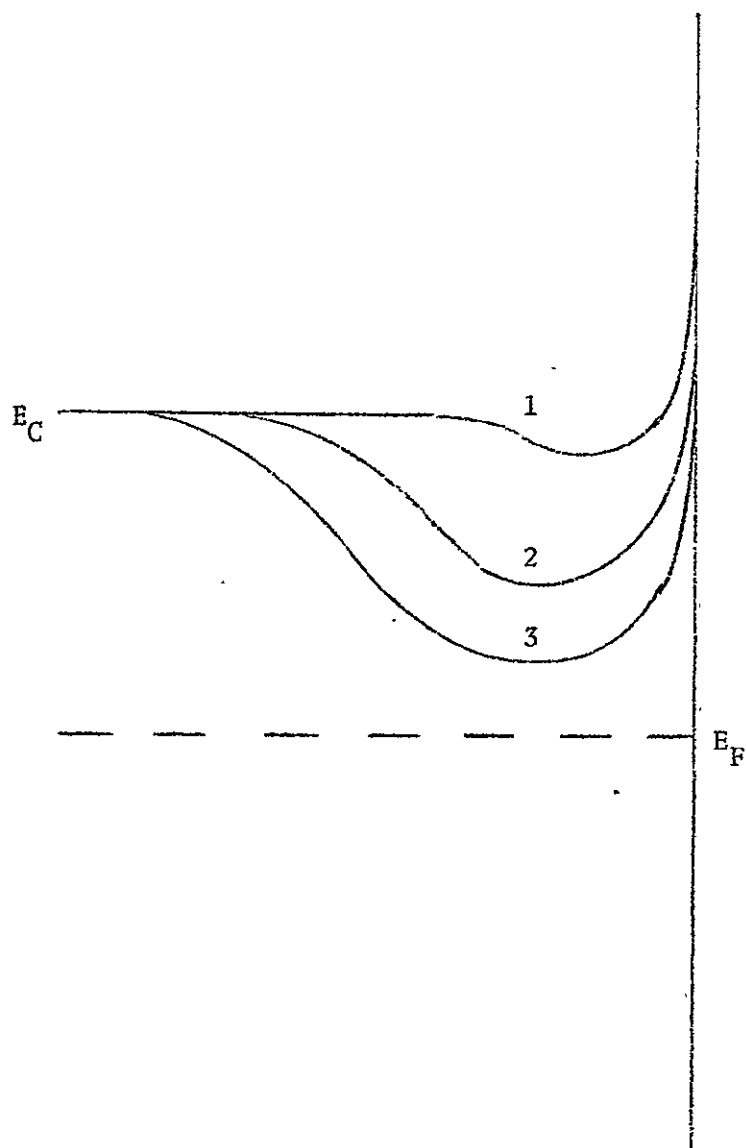
3 Desorption after 3.5 keV electron bombardment

FIGURE IIC-15:   Conduction band-edge in the surface-near region for successive

oxygen desorption (1-3).

conduction band (curves 2 and 3) and hence increasing the carrier density. This increase in the photoconductance can be seen in Fig. IIC-9, curves 1 to 4. Comparing Fig. IIC-9 with Fig. IIC-13, one sees that the photoconductance of a Class I crystal increases up to about 300° C at which point the oxygen desorption spectrum reaches a maximum. At this point the accumulation layer has been fully activated and consequently the photoconductance is at its maximum. Furthermore, up to this temperature the SDP is reasonably reversible upon oxygen backfill and even more so with a backfill of $[H_2O]:[O_2]$ = 5% as can be seen in Fig. IIC-11. If the crystal is heated to temperatures in excess of 300° C, the surplus surface cadmium as was suggested above starts to be desorbed and also diffuses into the bulk, causing a bulk sensitization. As this surplus surface cadmium which is responsible for the accumulation layer is desorbed, the photoconductance decreases. as a result of surface desensitization (Fig. IIC-9). At approximately 450° C this surface cadmium layer of ~ 10^{13} atoms-cm^{-2} is totally desorbed and the Class I crystal becomes a Class II crystal. The further upward shift after 525° C treatment is probably caused by the production of intrinsic defects. If the crystal in this Class II state is bombarded with 3.5 keV electrons, the Class I state can be restored[65]. This is because the accumulation layer has been partially restored by the "knocking out" of surface-near sulfur. The restoration of the surplus surface cadmium which is responsible for the accumulation layer is evident from the reappearance of the plateau in the cadmium desorption spectrum. It is this plateau in the cadmium desorption spectrum which is responsible for the accumulation layer. With oxygen readsorption, this restored accumulation is totally compensated and hence the crystal returns to the Class II state (Curve 4, Fig. IIC-9).

To substantiate the theory that the Class I state of CdS single-crystal platelets is caused by an excess of surface cadmium partially compensated by ad-

sorbed oxygen, crystals have been grown in our materials preparation laboratory at different relative concentrations of $[H_2S]:[N_2]$. If the $H_2S:N_2$ gas stream is not cut off until the crystal temperature has reached $\approx 200°$ C, we find that those crystals grown at concentrations of $[H_2S]:[N_2] \lesssim 0.31\%$ are Class I type, whereas those grown at concentrations of $[H_2S]:[N_2] > 0.31\%$ are Class II. This fact supports the theory that Class I CdS crystals are over-stoichiometric in surface cadmium since the low relative concentration of H_2S in the carrier gas stream has the effect of raising the partial pressure of cadmium in the gas surrounding the crystal during growth. As the concentration of H_2S is increased, the partial pressure of cadmium is reduced and hence the crystal becomes more stoichiometric resulting in a Class II crystal. This is because a CdS crystal is naturally over-stoichiometric in cadmium.

The effect of cooling the crystal down from a specified temperature lying between 50 and 500° C in the total absence of any H_2S in the carrier gas stream is currently being studied. Preliminary results indicate that a crystal which was grown at a concentration of $[H_2S]:[N_2] \lesssim 0.31$ % and cooled down to approximately 200° C before the H_2S was reduced to zero is Class I. However, if the crystal (having been grown at the same concentration of $[H_2S]:[N_2]$) is cooled down to 50° C before the H_2S is reduced to zero, the crystal is Class II.

From these results it can be seen that if stable photovoltaic cells are to be produced, the CdS crystal should definitely be a Class II crystal. The Class I crystal is far too sensitive to ambient and heat treatment.

3. Radiation-Damage Studies:

The defect structure of CdS can strongly influence its photo-electrical properties. The influence of impurities in CdS is beginning to be understood, but the influence of intrinsic defects is much less well understood. Progress in the identification of intrinsic defects has been slow because of their low concentrations and the difficulty in distinguishing between point defects and associated defects.

Heat treatments in the vapor of one of the components, thermal damage, radiation damage and self-diffusion experiments are capable of changing the intrinsic defect concentration. In the following, the intrinsic defect structure. was altered by the use of X-rays. Changes were detected by measuring the SDP and the TSC before and after irradiation. The effect of ambient pressure surrounding the crystal, the effect of heat treatment, the damage threshold, and the defects responsible for any observable changes were studied.

First we discuss some theoretical concepts. X-rays can cause damage in a crystal in the following manner: On entering a crystal, the X-rays interact with the atomic electrons by the Compton effect and the photoelectric effect (at energies less than ~ 1 MeV). An angular distribution of scattered electrons is produced which can collide with the lattice atoms of the crystal. If the energy of the electrons is sufficient, point defects may be produced.

There are several damage mechanisms which may be encountered as a result of the irradiation[88,89]. First, there is the possibility that one of the lattice atoms is displaced and deposited at a point distant from the resultant vacancy. Secondly, there is a possibility of an unfocused replacement event where the atom hit by the electron replaces a second atom, the second atom replaces a

third, etc., until the energy of the nth atom drops below the replacement energy threshold, and the nth atom goes into an interstitial position. Next, there is the possibility of a focused collision (or focuson); that is, the atom that is initially hit by the electron hits another atom in a row, etc., so that a substantial amount of the energy given to the first atom is transferred over many lattice distances. Therefore it is possible that a defect may be created quite far from the point of collision of the electron and the first atom. Another type of event that can occur is the focused replacement event. An atom is propagated down a line of atoms as a dynamic crowdion. A vacancy is left at the site of initial impact with the electron and an interstitial is created when the energy being transmitted along the line falls below the replacement threshold energy. Various things affect the occurrence of such events; for example, high temperatures would tend to defocus focusing events, whereas neighboring lines of atoms may assist focusing. The size of the atoms and their distance apart also influence focusing events. (As far as CdS is concerned, the requirements for focused collisions would most easily be fulfilled in the sulfur sublattice because of the large size of the sulfur atom.) Focusing and replacement events would require the lowest initial threshold energy.

Evidence for focusing exists in the case of metals subjected to sputtering. However, it is not known whether focusing occurs in a material like CdS.

It is important to know the crystal type if one is to discuss the results. As described above, CdS can be divided into two basic classes--Class I, where the near-surface region is the primary contributor to the photoconductivity, and Class II, where the bulk is the primary contributor to the photoconductivity in the extrinsic region and the surface the primary contributor in the intrinsic region.

Before we discuss our work, we mention some previous studies. A moderate amount of literature has appeared concerning radiation damage effects in CdS[77,90-113]. The studies in the literature, however, have been carried out using a wide variety of bombarding particles. Also, different electrical and optical methods have been used to detect radiation-produced changes. Various models have been proposed, but no unified picture exists as yet.

High-energy photons and electrons as well as low-energy heavy particles, such as protons, neutrons and alpha particles, tend to confuse the picture since they will cause damage in both the cadmium and sulfur sublattices. Therefore, to get the most meaningful results, it is best to confine an investigation to electrons and photons having an energy less than 1 MeV.

Böer, Weber and Wojtowicz[106] and Böer and Gutjahr[107] detected changes in the SDP with X-ray energies as low as 60 keV for measurements made in a vacuum of 10^{-6} torr. It is now felt that the results were affected by the residual gas left in the vacuum chamber. It is speculated that this gas was ionized and then bombarded the surface of the crystal, thereby causing the observed changes.

Kulp and Kelley[77] have studied the damage threshold in CdS using luminescence measurements to detect changes. They found that for 115 keV electrons, the green-edge luminescence first increases and then disappears and that a red luminescence band appears and grows in intensity. They found that the changes were irreversible. They attribute the edge emission to sulfur interstitials and the red emission to sulfur vacancies. The irreversibility was explained by radiation-enhanced diffusion of sulfur interstitials. More recent experiments by Bryand and Cox[109] confirm that 115 keV electrons cause damage to CdS crystals. Their explanation of the damage caused is consistent with Kulp and Kelley's explanation.

Kulp and Kelley's work is generally accepted as the definitive work on damage thresholds in CdS. However, the damage threshold values (8.7 eV for sulfur, 7.3 eV for cadmium) seem to be rather low. Bäuerlein[110] maintains that if CdS has a strong ionic component in its binding, then one would expect a significantly higher displacement threshold. Garlick et al.[91] suggest rather that lattice displacement is not involved but that damage takes place in a disordered region of the crystal.

There is also the possibility of sub-displacement threshold events--for example, replacement collisions and focused collisions. The energy transferred by these events may result in damage in disordered regions. It should be mentioned, however, that focused collisions are affected significantly by the temperature such that the higher the temperature, the more likely that defocusing will occur after a given number of collisions.

A problem also arises in the use of electrons as the bombarding particle. For one thing, the crystal is not uniformly irradiated; that is, electrons penetrate only a given distance in a crystal. Secondly, for electron energies just above threshold, only those atoms nearest the surface encounter damage-producing electrons. As the incident electron energy increases, an increasingly thicker layer will be the source of the damage. There is also the problem that a rather substantial amount of charge is injected into the crystal by the bombardment. This charge could possibly enhance damage produced in the crystal. As a result of these considerations, it would be better in some respects to use X-radiation since (1) the electrons that were capable of producing damage would be created uniformly throughout the crystal, and (2) no excess charge would be introduced into the crystal. X-irradiation, however, does have the disadvantage of not being monoenergetic and therefore the electrons produced are not monoenergetic.

As mentioned previously in this section, Böer et al. felt that the ambient atmosphere had a strong influence on the radiation damage results that they obtained. If this is the case, then the results of Kulp and Kelley would also be influenced by the ambient atmosphere. In fact, the use of electrons would enhance the problem as compared to the use of X-rays.

It is noteworthy that Kulp and Kelley were able to produce green-edge luminescence in their crystals above their threshold value. Green-edge luminescence appears to be connected with the near-surface region but not the bulk[81,114]. Therefore, Kulp and Kelley apparently caused changes in the near-surface region which may indicate that the ambient pressure was a significant factor in the damage. Damage in the near-surface region may require a considerably lower threshold than would be the case for the bulk.

More recently, O'Connell[111] irradiated Class II CdS crystals with X-rays. He found a damage threshold near 300 keV in a vacuum of 10^{-9} torr. He attributed the damage to the increase of sulfur vacancies and a decrease in recombination-center density. SDP and TSC measurements were used to monitor the damage. These results may indicate the significance of the ambient pressure in the vacuum chamber although the use of X-rays may also be significant.

Im and Bube[108] have caused damage in CdS crystals with electrons having an energy as low as 75 keV in an unspecified vacuum. The crystals tested had been treated in sulfur vapor prior to testing. They ascribe the changes as being due to changes in interstitial sulfur that was present as a result of the sulfur treatment. They also report an increase in electron lifetime for damage produced at electron energies less than 250 keV. At 700 keV, they noted a substantial decrease in the electron lifetime which they suggest might be due to both Cd and S being displaced from their lattice positions. They assumed the validity of

Kulp and Kelley's result when they proposed their model.

Wruck[113] has recently measured damage due to 280 keV electrons by using a sensitive a-c method. Extrinsic photoconductivity before and after irradiation was measured. At least six photoconductivity bands were found which were attributed to intrinsic lattice defects and to donor-acceptor associates involving intrinsic defects and residual impurities. The effect of radiation on these bands in conjunction with a variety of photoelectronic techniques were used to identify defect levels. It was assumed that the atomic displacement values of Kulp and Kelley are valid.

Now we discuss our experimental set-up. The crystals used in the experiments were grown in our laboratory as described in Sec. IIB1[56]. Platelets having a surface area of up to $1/2$ cm^2 (1 cm x $1/2$ cm) and a thickness of 50 to 100 μm were used. The crystals were not intentionally doped.

Ti/Al ohmic contacts were evaported onto the crystals[62]. A single crystal was then placed on a mica sheet which lay on a copper block (Fig. IIC-16). The crystal was held in place by two platinum wires under tension that also made electrical contact with the crystal electrodes. Thin copper wires connected the platinum wires to instruments that were used to make measurements. A 20 volt battery, a pico ammeter and a recorder were connected in series with the crystal. A copper constantin thermocouple was placed in a mica sheet on the copper block so that the temperature recorded by the thermocouple and the temperature of the crystal were the same.

The crystal holder (which is situated on the end of a stainless steel cold finger) was mounted in UHV system (Fig. IIC-17). Pressures as low as 10^{-10} torr were obtained using a Vac Sorb pump, a titanium-sublimation pump and a 15 liter/sec Vac Ion pump. A nude ionization gauge and the current drawn by
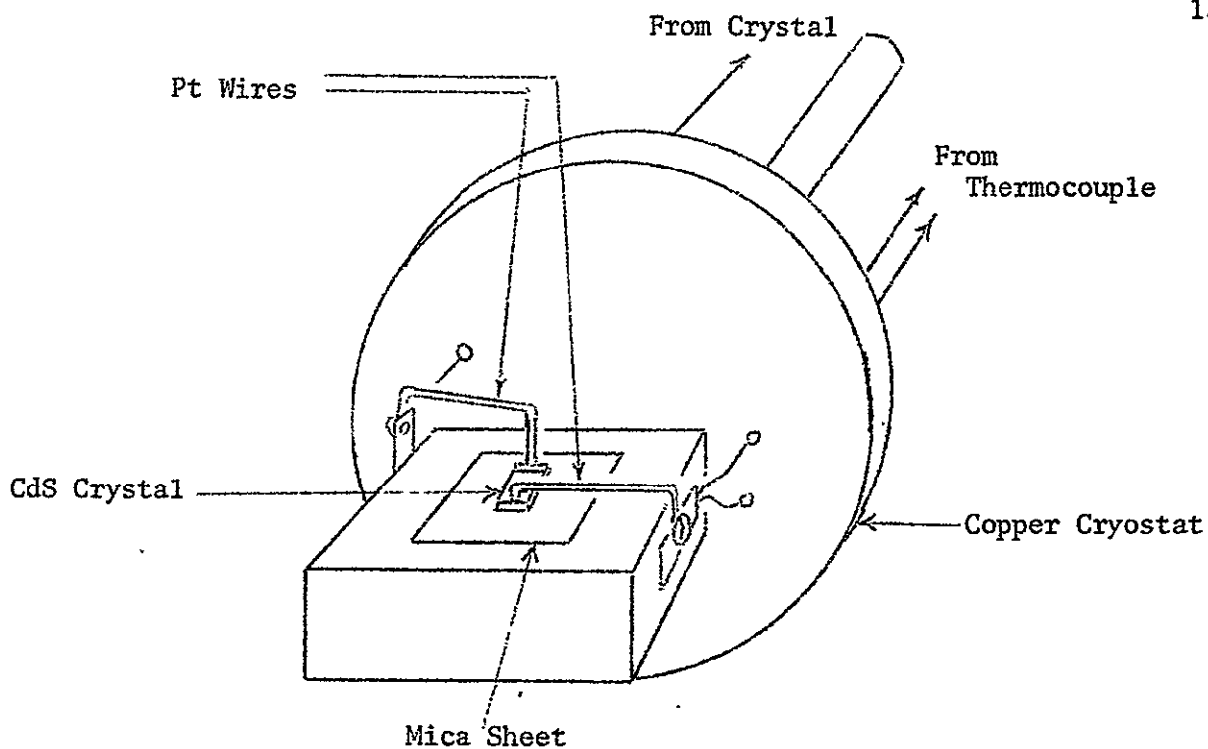
FIGURE IIC-16: Copper cryostat showing mounted crystal.
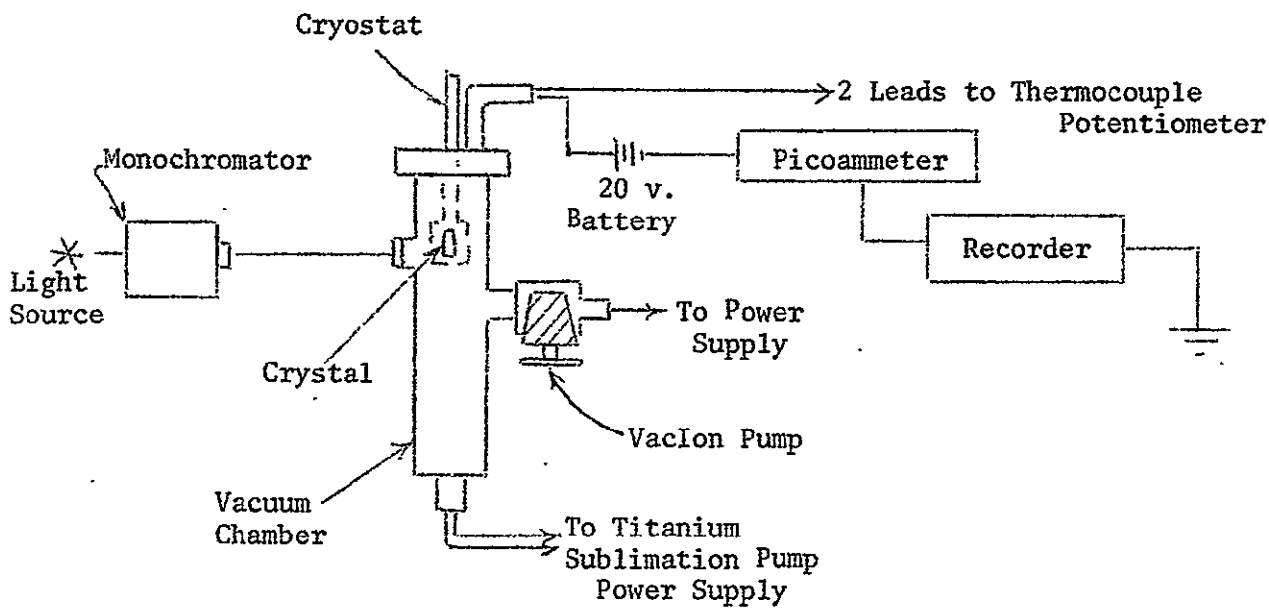

FIGURE IIC-17: Experimental apparatus.

the Vac Ion pump were used to measure the vacuum.

The crystals were illuminated using a high-intensity Bausch and Lomb monochromator. The spectral half-width of the light falling on the crystal was as small as 25 Å. The monochromator scan was driven at a rate which enabled the photocurrent to maintain equilibrium.

The source of X-rays for the experiments was located in Philadelphia, Pa. at Frankford Arsenal. An anti-cathode of tungsten was used to convert a mono-chromatic electron beam into a spectrum of X-rays. The maximum energy of the X-rays was 150 keV with an exposure time for the crystals being 1 hour.

Crystals were chosen that showed good photosensitivity. They were tested according to the following experimental program:

a. A virgin crystal is irradiated with 150 keV (maximum) X-rays while at a pressure, $p \lesssim 10^{-8}$ torr.

b. If there is damage, the crystal is subjected to temperature treatments starting at 50° C and increasing by 50° C at each treatment. After each treatment the crystal is subjected to 150 keV irradiation at 10^{-8} torr.

c. If there is no damage, the crystal is irradiated with 150 keV X-rays while at a pressure of $\sim 10^{-5}$ torr. Changes are measured and annealed if there is damage. If there is no damage, there is no necessity of annealing. In either case, then, the crystal is subjected to 200 keV X-rays at a pressure, $p \lesssim 10^{-8}$ torr.

    i. If there is damage, the crystal is temperature-treated at 50°C and in 50° C steps beyond 50° C. After each treatment the crystal is irradiated with 200 keV X-rays at $\lesssim 10^{-8}$ torr.

    ii. If there is no damage, the crystal is irradiated with 200 keV X-rays at 10^{-5} torr. If damage is observed, the crystal is annealed. Otherwise

no annealing is necessary. Then, the crystal is irradiated with 250 keV X-rays at $\leq 10^{-8}$ torr.

d. The above pattern is continued.

By this procedure, the threshold energy for damage, the effect of ambient pressure and the effect of temperature are to be determined.

The experimental techniques that were used to detect changes in the crystals were the measurement of the SDP at RT and LNT and the TSC. Before and after changing the conditions (either irradiation or heat treatment) to which the crystals were subjected, reproducible SDP and TSC measurements were obtained.

Crystals were irradiated at RT and immediately cooled to LNT in order to freeze-in any defects created. Within 2 hours, SDP and TSC measurements were started. Then, after completion of these measurements, the crystals were left in the dark at RT for several days before more measurements were made. Damage in the crystal was annealed if it was necessary.

The crystal which is presently being investigated is in the process of being put through the program mentioned in the above discussion. The crystal is a Class I crystal. Fig. IIC-18 shows the LNT SDP before and after irradiations with 150 keV X-rays at $p \leq 10^{-8}$ torr. Two irradiations were performed in order to check the reproducibility of the irradiation changes. It is to be noted that the irradiations produced similar changes in the LNT SDP; that is, the response in the intrinsic region decreased by approximately one-half an order of magnitude. The response in the extrinsic region can be attributed to a decay of the dark conductivity after the X-ray excitation. It is also to be noted that the peak at ~ 4870 Å decreases relative to the broad maximum at ~ 4750 Å as a result of the irradiation. Fig. IIC-19 shows the TSC curves before and after the first and second irradiations. Here, it is seen that the irradiations had a similar effect
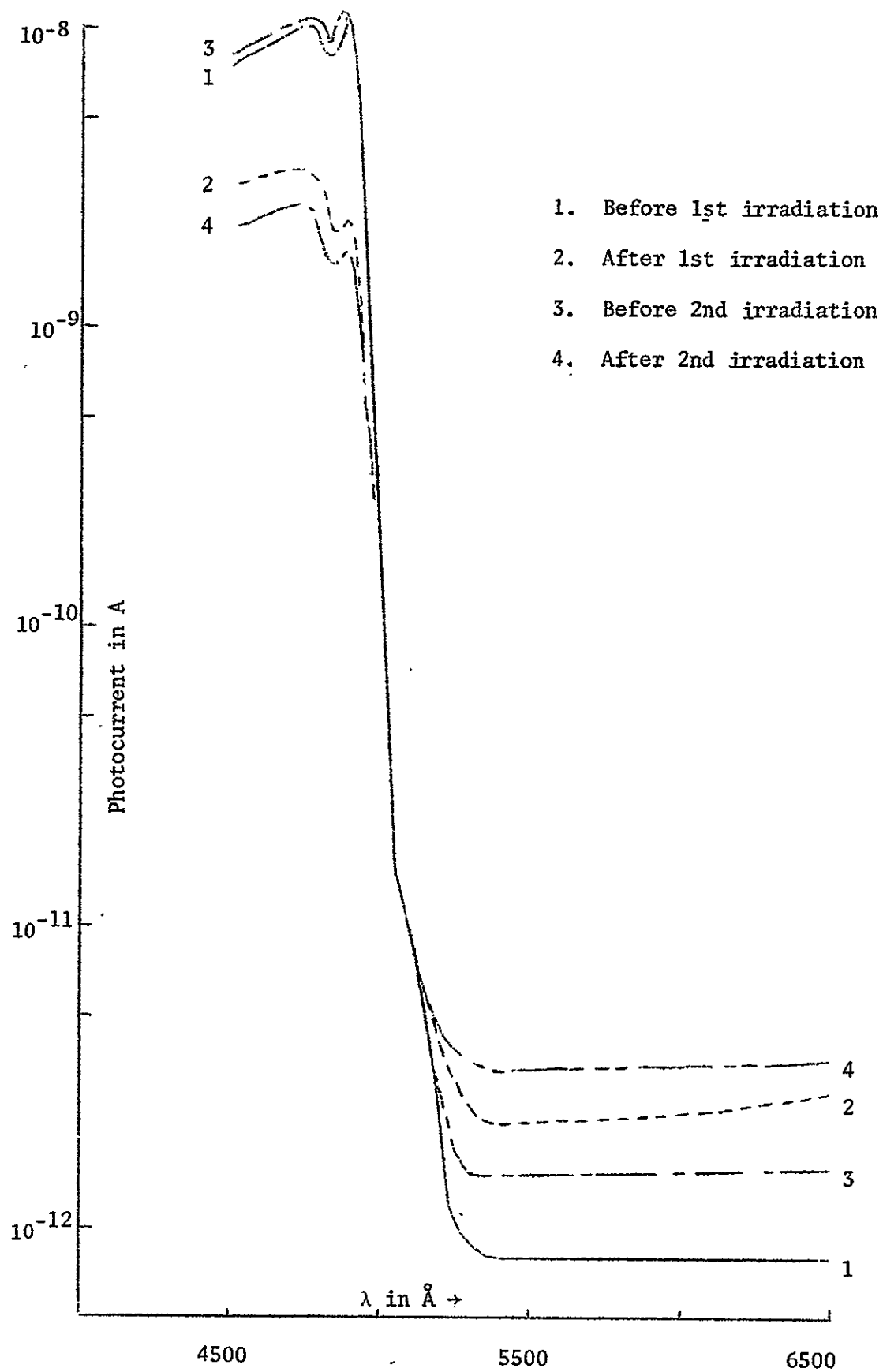
FIGURE IIC-18: LNT SDP before and after 150 keV irradiations for one hour.
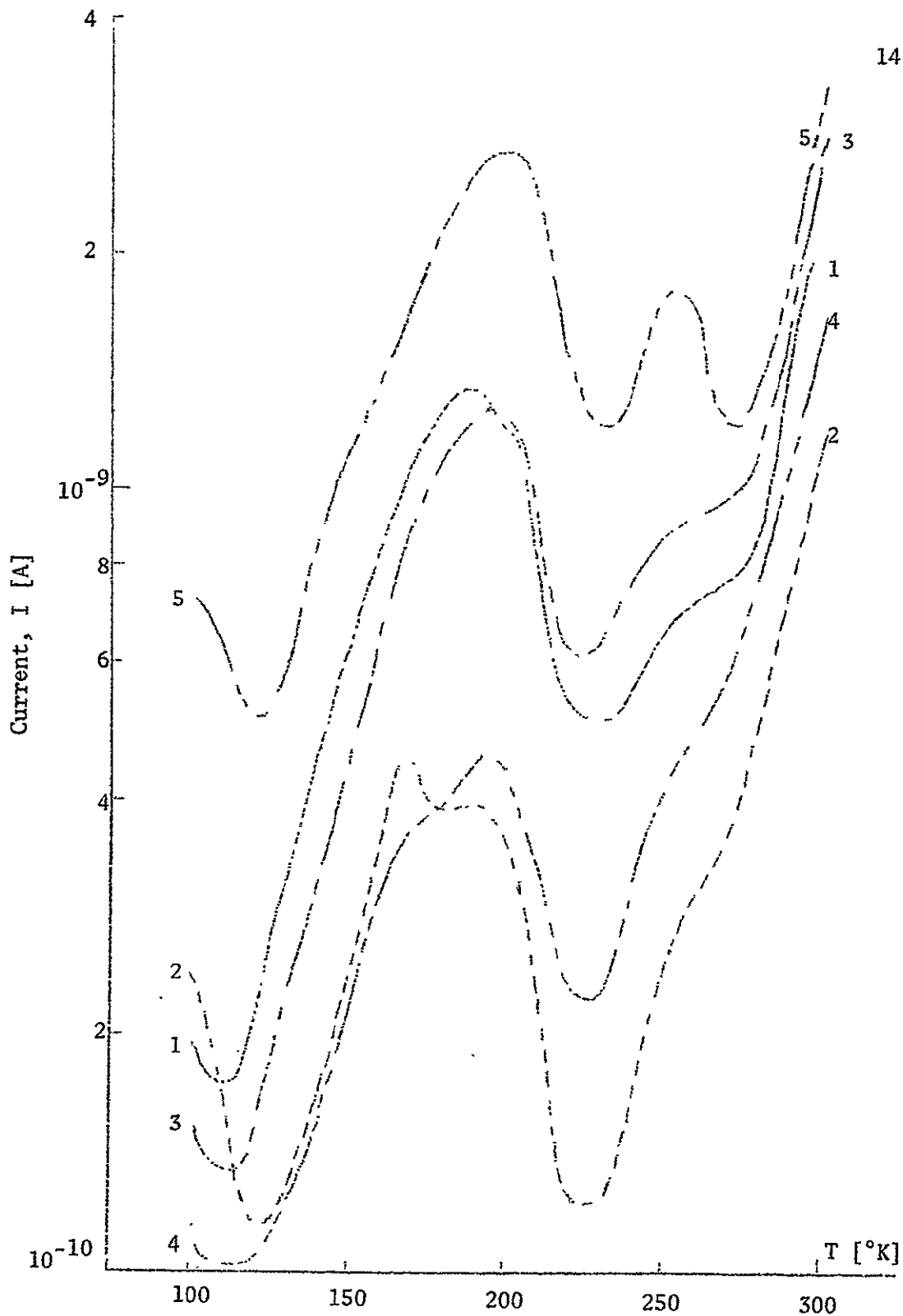
FIGURE IIC-19: TSC before and after 150 keV irradiations for one hour.

1. Before 1st irradiation
2. After 1st irradiation
3. Before 2nd irradiation
4. After 2nd irradiation
5. Several days after the 2nd irradiation

on the crystal, although the annealing after the second irradiation did not return the crystal to the pre-irradiation state. Next the crystal was heat-treated at 50° C for 1 hour with little apparent change in both the LNT SDP and the TSC measurements. Fig. IIC-20 shows the changes in the LNT SDP after another 150 keV X-irradiation. In this figure, the photoconductivity is resolved into components where the electric vector of the incident light is either perpendicular or parallel to the c-axis of the CdS crystal. This was done so that the excitonic structure could be resolved. A similar decrease of the photoconductivity in the intrinsic region is observed as a result of the irradiation. Also, annealing of the crystal by keeping it in the dark at RT returns the LNT SDP to that obtained before irradiation. The TSC results are seen in Fig. IIC-21. This also follows the behavior found after previous irradiations. Next, the crystal was heated to 100°C and then immediately cooled. Subsequent measurements within a few days showed an over-all decrease in the LNT SDP and an increase in the TSC response. However, after several weeks both the LNT SDP and TSC measurements returned to the pre-heat treatment levels. The investigations are continuing.

Now we discuss our results. The crystal that is being tested is a Class I crystal. Irradiation has the effect of decreasing the photo-response as well as decreasing the TSC. The decrease is approximately the same for the SDP and TSC measurements. This could be attributed to a decrease in lifetime in the crystal; that is, a greater amount of recombination is taking place (presumably at the surface) as a result of the irradiation. Whatever changes are caused in the crystal by the irradiation are annealed quickly when the crystal is left in the dark at room temperature; that is, recombination decreases.

Some changes are observable in both the LNT SDP and the TSC measurements other than a parallel shift. For example, the peak in the LNT SDP at ~ 4870 Å
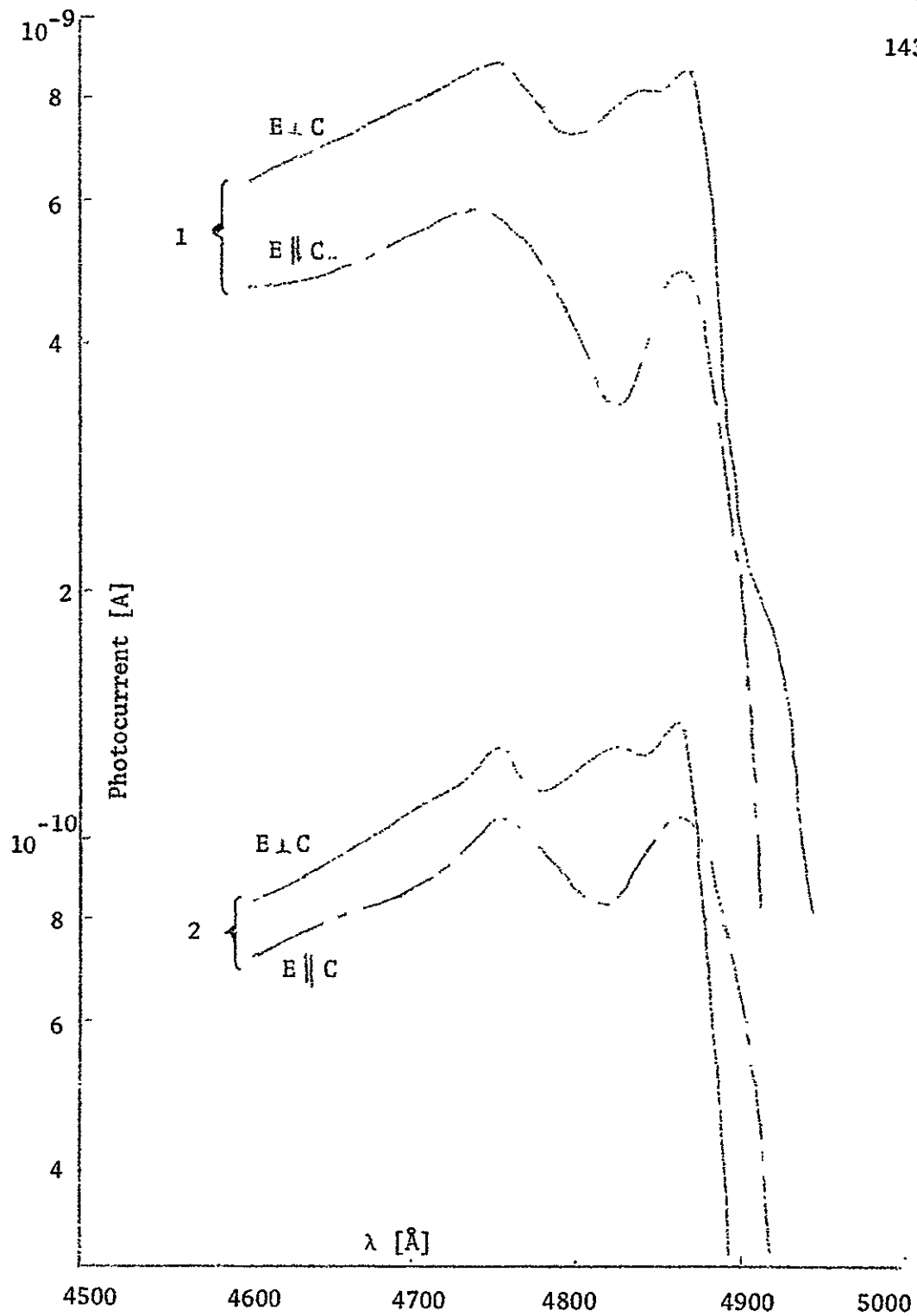
FIGURE IIC-20:   LNT SDP after a 150 keV irradiation for one hour.

1. After 50° C heat treatment and before 3rd irradiation
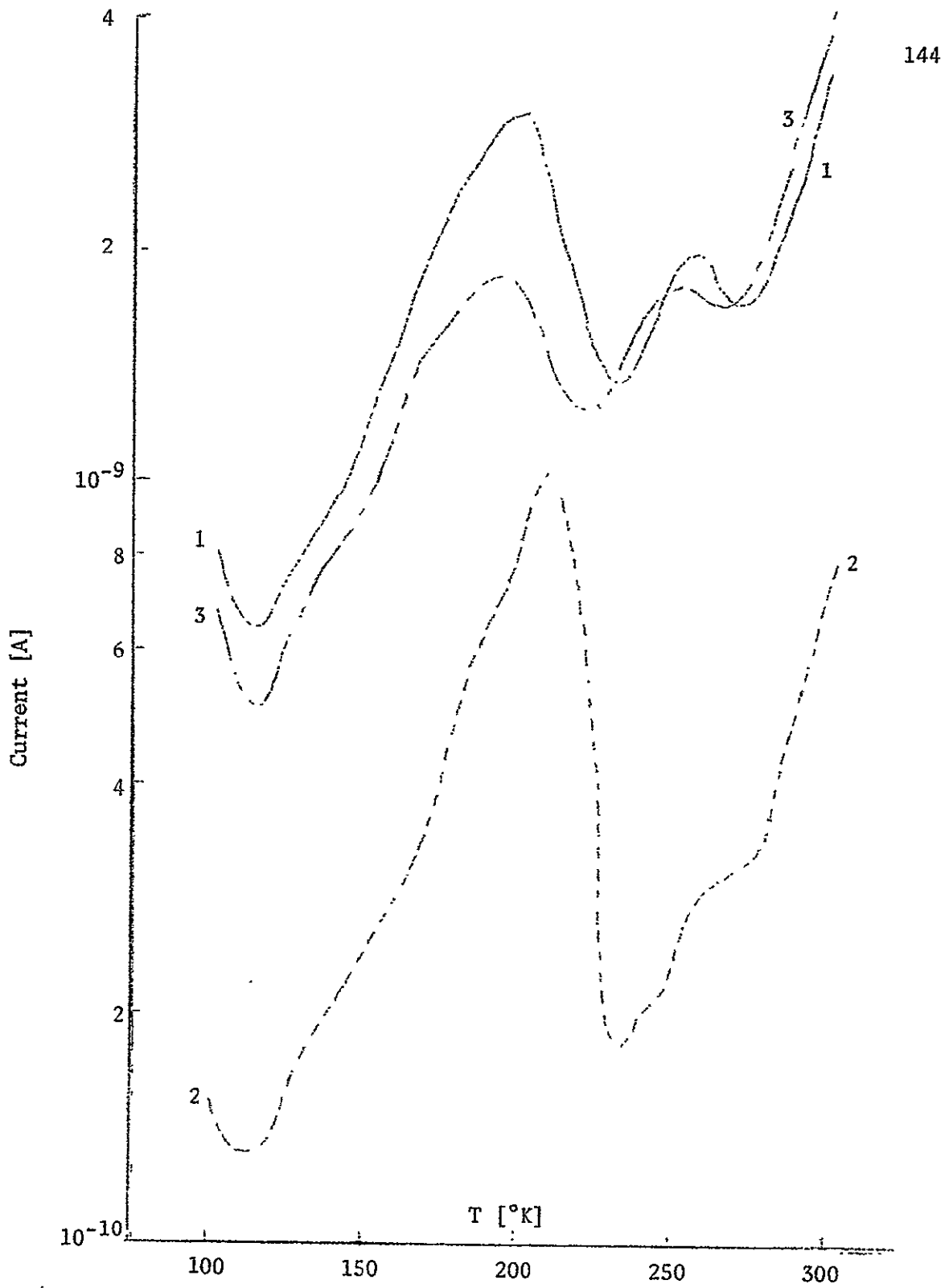2. After 3rd irradiation

FIGURE IIC-21: TSC before and after 3rd irradiation at 150 keV for 1 Hour.

1. After 50° C heat treatment and before 3rd irradiation
2. After 3rd irradiation
3. Several days after 3rd irradiation

decreases with respect to the ~ 4750 Å peak after irradiation. The peak at ~ 4870 Å is thought to be due to both the ionization of the A exciton and the ionization of an exciton bound to an impurity. Insufficient data is on hand to ascertain the precise behavior.

The TSC curves also show structural changes. For example, the irradiation caused the peak at ~ 200° K to become a double peak. Other indications of peaks remained after irradiation. Again, the TSC characteristics were annealed after the crystal was brought to RT and kept in the dark for several days. At this stage of the experiment, it is not possible to say much regarding the identification of defects associated with the TSC peaks. Further work is continuing in order to establish their nature.

It is significant that damage to this crystal was caused by 150 keV X-irradiation, as opposed to the almost 300 keV reported to be necessary by O'Connell[111]. This is apparently due to the fact that this crystal is a Class I crystal. Because the surface layer is most important for Class I crystals, any change in the surface layer would be particularly apparent. Kulp and Kelley[77] report that green-edge emission (which appears to be associated with Class I crystals[81,114]) could be made to disappear by bombarding crystals with electrons having energies ranging from 3 keV to 200 keV. The effect of the ambient atmosphere and the residual charge on the energy necessary to cause the green luminescence to disappear is unknown. Further experiments are underway to ascertain the significances of the various effects.

The following discussion summarizes the results of this Section. There are two different classes of CdS crystals. These exhibit substantially different behavior as a result of X-irradiation. Class I crystals have the photocurrent carried by a thin near-surface region (10^{-5} cm). Experiments up to now have

indicated that 150 keV (maximum) irradiation causes considerable changes in both SDP and TSC measurements. This may be attributed to the fact that the surface is especially sensitive either to ambient ions bombarding the surface or to actual radiation damage in the surface-near region. It is suggested that the damage threshold might be considerably lower for Class I crystals.

In Class II crystals, the photocurrent is carried in the bulk for extrinsic excitation and in the surface for intrinsic excitation. Measurements by O'Connell[111] indicate a higher damage threshold (~ 300 keV X-rays) for this class of crystal.

Although progress has been made in clarifying the picture regarding radiation damage in CdS crystals, more information clearly is needed. In particular, more information is needed on the respective damage thresholds of Class I and Class II crystals as well as the defects responsible for the damage observed in each type of crystal. We hope to obtain this information as a result of our subsequent investigations.

III.   CONCLUSIONS

. In the first phase (first year, which is conducted under the contract from the Jet Propulsion Laboratory) of the proposed research effort to improve the quality of CdS photovoltaic cells, specifically to improve the conversion efficiency over the currently achieved ~ 5%, the following results and conclusions were arrived at:

1. A research team of nine scientists/students (mostly working part-time for this contract) was formed (total effort averages about 3 man/year), and this team was familiarized with the general state of the art and the goal in photovoltaic research.

2. Three research groups within this team were established with close coordination of their research in the fields of (a) photovoltaic theory, (b) material, and (c) influence of external means (radiation, ambient atmosphere).

3. The results of the theoretical group with respect to an ideal junction analysis are encouraging. The consistent discussion of the Poisson- and extended transport equation using a graphical approach yields very useful results and shall be continued. Most important are the results in respect to the open circuit voltage yielding simple criteria for its maximum value.

4. The theoretical analysis of the real CdS:Cu$_x$S junction yields a model which allows explanation of many experimental results, some of which are not explainable otherwise.

5. A systematic discussion of photoconductor heterojunctions makes possible a number of recommendations with respect to selection of pairs of compounds with probably superior efficiency.

6. The discussion of the kinetics of the field distribution near a contact is very helpful because of two reasons:

  (a) At least one contact of a photovoltaic cell will be close to the active volume of the cell for maximum efficiency.

  (b) The field distribution in a heterojunction is very similar to the one near a contact and most of the results obtained can readily be used for the junction.

We have used this approach since here experimental results were already available. The theory shall be expanded for junctions.

7. The experimental group involved in crystal growth, doping and production of the heterojunction has successfully completed this task with respect to reproducible production of CdS-platelet/Cu_xS junctions and with controlled CdS-doping as required for high-field domains.

8. The use of high-field domains for obtaining further experimental information on the field distribution and electron concentration within the junction shall be further analysed.

9. Investigation of the spectral distribution of the photovoltaic effect at different temperatures at partially illuminated p-n junctions provided the experimental evidence for the high-strain model suggested for the actual junction and causing the photovoltaic dip at the CdS-band-edge.

10. The investigation of the influence of the ambient atmosphere on photoelectric parameters was successfully concluded with respect to oxygen. This part resulted in two publications (Refs. 64 and 65).

11. Investigation of the post-growth treatment resulted in a method to obtain oxygen-ambient-insensitive CdS crystals by cooling the freshly grown crystals in a H_2S-rich N_2-atmosphere ($\sim$ 5% H_2S) to below 200° C.

12. X-ray damage experiments have shown a first threshold of some
CdS platelets in 10^{-5} torr air ambient at 115 keV, -- other platelets in
10^{-9} torr ambient have the first threshold at ~ 275 keV. There are experimental
indications that differences in the native defect distribution and possibly in
the ambient atmosphere are reasons for this difference in threshold. Also some
differences in annealing temperatures are detected. Such findings can become
important for producing highly damage-resistant photocells.

IV. RECOMMENDATIONS

Since the research program was started only twelve months ago, most of the findings are of preliminary nature and recommendations are made with some reservations.

1. For maximum open-circuit voltage the material should be doped in such a way that the (dark) Fermi-level lies close to the respective band and the quasi-Fermi level for minority carriers shifts as close as possible to the opposite band with light. A small density of levels in the center part of the band gap seems essential for this.

2. Material which is more than a random-walk length for minority carriers separated from the junction is useless for the photovoltaic effect and can only reduce it because of additional optical absorption. It should also be eliminated because it acts as undesired series resistance which can only be neglected for high doping levels, which in turn are undesired since they oppose point 1 of these recommendations.

3. Since the random-walk length of minority carriers and the Debye screening length are of the order of (or below) 10^{-5} cm, only a very thin slab of the (not graded) photovoltaic device is active; hence large optical absorption ($\kappa \gtrsim 10^5$ cm^{-1}) is required for efficient photogeneration of carriers. This requires extreme doping densities in the junction, i.e., grading of the junction and illumination through the wide band gap material for maximum efficiency. The thickness of the graded part should not exceed the Schubweg of the minority carriers in the junction field.

4. For efficient transport of the carriers to the electrodes the width of each side of the device (measured from the centerplane of the junction) shall be smaller than the random-walk length of the majority carrier.

This asks for rather thin backwall devices (less than 1 µm). Technical difficulties in producing thin pinhole-free layers with perfectly laminated graded junction determine the currently used optimum thickness of about 100 x the theoretical optimum. Therefore intensive studies of economical means of laminated deposition of thin graded junctions are highly recommended. The development of a highly transparent front-electrode (e.g., n^+-CdS) with an ohmic metal grid (Ti/Al) is suggested.

Recommendations continued.

V. NEW TECHNOLOGY

1. In CdS:Cu$_x$S photocells care should be taken to prevent the formation of an interlayer of Cu$_{1.96}$S by sufficient reduction of the copperchloride solution, a light treatment of the cell and low temperature operation.

2. To reduce the stress at the Cu$_x$S:CdS boundary and excessive Cu-diffusion into CdS a thin interlayer of a II-VI alloy (possibly Zn/CdS/Se) is suggested.

VI. REFERENCES

1. W. D. Gill and R. H. Bube, J. Appl. Phys. $\underline{41}$, 3731 (1970).

2. H. Rau, J. Phys. Chem. Solids $\underline{28}$, 903 (1967).

3. L. R. Shiozawa, F. Augustine, G. A. Sullivan, J. M. Smith, and W. R. Cook, Jr., Final Rept.; Contract AF 33 (615)-5224, Aerospace Research Labs., May 1969.

4. L. Eisenmann, Ann. Phys. $\underline{10}$, 129 (1952).

5. R. Marshall and S. S. Mitra, J. Appl. Phys. $\underline{36}$, 3882 (1966).

6. G. B. Abdullaev, Z. A. Alirarova, E. H. Zamanova, and G. A. Asadov, Phys. Stat. Sol. $\underline{26}$, 65 (1968).

7. G. P. Sorokin, Yu. M. Papshev, and P. T. Oush, Sov. Phys.-Solid State $\underline{7}$, 1810 (1966).

8. N. Nakayama, Jap. J. Appl. Phys. $\underline{8}$, 450 (1969).

9. W. R. Cook, Jr., L. Shiozawa, and F. Augustine, J. Appl. Phys. $\underline{41}$, 3058 (1970).

10. Reference 3, pp. 38 ff.

11. N. Miya, Jap. J. Appl. Phys. $\underline{9}$, 768 (1970).

12. Reference 3, p. 105.

13. R. H. Bube, J. Appl. Phys. $\underline{35}$, 586 (1964).

14. L. R. Shiozawa, F. Augustine, and W. R. Cook, Jr., Final Rept.; Contract F33615-69-C-1732, Aerospace Research Labs., July 1970, pp. 30 ff.

15. R. R. Chamberlin and J. S. Skarman, Sol. St. Elect. $\underline{9}$, 819 (1966).

16. H. J. Queisser, J. Appl. Phys. $\underline{32}$, 1776 (1961).

17. M. S. Abrahams, L. R. Weisberg, J. J. Tietjen, J. Appl. Phys. $\underline{46}$, 3754 (1969).

18. Y. Sugita, M. Tamura, K. Sugawara, J. Appl. Phys. 40, 3089 (1969).

19. J. R. Dale, Phys. Stat. Sol. 16, 351 (1966).

20. Reference 3, p. 15.

21. Reference 3, p. 103.

22. K. W. Böer, G. Döhler, G. A. Dussel, P. Voss, Phys. Rev. 169, 700 (1968).

23. K. W. Böer, G. A. Dussel, P. Voss, Phys. Rev. 179, 703 (1969).

24. R. Stirn, K. W. Böer, G. A. Dussel, P. Voss, Proc. Int. Conf. Photocon-
    ductivity, Stanford (1969) (in print).

25. A. Rose, Concepts in Photoconductivity and Allied Problems, Wiley,
    New York (1963).

26. W. Ruppel, Semiconductors, Vol. 6, Ch. 5, Academic Press (1970).

27. A. J. Bennett and C. B. Duke, Phys. Rev. 160, 541 (1967); Phys. Rev. 162,
    578 (1967).

28. G. H. Parker and C. A. Mead, Appl. Phys. Lett. 14, 21 (1969).

29. G. A. Dussel and K. W. Böer, Phys. Stat. Sol. 39, 375 (1970).—

30. W. Franz, Handbuch der Physik, XVII, 153 (1956). See, e.g., G. A. Dussel,
    Ph.D. Dissertation, Univ. of Del. (1970).

31. L. J. van Ruyven and F. E. Williams, Am. J. Phys. 35, 705 (1967).

32. W. Palz and W. Ruppel, Phys. Stat. Sol. 6, K161 (1964).

33. E. D. Hinkley and R. H. Rediker, Sol. St. Elect. 10, 671 (1967).

34. W. D. Gill and R. H. Bube, J. Appl. Phys. 41, 1694 (1970).

35. Reference 3, p. 146.

36. Reference 3, p. 97.

37. L. J. van Ruyven and I. Dev, J. Appl. Phys. 37, 3324 (1966).

38. Y. Marfaing, G. Cohen-Solal, and F. Bailly, Physics of Semiconductors,
    p. 1245, Dunod, Paris (1964).

39. M. Glicksman, D. Gutman, and W. M. Yim, Appl. Phys. Lett. 16, 366 (1970).

40. B. Agusta and R. L. Anderson, J. Appl. Phys. 36, 206 (1965).

41. K. J. Siemsen and H. D. Riccius, Phys. Stat. Sol. 37, 445 (1970).

42. W. Michael Yim, J. Appl. Phys. 40, 2617 (1969).

43. A. Kremheller, A. K. Levine, G. Gashurov, J. Electrochem. Soc. 107, 12 (1960).

44. M. V. Kot, V. G. Tyrziu, A. V. Simaskevich, Yu. E. Maronchuk, and V. A. Mshenskii, Sov. Phys.-Solid State 4, 1128 (1962).

45. M. R. Lorenz, Physics and Chemistry of II-VI Compounds, p. 112, Wiley, New York (1967).

46. N. I. Vitrikhovskii and I. B. Mitsetskaya, Sov. Phys.-Sol. St. 1, 912 (1959).

47. S. Larach and W. H. McCarroll, J. Phys. Chem. 60, 604 (1956).

48. A. G. Fischer and R. J. Paff, J. Phys. Chem. Sol. 23, 1479 (1962).

49. J. C. Woolley, Compound Semiconductors, Vol. 1, p. 3, Reinhold, New York, (1962).

50. N. A. Goryunova, The Chemistry of Diamond-like Semiconductors, p. 125, M. I. T., Cambridge (1965).

51. Reference 50, p. 138.

52. E. K. Müller and J. L. Richards, J. Appl. Phys. 35, 1233 (1964).

53. Reference 50, p. 148.

54. A. D. Stuckes and R. P. Chasmar, J. Phys. Chem. Sol. 25, 469 (1964).

55. N. A. Goryunova, F. P. Kesamanly, and D. N. Nasledov, Semiconductors and Semimetals, Vol. 4, p. 413, Academic Press, New York (1968).

56. L. van den Berg, Master's Thesis, Univ. of Delaware (1969).

57. E. F. Gross and B. V. Novikov, J. Phys. Chem. Sol. 22, 87 (1961).

58. K. W. Böer and P. Voss, Phys. Rev. 171, 899 (1967).

59. K. W. Böer, H. J. Hänsch, and U. Kümmel, Z. Physik 155, 460 (1959).

60. W. Franz, Z. Naturforsch. 13a, 484 (1958); I. V. Keldysh, Zh. Eksperim. i Teor. Fiz. 34, 1138 (1958) [English transl.: Sov. Phys.-JETP 6, 788 (1958)].

61. G. A. Dussel and K. W. Böer, Phys. Stat. Sol. 39, 391 (1970).

62. K. W. Böer and R. B. Hall, J. Appl. Phys. 37, 4739 (1966).

63. Reference 3, p. 82.

64. R. Schubert and K. W. Böer, J. Phys. Chem. Sol. (in print).

65. C. Wright and K. W. Böer, Phys. Stat. Sol. 38, K51 (1970).

66. P. Mark, J. Phys. Chem. Sol. 25, 911 (1964); 26, 959 (1965).

67. R. H. Bube, J. Chem. Phys. 21, 1409 (1955).

68. H. Berger, K. W. Böer and E. H. Weber, Z. Physik 158, 501 (1960).

69. E. H. Weber, Phys. Stat. Sol. 28, 649 (1968).

70. E. F. Gross et al., Proc. of the 7th Int. Conf. of Semiconductors, p. 5, Paris (1964).

71. R. V. Grigoriev, B. V. Novikov and A. E. Cherednichenko, Phys. Stat. Sol. 28, K85 (1968).

72. F. I. Kreingold'd, Soviet Physics-Solid State 4, 2499 (1963).

73. J. Auleytner, E. F. Gross, A. A. Kralina and B. S. Razbirin, Phys. Stat. Sol. 24, K107 (1967).

74. H. B. de Vore, Phys. Rev. 102, 86 (1956).

75. V. V. Eremenko and E. V. Matyushkin, Soviet Physics-Solid State 6, 321 (1964).

76. J. Voigt and E. Ost, Phys. Stat. Sol. 33, 381 (1969).

77. B. A. Kulp and R. H. Kelley, J. Appl. Phys. 31, 1057 (1960).

78. J. J. Lambe, C. C. Klick, and D. L. Dexter, Phys. Rev. 103, 1715 (1956).

79. Y. S. Park and D. C. Reynolds, Phys. Rev. 132, 2450 (1963).

80. H. Kukimoto and S. Shionoya, J. Phys. Soc. Japan 29, 520 (1970).

81. J. A. Bragagnolo and K. W. Böer, Journal of Luminescence 1, 572 (1970).

82. R. A. Titov, Soviet Physics-Solid State 5, 2553 (1964).

83. R. I. Shekhmamet'ev and B. V. Novikov, Soviet Physics-Solid State 6, 1353 (1964).

84. R. E. Halsted, Physics and Chemistry of II-VI Compounds, p. 385, North Holland (1967).

85. D. C. Reynolds, C. W. Litton and T. C. Collins, Phys. Stat. Sol. 9, 645 (1965); 12, 3 (1965).

86. J. Voigt and F. Spiegelberg, Phys. Stat. Sol. 30, 659 (1968).

87. Reference 64 and references contained therein.

88. Lewis Chadderton, Radiation Damage in Solids, Methuen and Co. Ltd., London, 1965.

89. B. T. Kelly, Irradiation Damage to Solids, Pergamon Press Ltd., Oxford, 1966.

90. B. A. Kulp, Phys. Rev. 125, 1865 (1962).

91. G. F. J. Garlick, F. J. Bryant and A. F. J. Cox, Proc. Phys. Soc. 83, 967 (1964).

92. A. P. Galushka and I. D. Konozenko, Atom. Energ. 13, 277 (1962).

93. A. D. Galushka, I. B. Evnolovich, N. E. Korsunskaya, I. D. Konozenko and M. K. Sheinkman, Fiz. Tver. Tela 8, 1070 (1966), Sov. Phys. Sol. State 8, 831 (1966).

94. R. B. Oswald and C. Kukuchi, Tech. Rept. of College of Eng., Univ. of Michigan (1964).

95. W. Schweinberger and D. Wruck, Phys. Stat. Sol. 15, 355 (1966).

96. S. Tanaka and T. Tanaka, J. Phys. Soc. Japan 14, 113 (1959).

97. M. Barjon, C. Bracket, M. Lambert, M. Martineau and J. Schmouker, C. R. Acad. Sci. 248, 83 (1959).

98. V. I. Broser and R. Warminsky, Z. Natur. forsch. 6a, 85 (1951).

99. T. Y. Sera, V. V. Serdyuk and I. M. Shavihenko, Fiz. Tverd. Tela 3, 3537 (1691).

100. R. O. Chester, ORNL Report 3767 (1965).

101. S. Ibuki, J. Phys. Soc. Japan 19, 1196 (1959).

102. M. R. Lorenz, M. Aven and A. H. Woodbury, Phys. Rev. 132, 143 (1963).

103. H. Saito, M. Kitagawa and M. Hirata, Proc. Japan Conf. on Radioisotopes 5, 207 (1963).

104. E. A. Niekisch, Semicond. Phys. Conf., Prague, p. 1064 (1960).

105. R. J. Collins, J. Appl. Phys. 30, 1135 (1959).

106. K. W. Böer, E. H. Weber and B. Wojtowicz, Z. Physik 168, 115 (1962).

107. K. W. Böer and H. Gutjahr, Z. Physik 152, 203 (1958).

108. H. B. Im and R. H. Bube, J. Appl. Phys. 39, 2908 (1968).

109. F. J. Bryant and A. F. J. Cox, Proc. Roy. Soc. A 310, 319 (1969).

110. R. Bäuerlein, Proc. Int. School of Physics, Enrico Fermi, on Radiation Damage in Solids, Academic Press, New York, London, p. 358, 1963.

111. J. C. O'Connell, Ph.D. Dissertation, Univ. of Delaware, 1967.

112. K. F. Lider, B. V. Novikov and S. A. Permogorov, Phys. Stat. Sol. 18, K1 (1966).

113. D. Wruck, Phys. Stat. Sol. 37, 165 (1970).

114. V. D. Egorov, Phys. Stat. Sol. 20, 705 (1967).

KARL WOLFGANG BÖER

Born: March 26, 1926
       Berlin, Germany

Education:

1944-49 Humboldt University of Berlin
1949   Diplom Physicist
1952   Dr. rer. nat.
1955   Dr. rer. nat. habil.

Employment:

1949-55 assistant and "ober"-assistant in II Physics
         Department of Humboldt University
1955-58 docent - Humboldt University (Lecturer)
1958-61 Associate Professor and head of the IV Physics
         Department
1961   Full Professor at Humboldt University
1955-61 Director of the laboratory of dielectric breakdown
         at the German Academy of Sciences (simultaneously
         with the above-mentioned appointments)
1961-62 research professor at New York University
1961   founder and editor-in-chief of Physica Status Solidi
1962-date Associate Professor at the University of Delaware
1965 (summer) guest professor at Stanford University

~150 130 117 publications in the field of electrical and optical properties
of CdS

Books:

Grimsehl - Lehrbuch der Physik (section on solid state physics)

Siemon, Suhrmann - Photozellen (part on photoconductivity)

2 research films on dielectric breakdown

Book on Instabilities in Semiconductors (1971)

Chapter on Photoconductivity in book ed. by Pick Bube (1971)